MODELLING FOR ENGINEERING AND HUMAN BEHAVIOUR 2013

Instituto de Matemática Multidisciplinar

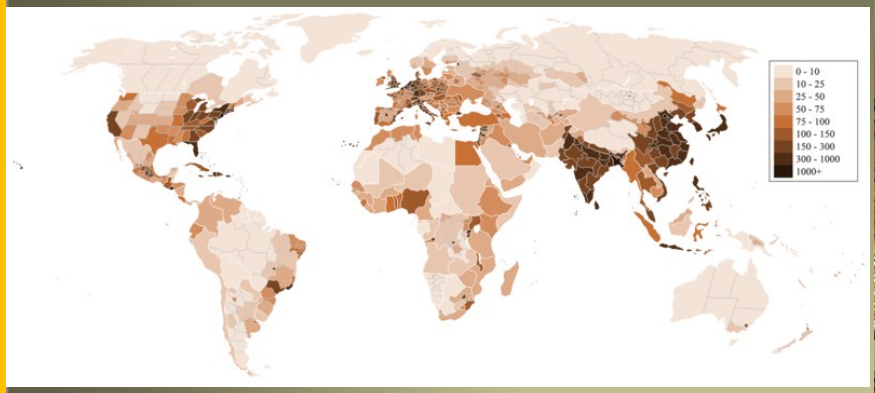

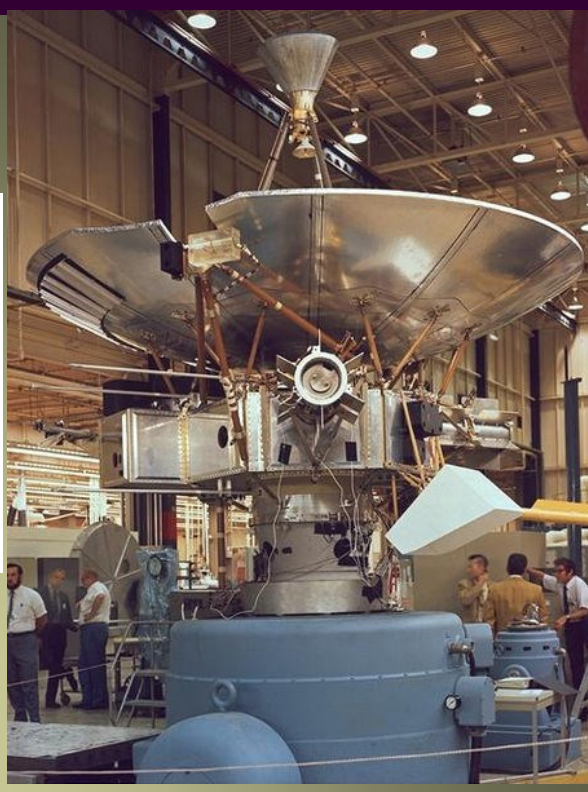

I. Jódar, L. Acedo, J. C. Cortés and M. Ehrhardt,

Editors

Instituto Universitario de Matemática Multidisciplinar

im² Instituto de Matemática Multidisciplinar

UNIVERSIDAD POLITECNICA DE VALENCIA

MODELLING FOR ENGINEERING, & HUMAN BEHAVIOUR 2013

Instituto Universitario de Matemática Multidisciplinar
Universidad Politécnica de Valencia
Valencia 46022, SPAIN

Edited by
Lucas Jódar, Luis Acedo, Juan Carlos Cortés and Matthias Ehrhardt*
Instituto Universitario de Matemática Multidisciplinar
($\star$) Bergische Universität Wuppertal
I.S.B.N.: 978-84-695-9340-0

CONTENTS

Distributed computation in epidemiology

J. Villanueva-Oller[♭] , L. Acedo[⋆] [*], J. A. Moraño[⋆],
and A. Sánchez-Sánchez[⋆]

(♭) Centro de Estudios Superiores Felipe II,

Aranjuez, Madrid, Spain

(⋆) Instituto Universitario de Matemática Multidisciplinar,

Building 8G, Door C, Second Floor,

Universitat Politècnica de Valéncia, 46022 Valencia, Spain

November 30, 2013

1 Introduction

Networks provide an alternative to the traditional continuous differential equations approach in mathematical epidemiology [1, 2, 3]. Although differential equations are a powerful and well-known mathematical tool for studying the dynamics of any system, they are not always the most suitable one because they do not allow to model the effects arising from the different individuals as separate entities. Typically, in these models we consider the fraction of susceptible (S), infected (I) and recovered (R) individuals and propose a compartmental model for the transitions between these states. The resulting model has been widely studied [3, 4] but, albeit it is a good approximation in some cases, it is clear it cannot be the final word in the epidemiology of any real disease. The continuous approach cannot, by its own nature, distinguish among individuals and, consequently, the effects of age, sex, previous illnesses and any other parameters influencing the propagation of the epidemic under study are difficult to implement.

[*]e-mail: luiacrod@imm.upv.es

Unfortunately, networks are a more sophisticated and difficult to tackle paradigm and exact solutions for these models cannot be found analytically. The computational problem is of such a magnitude that studies of real social networks are restricted to a relatively small number of individuals usually not larger than 10,000 individuals [5]. However, pandemics involve large number of people in the range of millions. So, the development of a distributed computing solution for simulating pandemics in very large networks is a necessary challenge to be dealt with in epidemiology.

In this work we describe how we tackled the problem by using two computational systems which follow the paradigm of distributed computing that allowed us to estimate the parameters in random network epidemic models, depending on the amount of tasks to be carried out: one of them, Sisifo, designed by us to work in intranets, is simpler, uses less resources and has a quicker development, implementation and deployment; the other is the well-known Berkeley Open Architecture for Network Computing (BOINC) platform [6]. The main difference among Sisifo and BOINC concerns the security issues and the possibility of widespread distributed computing in personal computers of clients connected to Internet, in the case of BOINC, in contrast with the limitation of Sisifo to a computer intranet where security issues are not so important. In particular, BOINC implements public-key encription against virus attack which we did not considered in Sisifo.

In this note we will discuss briefly both distributed computing systems (Sisifo and BOINC) as well as a simple example of the computational capabilities of these systems in the study of emergent behaviour in epidemic propagation in random networks with one million nodes.

2 The Sisifo distributed-computing system

Sisifo was our first proposal [7] for a distributed computing system, quite simpler than BOINC, requiring less resources and providing a significantly quicker development, implementation and deployment. Although our first objective is to use Sisifo to estimate parameters in epidemic models, of course it can also be used to solve other kind of problems if they match the requirements for distributed computing. Taking into account that we have previous experience in the developing of client/server systems with centralized databases and TCP/IP communication [8], we have used that background to build Sisifo.

To implement the Sisifo system we need the following strategy: the problem we want to solve (for instance, simulation of the propagation of an epidemic in different conditions) should be divided into independent tasks, in the sense that they can be computed in a client separately from the others. Tasks are coded in text files and they indicate all necessary data to start the running of a simulation once received by the clients.

Each client computer has a Sisifo client installed which requests tasks to the server. The server provides to the client a package containing the solver (the computer program which runs the simulation) and the task to be solved. The task is then marked as pending by the server. Once the client has received the package, it runs the solver with the data provided by the task and waits for the solver to finish. Then, the client takes the obtained results and transmits them back to the server. The results are received by the server, stored and the related task is marked as done. Then, the client requests a new task and the cycle starts again until all tasks have been solved.

3 A BOINC project for distributed computation in epidemiological networks

Although the first experiment with Sisifo gave us satisfactory results in a very short period of time, during the computations a lot of tasks were unsuccessful because with our first set of tasks, the total number of infected became zero and therefore, nobody could be infected. We needed a deeper search into the solution space to find what parameters were able to produce a network where the disease did not die out. This required processing a much higher number of tasks, but the intranet where Sisifo was running had not enough power to cope with all computations in a reasonable time and we wondered if we could boost this.

For this reason we decided to try out BOINC. BOINC is an open source software actively maintained and used by the scientific community to manage projects of distributed computing as the above mentioned SETI@home [9, 10], ROSETA [11] or Climate Prediction [12]. BOINC protects against several types of attacks and the distribution of viruses using digital signatures based on public-key encryption, its server architecture is highly scalable and the core client is available for most common platforms. These are some of its main features that assure the correct transmission and reception of the task

results [13].

To do that we requested the help of the Falua project [14, 15], an initiative supported by the CES Felipe II of Aranjuez (campus of the Universidad Complutense de Madrid) which provides ad-hoc BOINC deployment and computing power for small to medium computation problems. They adapted our solver to the BOINC platform and opened the possibility of foreign collaboration from the BOINC community.

4 An application to a SIRS epidemiological model in a random network

We have tested the distributed computing solution discussed above by using a SIRS [16] (Susceptible-Infected-Recovered-Susceptible) epidemiological model in a random network. Our objective is to fit data for the hospitalization of children with Respiratory Syncytial Virus (RSV) in the Autonomous Region of Valencia (Spain) [17]. The solver implementation for RSV in order to estimate the parameters b (transmission rate) and k (average node degree), has taken ten weeks. Then, we prepared 60 120 tasks for

- a million nodes, divided into age groups following a Foster-McKendrick constant demographic model as described in Ref. [17]. In this model individuals within the same year of age constitute an age-group,
- each node is labelled by age and state respect to RSV,
- a Poisson nodes distribution with mean $k = 5, 6, \ldots, 124$,
- a transmission rate b from 0 to 1/200 with steps of 10^{-5},
- an average time of infection of 10 days,
- an average time of immunity after the infection of 200 days according to Weber el at. [18],
- an initial situation where all the population is susceptible, but for 1% of infected.

The fitting is depicted in Figure 1. Notice that the parameter s, the fraction of infected children under one year old, which become hospitalised

as a consequence of RSV infection is also a fitting parameter. We considered a fraction s of the children aged one year old or less and compared with the real data to find the optimum result. We found a best fit for $s = 4.979$ (4.979% of the weekly infected children under one year old are hospitalized)

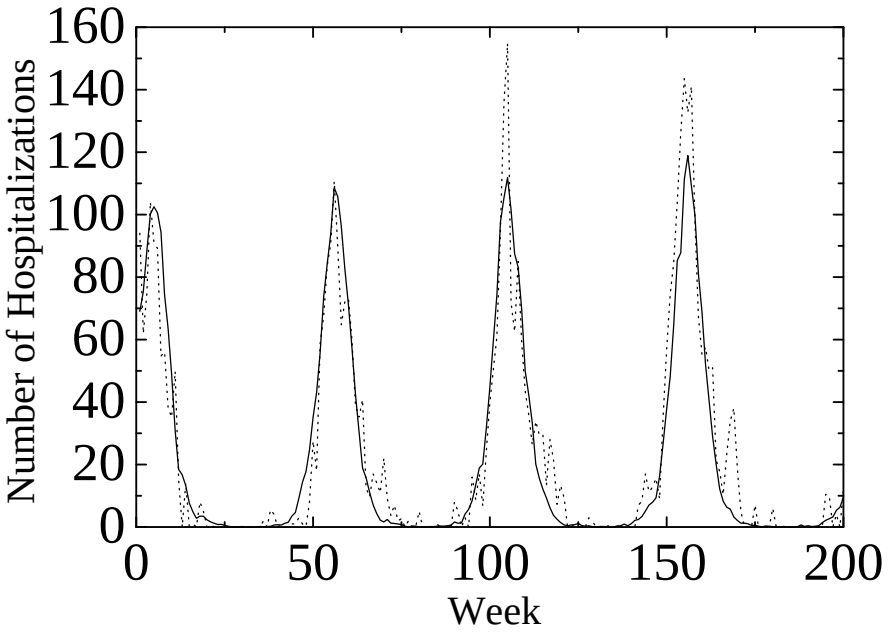

Figure 1: The number of hospitalisations of children under 1 year of age in the Spanish region of Valencia: real data (dotted line) and fitting corresponding to the random network model (solid line). The period of time goes from January 2001 to December 2004.

The interesting fact about the results depicted in Fig. 1 is that the oscillatory behaviour was obtained without resorting to external forcing as usually considered in continuous models [17, 18].

5 Conclusions

We have discussed two computing distributed techniques in order to accelerate the simulation of epidemic models in very large random networks. The

first one is an Intranet solution (Sisifo) which is simpler to implement and operate while the second one is based on the BOINC software and has the advantage of being distributed throughout the whole Internet with the help of volunteers.

By using this distributed architecture we have been able to tackle the problem of double statistical average in networks: We consider a set of different random networks characterized by the connectivity, k, and for each of them a simulation of the propagation of the epidemic is performed. Then, an average over the propagation of the disease in a random network with a given k can be given. This is a fundamental statistical problem in many models arisen in Statistical Physics and our solution provides an efficient way to implement a computational solution even for very large systems. In order to test its efficiency we have considered epidemic propagation in random networks as an example.

The tools developed in this work could be applied to a variety of situations ranging from infectious diseases epidemics to social models of contagion of habits such as tobacco or drug addiction [5].

References

[1] W. O. Kermack, A. G. McKendrick, Contributions to the mathematical theory of epidemics - Part I, Proc. Roy. Soc. 115 (1927), pp. 33–55.

[2] L. Edelstein-Keshet, Mathematical models in Biology, SIAM, 2005.

[3] J. D. Murray, Mathematical Biology: I. An Introduction, Springer-Verlag, Berlin, 2002.

[4] H. W. Hethcote, The mathematics of infectious diseases, SIAM Rev. 42 (2000), pp. 599–653.

[5] N. A. Christakis, J. H. Fowler, The collective dynamics of smoking in a large social network, New England Journal of Medicine 358 (21) (2008), pp. 2249–2258. doi:10.1056/NEJMsa0706154.

[6] http://boinc.berkeley.edu/, BOINC, open-source software for volunteer computing and grid computing, [cited March 2nd, 2011].

[7] For further details and to download Sísifo software under request visit: http://sisifo.imm.upv.es

[8] J. Villanueva-Oller, R. Villanueva, S. Díez, CASANDRA: A prototype implementation of a system of network progressive transmission of medical digital images, Computer Methods and Programs in Biomedicine 85 (2) (2007), pp. 152 – 164. doi:10.1016/j.cmpb.2006.10.002.

[9] E. Korpela, D. Werthimer, D. Anderson, J. Cobb, M. Leboisky, Seti@home-massively distributed computing for SETI, Computing in Science & Engineering 3 (1) (2001), pp. 78 – 83. doi:10.1109/5992.895191.

[10] SETI@home [cited March 2nd, 2011]. http://setiathome.berkeley.edu

[11] ROSETTA@home [cited March 2nd, 2011]. http://boinc.bakerlab.org/

[12] Climate prediction [cited March 2nd, 2011]. http://climateprediction.net/

[13] The Respiratory Syncytial Virus BOINC project webpage: http://falua.cesfelipesegundo.com/VRS

[14] D. Martín, J. Villanueva-Oller, I. Hidalgo, M. Alberquilla, I. Contreras, Anales de Ingeniería Técnica Informática de Sistemas 3, CES Felipe II, 2010, Ch. Superordenadores virtuales y computación distribuida con BOINC (Virtual supercomputers and distributed computing with BOINC).

[15] J. Villanueva-Oller, D. Martín, I. Hidalgo, M. Alberquilla, I. Contreras, El proyecto Falúa: computación distribuida mediante BOINC en el campus de Aranjuez de la UCM (Falúa project: distributed computing using BOINC in the Aranjuez campus of UCM), in: CEDI2010 (Ed.), Congreso Español de Informática 2010 - XXI Jornadas de Paralelismo, Valencia (Spain), September 8th-12th, 2010.

[16] W. O. Kermack, A. G. McKendrick, Contributions to the mathematical theory of epidemics - Part I, Proc. Roy. Soc. 115 (1927), pp. 33–55.

[17] L. Acedo, J. Díez-Domingo, J. A. Moraño, R. J. Villanueva, Mathematical modelling of respiratory syncytial virus (RSV): vaccination strategies and budget applications, Epidemiology and Infection 138 (2010), pp. 853–860. doi:10.1017/S0950268809991373.

[18] A. Weber, M. Weber, P. Milligan, Modeling epidemics caused by respiratory syncytial virus (RSV), Mathematical Biosciences 172 (2) (2001) pp. 95 – 113. doi:10.1016/S0025-5564(01)00066-9.

How long will the two-party system last in Spain?

E. De la Poza[‡] [*], A. Pricop[‡], M. Alkasadi[†], L. Jódar[†]

(†)Instituto Universitario de Matemática Multidisciplinar,

(‡)Facultad de Administración y Dirección de Empresas,

Universitat Politècnica de València,

(†) (‡)Universitat Politècnica de València,Camino de Vera s/n. 46022,

Valencia, Spain.

1 Introduction

The depth and length of the European economic crisis with high levels of unemployment (mainly youth), public debt, increasing taxation and welfare deterioration combined with a lack of solutions by Government parties as well as the so called "cartelization" of the political parties are producing the emergence of political offers breaking the limits of traditional European trends. Thus, the populist and extremist political offers are not infrequent at the present times [1] and the Government parties are losing their power by each election period since 2008.

In this research we propose a population discrete mathematical model represented by a system of difference equations [2][3] to forecast in the short-term horizon 2015 the electoral support of establishment and extremist parties as well as the level of abstention and blank voters. In fact the present situation in Spain is very special due to the combination of the economic and institutional crisis [4, 5, 6, 7].

The Spanish vote election population was divided into three subpopulations:

[*]e-mail:elpopla@esp.upv.es

the extremist voters (EX) defined as followers of any of these three alternatives: breakers of the constitutional order (separatists), breakers of the capitalist system or disrespectful of the human rights (racists of gender, race, minorities.....); the second subpopulation is composed by the abstention's (AB),those potential electors who do not vote or plan to vote [8] and finally the establishment voters (ES) composed by those citizens planning to vote a non-extremist party that also achieved representation on the Spanish parliament for at least the last three national elections.
Initial data was taken from the last three Spanish general elections(2004, 2008, 2011), in order to know the initial level of each subpopulation.
The paper is organized as follows: Section2, deals with mathematical model construction with an explicit computation of the subpopulations coefficients transits. Results and simulations are included in section 3. Section 4, shows the robustness of the model throughout changes in the Government labor indicator (GLI) and also the political trust indicator. Finally, conclusions and recommendations section is included.

2 Mathematical model

The target population is composed by the Spanish citizens older than 18 years old. Through a discrete dynamic epidemiological model quarterly forecasted is estimated the citizenship vote intention of the Spanish national elections from January 2012 until January 2016.

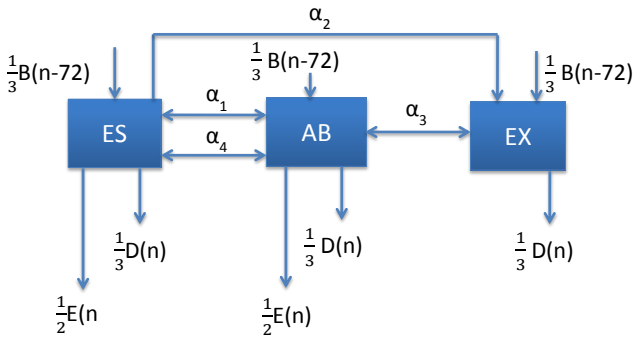

Figure 1: Block diagram showing the transits between the three subpopulations.

Our starting hypothesis is that subpopulations change dynamically and these variations depend mainly of demographic factors: emigration-E(n), birth - B(n) and death rate -D(n), economic ones: unemployment rate $-\alpha_1$, poverty indicator $-\alpha_3$, sociological trends such as Government $-\alpha_4$ and political trust indicators $-\alpha_2$. The transit between subpopulations (ES, AB, EX) is modeled by dynamic coefficients built on data provided by direct sources of information such as [9, 10, 11, 12, 13] combined with our hypotheses and analysis.

The dynamic of population can be described by the following equations:

$$\left.\begin{aligned} ES(n) = ES(n-1) - \alpha_1(n)ES(n-1) - \alpha_4(n)ES(n-1) - \\ \alpha_2(n)ES(n-1) + \frac{1}{3}B(n-72) - \frac{1}{3}D(n) - \frac{1}{2}E, \\ AB(n) = AB(n-1) + \alpha_1(n)ES(n-1) + \alpha_4(n)ES(n-1) - \\ \alpha_3(n)AB(n-1) + \frac{1}{3}B(n-72) - \frac{1}{3}D(n) - \frac{1}{2}E, \\ EX(n) = EX(n-1) + \alpha_2(n)ES(n-1) + \alpha_3(n)AB(n-1) + \\ \frac{1}{3}B(n-72) - \frac{1}{3}D(n). \end{aligned}\right\} \quad (1)$$

It is preceded with the explanation of all parameters:

B $(n-72)$: as the number of children born at $n-72$ quarters (18 years ago) that it was distributed equally between the subpopulations - people that can vote by law [9].

D (n): as the number of persons who passed away at n quarter of year distributed equally between the three subpopulations [9].

E : as the number of emigrants at n quarter distributed equally between ES and AB that remains constant during all period 18.750 (around 150.000 people per year)[9].

$\alpha_1(n)$: is the unemployment economic transit effect between quarter n and $n-1$ from ES to AB or vice versa. It is defined as :

$$\alpha_{e1}(n) = \begin{cases} 0.01 \times (\gamma(n) - \gamma(n-1) & , when \quad \gamma(n) \neq \gamma(n-1), \\ 0.01 & , when \quad \gamma(n) = \gamma(n-1). \end{cases} \tag{2}$$

where $\gamma(n)$: is the unemployment rate at quarter n [11, 12, 13].

$\alpha_2(n)$: is the lack of political trust transit from ES to AB defined as $C \times (\beta(n) - \beta(n-1)$, where C (sociological constant) $= 0,00299$ and $\beta(n)$ = CIS political trust indicator [10].

$\alpha_3(n)$: is the rate of radicalization due to Spanish poverty indicator transit from AB to EX constant to 0.5% [14].

$\alpha_4(n)$: is the coefficient transit form ES to AB of disappointed established voters defined as $D \times (f(n-1) - f(n)$, where D is the proportion of susceptible ES voters that can change their vote(32.9%) and $f(n)$ is the CIS Government labor indicator(%)[10].

3 Results and forecast

The mathematical model allows us to compute the subpopulations ES(n), AB(n) and EX(n) at a quarter of year n. As a result we simulate two possible scenarios according to the annual levels of unemployment and political trust. It was used data from [10, 11, 12, 13]and also our own estimations for year 2016.
Table 1: indicates our findings in term of Spanish citizens vote support for the following quarters of year:

Table 1: Forecasted subpopulations by quarters.

Quarter	ES		AB		EX	
	Op	**Pe**	**Op**	**Pe**	**Op**	**Pe**
Jan-12	19,238,081	19,238,081	11,764,115	11,764,115	3,975,684	3,975,684
Apr-2012	19,191,070	19,191,070	11,418,760	11,418,760	4,328,902	4,328,902
Jul-12	18,575,355	18,575,355	11,678,532	11,678,532	4,645,003	4,645,003
Oct-12	17,768,050	17,768,050	12,103,273	12,103,273	4,987,024	4,987,024
Jan 2013	17,805,227	17,623,338	12,005,133	12,026,023	4,956,742	5,117,742
Apr-13	17,595,761	17,489,724	11,993,195	12,023,580	5,122,528	5,198,179
Jul-13	17,423,610	17,320,809	12,020,360	12,055,407	5,210,029	5,277,783
Oct-13	17,361,189	17,248,098	11,936,752	11,989,883	5,296,712	5,356,672
Jan -14	17,298,280	17,174,964	11,852,936	11,923,981	5,382,237	5,434,508
Apr-14	17,248,253	17,119,914	11,778,890	11,841,857	5,447,243	5,512,615
Jul-14	17,199,008	17,065,668	11,705,893	11,760,845	5,512,554	5,590,941
Oct-14	17,150,543	17,012,227	11,633,942	11,680,938	5,578,174	5,669,494
Jan -15	17,102,858	16,959,588	11,563,031	11,602,133	5,644,111	5,748,279
Apr-15	17,069,824	16,783,681	11,483,534	11,659,030	5,702,907	5,813,555
Jul-15	17,036,449	16,608,988	11,404,072	11,713,840	5,760,934	5,878,626
Oct-15	17,002,733	16,435,501	11,373,139	11,766,587	5,769,698	5,943,482
Jan -16	16,968,678	16,263,210	11,341,868	11,817,290	5,778,069	6,008,115

Op: Scenario Optimistic; **Pe**: Scenario Pessimistic

As it is shown, at the end of the period of study, January 2016, the expected electoral support of ES parties achieves the 47.71% in the pessimistic case while in the optimistic one the ES electoral support amounts the 49.78%. With respect to the extremist support (EX) for the optimistic scenario is 16.95% and 17.62% for the pessimistic one. Finally with respect to the abstentions (AB) the 33.27% in the optimistic scenario while 34.67% in the

pessimistic one.

4 Robustness of the model

Regarding the uncertainty of the labor indicator of the Government it was studied what happens if this coefficient changes (diminish to -0.5 and increase to 0.25) and contrast the results. There were no important differences revealed between the three subpopulations.

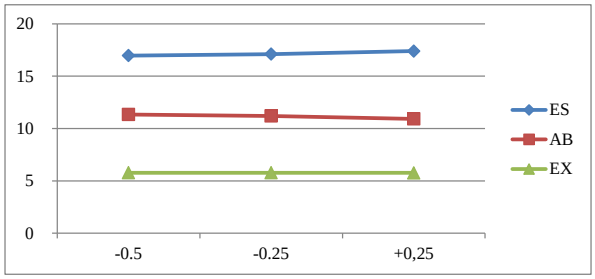

Figure 2: Sensitivity analysis of trust on the GLI (Millions of predicted voters).

The coefficient that explains the transit from ES to EX due to the political trust is built by the expression $\alpha_2(n) = C(\beta(n) - \beta(n-1))$, where $\beta(n)$ is the value of the political trust indicator at quarter n and C is a sociological constant that is adjusted taking into account the electoral data of the last three Spanish general elections. As a result C was estimated in the value interval $[1/2C, 3/2C]$, what allow us to compute the subpopulations results at 2016, (see Figure 4).

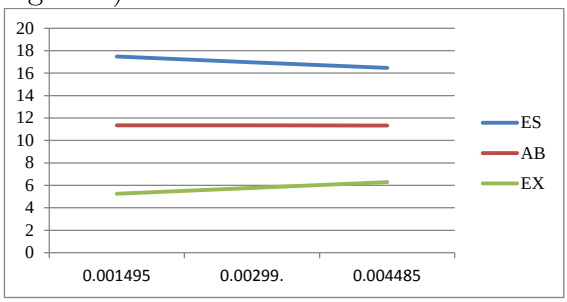

Figure 3: Sensitivity analysis of the political trust indicator, (Millions of predicted voters).

The results for both sensitivity analysis confirm the robustness of our model.

5 Conclusions and recommendations

The model predicts that the support of abstentions and blank voters, i.e. the subpopulation AB remains approximately constant since the last election November 2011 until the expected time (if general elections are not held in advance) in spite of the reduction of the electoral register about 800,000 Spanish citizens coming who emigrate looking for a job (we assume they do not vote).
On the other hand, the predicted electoral support of the two main parties (PP and PSOE) scarcely will achieve the 40% in the next general elections while in the previous general elections got a support of 49% of the register. This scenario includes an important increase of minor ES parties like UPyD, Ciutadants. This situation is combined with a highly important growth of support of extremist parties, moving from 11% to 17.5% that in absolute terms means to be an increase of more than 2 million of supporters.
The previous results imply that probably is not going to be possible to get sufficient electoral support to constitute a Government without extremist parties. It looks like the only possible imagined Government coalition would involve at least three parties, including between them one extremist party.
As results of the model show, the economic crisis favors the shift of a part of ES voters to AB and from AB to EX. Thus, all type of measures addressed to improve the economic scenario of the country will help to stop this trend. Some of the measures would be: a reform of the constitution, to stabilize the political territorial Administration (against the separatist stresses), the elimination of the public financial support to labor unions and firm associations, new formulas of management for expensive public services. It is also urgent a reform of the current political parties law to improve the transparency of the political system as well as a change of the electoral law that punishes the appearance of new emergent political offers [5, 7, 15].

References

[1] T. Pauwels. The populist voter, Phd thesis, Universit Libre de Bruxelles, 2012.

[2] E. De la Poza, N. Guadalajara, L. Jódar and P. Merello. Modeling Spanish anxiolytic consumption: Economic, demographic and behavioral influences *Mathemtical Computer Modelling,* 57(7-8):1619-1624, 2013.

[3] E. De la Poza, M. Del Líbano, I. García, L. Jódar, and P. Merello. Predicting workaholism in Spain: a discrete mathematical model *International Journal of Computer Mathematics*, http:// dx.doi.org / 10.1080/00207160.2013.783205, 2013.

[4] C. M. Reinhart, and K. Rogoff. This Time is Different: Eight centuries of financial folly, Princeton , University Press, 2009.

[5] S. Muñoz-Machado. Informe Sobre España. [*In Spanish*] , Barcelona, Critica, 2012.

[6] J. R. Rallo. Una alternativa liberal para salir de la crisis. [*In Spanish*], Barcelona, Deusto, 2012.

[7] A. Vidal-Quadras. Ahora, Cambio de Rumbo: Agenda urgente para recomponer España. Barcelona, Planeta, 2012.

[8] E. Anduiza, A. Bosch, Comportamiento político y electoral, [*in Spanish*], Barcelona, Planeta, 2012.

[9] Spanish Statistics Institute (INE). Available at: www.ine.es.

[10] Center for Sociological research (CIS). Available at: http://www.cis.es/cis/opencms/EN/.

[11] The Organization for Economic Co-operation and Development(OECD), France, 2013. Available at:http://www.oecd.org/eco/outlook/spaineconomicforecastsummary.htm.

[12] Cross Asset Research. Société Générale (SG), France, 2013. Available at: https://publication.sgresearch.com/en/3/0/172963/125179.html?sid=5b4256d8671034005116a674000337f9.

[13] International Monetary Fund (IMF), USA, 2013. Available at: http://www.imf.org/external/pubs/ft/scr/2013/cr1354.pdf .

[14] C. Herrero, A. Soler, A. Villar, R. Aragón, and S. Sabater. La pobreza en España y sus Comunidades Autónomas, 2006-2011. Instituto Valenciano de Investigaciones Económicas, S.A., Valencia, 2012.

[15] A. Nieto.El desgobierno de España, [*in Spanish*] , Barcelona, Ariel,2012.

Modelling Oil-Spill Detection with Swarm Drones

Fidel Aznar*, Mireia Sempere*,
Mar Pujol*, Maria José Pujol‡, and Ramón Rizo*

(*) Department of Computer Science and Artificial Intelligence.

(‡) Department of Applied Mathematics,

University of Alicante, San Vicent del Raspeig, Alicante (E-03080). Spain.

November 30, 2013

Nowadays, swarm robotics is an important research topic due to the benefits derived from its use, such as robustness, parallelism and flexibility. Unlike distributed robotic systems, swarm robotics emphasizes a large number of robots, and promotes scalability. Among the multiple [2] applications of such systems we could find exploring unstructured environments, resource monitoring or distributed sensing. Two of these applications, monitoring and perimeter/area detection of a given resource have several ecological uses. One of them is the detection and monitoring of pollutants to delimit its perimeter and area accurately.

One of the locations where such detection takes special importance is oceans. Maritime activity has been increasing gradually in recent years. Many ships carry products that can adversely affect the environment, such as oil, which can produce high levels of pollution in case of being spilled at sea. This problem is even more important if we consider that in common loading/unloading operations often occur accidents that could spill small amounts of these substances into the ocean.

In this paper we will present a distributed system which monitors, cover and surround a resource using a swarm of homogeneous low cost drones.

*Contact author mail: fidel@dccia.ua.es. This work has been supported by the Spanish Ministerio de Ciencia e Innovación, project TIN2009-10581

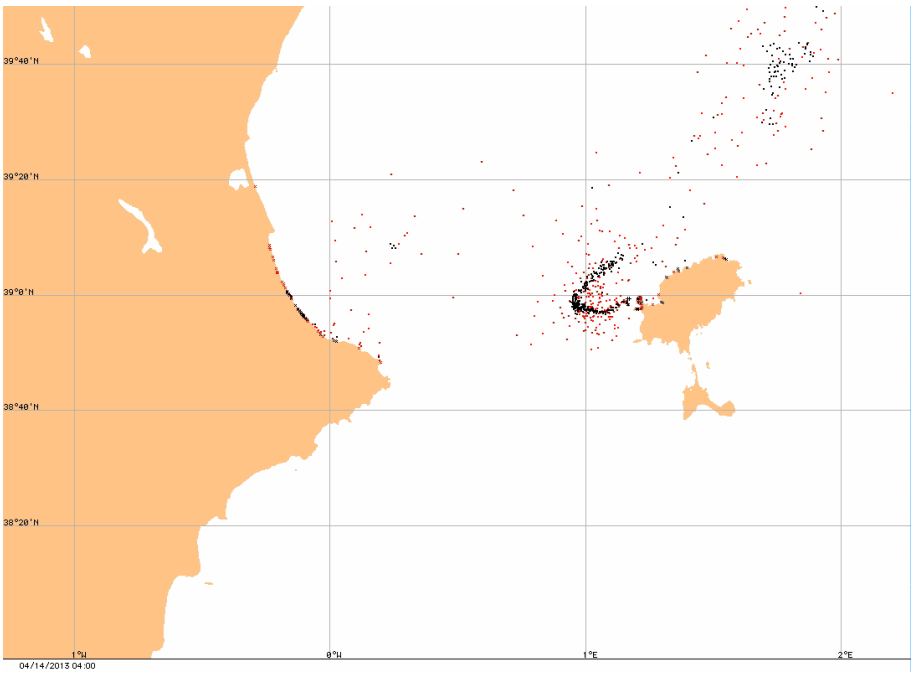

Figure 1: Oil spill simulated using GNOME model at the Spanish mediterranean coast

These drones only use its local sensory information and will not require any direct communication between them.

More specifically, in this work, we will base on the model provided by the National Oceanic & Atmospheric Administration (NOAA) of the USA to model an oil spill. This model is known as GNOME [1] and allows us to use real weather maps, for both ocean and winds currents, making it possible to complete a realistic simulation of an oil spill in Spanish coasts.

Taking into account the properties of this kind of oil spills we will present a microscopic model for a swarm of drones, capable of monitoring these spills properly. Furthermore we will analyze the proper macroscopic operation of the swarm, considering for example the convergence of the agents depending on the size of the cluster, moving speed, the number of divisions or new spots generated by the main spill. The analytical and experimental results presented here showed the proper operation of our system.

1 Results

This paper describes a microscopic model that is able to locate and mark the perimeter of an oil spill. The microscopic behaviour presented does not require direct communication between agents. This limitation can cause that the convergence of the swarm on the spill take more time, depending on the number of drones and the size of the spill. However, this behaviour is versatile and easy to implement and develop, even in areas without GPS coverage. It is important to highlight that a swarm system, that requires direct communication between agents, is a limited system because of the maximum range of each agent and the saturation of the radio frequency space if the system needs a large number of agents.

Moreover, we have demonstrated that the process of locating and marking the perimeter of the spill without communication is robust and efficient. We have shown that the swarm system is able to completely delimit the spill if the number of agents is sufficient. In order to achieve this task, an agent must be able to detect drones that are nearby. There are several ways, as for example, using a camera or transmitting the GPS position.

We propose the use of signal intensity (at a given frequency) for obstacle avoidance tasks. This strategy may show some problems (we have implemented it by using a reactive behaviour), however, it has several advantages. Many countries require that drones broadcast a continuous signal indicating their position. Europe uses 433MHz frequency for this purpose. The intensity of the signal in a particular area can be detected by using the same infrastructure. If the intensity of the signal grows with the movement of the agent, this agent must change its direction. We emphasize that, as a swarm approach, this is not a communication between agents, but simply a *beacon*, that we can use, if necessary, to know the position of drones.

The proposed macroscopic model demonstrates that the tendency of the swarm, for a sufficient number of drones, is the same that can be perceived in the microscopic model. The connection of both models has been tested for a complex spill, generated with GNOME. These experiments have shown that the fundamental characteristics of the behaviour (detection and monitoring) are reflected in both models. It is advisable not to forget the differences between the two models.

The microscopic model defines the individual behaviour. Because of this it is easy to understand at local level. However, this model does not define the behaviour of all the swarm. In order to analyse the global behaviour, a

set of tests can be defined for a large number of agents. However, these tests can be expensive, difficult and are not exempt from problems.

The macroscopic model defines the global behaviour of the swarm. It allows to verify the emergent behaviour from the interaction between all agents that run the microscopic model. The macroscopic model demonstrates the tendency of the swarm for a large number of agents. The analysis of this model is complex, because of the use of differential equations that, for example, force us to choose a single point to start the simulation. Even so, this model has remarkable advantages: continuous analysis for any point of the environment, time of the probability that an agent is located in a given location, simulation time negligible compared to microscopic model...

We are currently working on the implementation of this system in a real swarm of drones. Our immediate future research focuses on this real swarm, since it allows us to adjust the algorithms for a real system. We are already in the testing phase for small swarms (5 drones), obtaining satisfactory results in our preliminary tests.

References

[1] Zelenke, B., C. O'Connor, C. Barker, C.J. Beegle-Krause, and L. Eclipse (Eds.). 2012. *General NOAA Operational Modeling Environment (GNOME) Technical Documentation.* U.S. Dept. of Commerce, NOAA Technical Memorandum NOS OR&R 40. Seattle, WA: Emergency Response Division, NOAA. 105 pp.

[2] Alessandro Farinelli and Ro Farinelli and Luca Iocchi and Daniele Nardi. 2004. *Multi-Robot Systems: A classification focused on coordination.* IEEE Trans. Syst., Man, Cybern. B (34), 2015–2028.

The Operation of Infimal/Supremal Convolution in Mathematical Economics

L. Bayón* ⁎, P.J. García Nieto*, R. García-Rubio†
J.M. Grau*, M.M. Ruiz* and P.M. Suárez*

(*) University of Oviedo, Department of Mathematics, Spain

(†) University of Salamanca, Department of Economy, Spain

November 30, 2013

1 Introduction

The infimal convolution (IC) operation is a fundamental fact in discrete convex analysis that is often usefully applied in mathematical economics. A excellent review of the literature on IC within the context of optimal risk exchange and optimal allocation problems can be found in [1]. In two previous papers the authors of the present paper presented two new applications of the IC: in [2] the firm's cost-minimization (FCM) problem with the Cobb-Douglas production function, and in [3] the FCM problem with the linear production function in economies of scale.

In this paper we present a new application to demonstrate the enormous potential of this mathematical tool in the field of economics: the analytical solution of the utility maximization problem. We shall address this problem in an exact way in this paper, transforming it into the constrained supremal convolution problem of the log-concave functions. Moreover we do not solve a particular problem for a particular level of budget level ξ, but for a family of problems: all those posed when considering all the permissible levels of budget level ξ.

⁎e-mail: bayon@uniovi.es

2 The Utility Maximization Problem

In this paper we shall consider the Utility Maximization (UM) problem for the case of the utility function following the Cobb-Douglas model, $\prod_{i=1}^{m} x_i^{\alpha_i}$, and the availability of the commodities having upper constraints. In the UM problem the aim is to choose the best among all possible options subject to the budget constraint: $\sum_{i=1}^{m} p_i x_i = \xi$ and to the available amount of commodities: $0 \leq x_i \leq N_i$, such that the utility is maximized, where $\mathbf{p} = (p_1, \ldots, p_m)$ is the price vector of the different commodities, i.e.:

$$\begin{aligned} u(\mathbf{p}, \xi) &= \max \prod_{i=1}^{m} x_i^{\alpha_i} \\ \text{s.t.} \quad \sum_{i=1}^{m} p_i x_i &= \xi; \quad 0 \leq x_i \leq N_i \end{aligned} \tag{1}$$

This problem is equivalent to a new problem:

$$\begin{aligned} \widetilde{u}(\mathbf{p}, \xi) &= \max \sum_{i=1}^{m} \alpha_i \ln\left(\tfrac{y_i}{p_i}\right) \\ \text{s.t.} \quad \sum_{i=1}^{m} y_i &= \xi; \quad 0 < y_i \leq p_i N_i = M_i \end{aligned} \tag{2}$$

with $\alpha_i, p_i > 0, i = 1, ..., m$, in which only the following change in the variables needs to be taken into account: $p_i x_i = y_i$. The function $\widetilde{u}(\mathbf{p}, \cdot)$ is in fact the supremal convolution of the log-concave functions:

$$F_i(y_i) := \alpha_i \ln\left(\frac{y_i}{p_i}\right)$$

3 Solution of the Problem

In this section we shall calculate the supremal convolution for the functions $F_i(y_i)$ and then go on to prove that it belongs to the class C^1. The demonstration of the results not shown will be analogous to those developed in a previous paper [2] for exponential functions. Let C_ξ be the set:

$$C_\xi := \{(y_1, \ldots, y_m) \in (0, M_1] \times ... \times (0, M_m] \ / \ \sum_{i=1}^{m} y_i = \xi\}$$

The supremal convolution of the $\{F_i\}_{i=1}^m$is:

$$(F_1 \circledast \cdots \circledast F_m)(\xi) := \max_{C_\xi} \sum_{i=1}^{m} F_i(y_i)$$

Definition 1. Let us call the function $\Psi_i : \left(0, \sum_{j=1}^m M_j\right] \longrightarrow (-\infty, M_i]$ *the i-th distribution function,* defined by:

$$\Psi_i(\xi) = y_i, \quad \forall i = 1, \ldots, m$$

where $(y_1, \ldots, y_m)$ is the unique maximum of F on the set C_ξ, i.e.:

$$\sum_{i=1}^{m} \Psi_i(\xi) = \xi \quad \text{and} \quad \sum_{i=1}^{m} F_i(\Psi_i(\xi)) = (F_1 \circledast \cdots \circledast F_m)(\xi)$$

Theorem 1. *For every $k = 1, \ldots, m$ the k-th distribution function is*

$$\Psi_k(\xi) = \begin{cases} \dfrac{\alpha_k}{\sum_{i=1}^{m} \alpha_i} \xi & if \qquad \xi < \theta_m \\ \dfrac{\alpha_k}{\sum_{i=1}^{j-1} \alpha_i} \left[\xi - \sum_{i=j}^{m} M_i \right] & if \quad \theta_j \le \xi < \theta_{j-1} \le \theta_k \\ M_k & if \qquad \xi \ge \theta_k \end{cases}$$

with the coefficients:

$$\theta_k = \sum_{i=k}^{m} M_i + \frac{M_k}{\alpha_k} \sum_{i=1}^{k-1} \alpha_i$$

Theorem 2. *The supremal convolution of the log functions $F_i(y_i)$ is a logarithmic piecewise function:*

$$(F_1 \circledast F_2 \circledast \cdots \circledast F_m)(\xi) = \begin{cases} \widetilde{\beta}_{m+1} + \sum_{i=1}^{m} \alpha_i \ln\left(\frac{\xi}{p_i}\right) & if \qquad \xi < \theta_m \\ \widetilde{\beta}_k + \sum_{i=1}^{k-1} \alpha_i \ln\left(\xi - \sum_{i=k}^{m} M_i\right) & if \quad \theta_k \le \xi < \theta_{k-1} \end{cases}$$

with the coefficients:

$$\widetilde{\alpha}_k = \sum_{i=1}^{k} \alpha_i; \quad \widetilde{\beta}_k = \sum_{i=1}^{k-1} \alpha_i \ln\left(\frac{\alpha_i}{\widetilde{\alpha}_{k-1}}\right) + \sum_{i=k}^{m} \alpha_i \ln\left(\frac{M_i}{p_i}\right)$$

Moreover, it belongs to the class C^1.

Having calculated the function $\widetilde{u}(\mathbf{p}, \xi)$, and considering the fact that $u(\mathbf{p}, \xi) = \mathbf{e}^{\widetilde{u}(\mathbf{p},\xi)}$, the solution of problem (1) is evident.

4 Example

We shall now consider an example with $m = 20$ commodities that has also been used in [2]. Figure 1 shows the graph of the utility function, $u(\mathbf{p}, \xi)$, obtained for each budget level ξ.

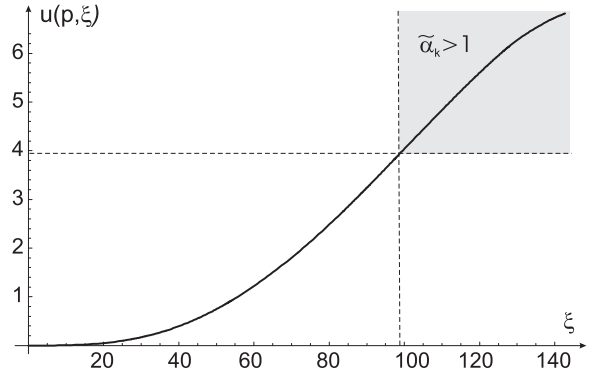

Figure 1. Utility function, $u(\mathbf{p}, \xi)$.

References

[1] D. Filipovic, M. Kupper. Monotone and cash-invariant convex functions and hulls, *Insurance: Mathematics and Economics,* 41(1):1–16, 2007.

[2] L. Bayon, J.M. Grau, M.M. Ruiz and P.M. Suarez. The explicit solution of the profit maximization problem with box-constrained inputs, *Applied Mathematics and Computation*, 217(21): 8705–8715, 2011.

[3] L. Bayon, J.A. Otero, M.M. Ruiz, P.M. Suarez and C. Tasis. The Profit Maximization Problem in Economies of Scale, *J. Comput. Appl. Math.* 236(12): 3065–3072, 2012.

Consistent completion of reciprocal matrices

J. Benítez* *, L. Carrión†, J. Izquierdo‡, and R. Pérez-García‡

(*) Instituto de Matemática Multidisciplinar,

Universidad Politécnica de Valencia, Camino de Vera s/n 46022, Valencia (Spain),

(†) Universidad Politécnica de Valencia,

Universidad Politécnica de Valencia, Camino de Vera s/n 46022, Valencia (Spain),

(‡) Fluing, Instituto de Matemática Multidisciplinar,

Universidad Politécnica de Valencia, Camino de Vera s/n 46022, Valencia (Spain).

November 30, 2013

1 Introduction and a brief approach of AHP

The so-called analytic hierarchy process (AHP) [3, 4], has been accepted as a leading multi-attribute decision-aiding model both by practitioners and academicians, since it is designed to make better choices when faced with complex decisions involving several dimensions.

In participatory making decision processes, some actors may not be completely familiar with several elements about which they have to issue their judgement. As a result, it is difficult to gather complete information about the preferences of such a stakeholder at a given moment. It seems reasonable to allow such an actor to express their preferences several times at his or her own convenience. Meanwhile, partial results based on partial preference data may be generated from data collected at various times – and this data may eventually be consolidated when the information is complete. Based on a process of linearization [1] that minimizes a matrix distance defined in terms of the Frobenius norm, in [2] the authors have initiated a line towards

*e-mail: jbenitez@mat.upv.es

a dynamic model of AHP by addressing the problem of adding new criteria or deleting obsolete criteria. The consistent completion of a reciprocal matrix as a mechanism to obtain a consistent body of opinion issued in an incomplete manner by a specific actor was addressed. This feature help stakeholders not fully problem-acquainted in their integration within participatory processes.

Here we provide a solution to this issue by solving the following problem: to characterize when an incomplete and reciprocal matrix can be completed to be a consistent matrix. We show that this characterization reduces to the solution of a linear system of equations –a straightforward procedure. Finally, by using graph theory some properties of this completion are studied.

2 Characterization of the consistent completion

The standard basis of $\mathbb{R}^n$ is denoted by $\{\mathbf{e}_1, \ldots, \mathbf{e}_n\}$. We will use the mappings $L : \mathbb{R}^+_{n,m} \to \mathbb{R}_{n,m}$ and $E : \mathbb{R}_{n,m} \to \mathbb{R}^+_{n,m}$ given by $L(A) = (\log(a_{ij}))$ and $E(A) = (\exp(a_{ij}))$, respectively, where $A = (a_{ij})$. Evidently one has that for $A \in \mathbb{R}^+_{n,n}$, A is reciprocal if and only if $L(A)$ is skew Hermitian. We define $\mathcal{L}_n = \{L(A) : A \in \mathbb{R}^+_{n,n} \text{ is consistent}\}$. From now on, we define for $1 \leq i < j \leq n$ the following skew-Hermitian matrices: $B_{ij} = \mathbf{e}_i\mathbf{e}_j^T - \mathbf{e}_j^T\mathbf{e}_i$.

THEOREM 1: *Let $1 \leq i_1, j_1, \ldots, i_k, j_k \leq n$ be indices such that $i_r < j_r$ for $r = 1, \ldots, k$. Denote $I = \{(i_1, j_1), \ldots, (i_k, j_k)\}$ and $J = N_n \setminus I$. Let $C_0 = \sum_{(i,j)\in J} \rho_{ij} B_{ij}$. The following statements are equivalent*

(i) *There exist $\lambda_1, \ldots, \lambda_k \in \mathbb{R}$ such that $C_0 + \sum_{r=1}^k \lambda_r B_{i_r j_r} \in \mathcal{L}_n$.*

(ii) *There exists $\mathbf{w} = (w_1, \ldots, w_n)^T \in \mathbb{R}^n$ such that $\rho_{pq} = w_p - w_q$ for any $(p, q) \in J$.*

Furthermore, if the case that the statements hold, then $\lambda_r = w_{i_r} - w_{j_r}$ for any $r \in \{1, \ldots, k\}$.

3 Conection with graph theory

For an $n \times n$ incomplete reciprocal matrix $A = (a_{ij})$, we use this procedure to construct a directed graph, denoted by G_A: If $i \geq j$, then there is no arrow from i to j. If $i < j$ and we do not know the entry a_{ij}, then there is no arrow

from i to j. If $i < j$ and we know the entry a_{ij}, then there is an arrow from i to j. Now, we construct the incidence matrix of G_A, denoted by M_A.

To describe the linear system that appears in item (ii) of Theorem 1, we define, for an incomplete reciprocal matrix $A \in \mathbb{R}_{n,n}$, the vector $\mathbf{b}_A = (b_1, \ldots, b_m)^T \in \mathbb{R}^m$, being m the number of columns of M_A, by the following procedure: For $r = 1, \ldots, m$, let us pay attention to the r-th column of M_A and let i, j be the unique indices such that the entry (i, r) of M_A is 1 and the entry (j, r) of M_A is -1. We set $b_r = \log(a_{ij})$.

Theorem 1 can be rephrased as follows: If A is an incomplete reciprocal matrix, then A can be completed to be a consistent matrix if and only if the system $M_A^T \mathbf{w} = \mathbf{b}_A$ is consistent.

THEOREM 2: *Let $A \in \mathbb{R}_{n,n}$ be a reciprocal incomplete matrix and $2k$ be the number of void entries. If G_A has p connected components and $2k \geq n^2 - 3n + 2p$, then A can be completed to be consistent.*

THEOREM 3: *Let $A \in \mathbb{R}_{n,n}$ be a reciprocal incomplete matrix and $2k$ be the number of void entries. If $2k < n(n-1)$, G_A is connected, and there exists a consistent completion of A, then this completion is unique.*

Let us observe that the linear system $M_A^T \mathbf{w} = \mathbf{b}_A$ is consistent if and only if $\mathbf{b}_A \in \mathcal{R}(M_A^T)$. But by standard linear algebra one has $\mathcal{R}(M_A^T) = \mathcal{N}(M_A)^\perp$. Hence we have that the linear system $M_A^T \mathbf{w} = \mathbf{b}_A$ is consistent if and only $\mathbf{b}_A^T \mathbf{x} = 0$ for any $\mathbf{x} \in \mathcal{N}(M_A)$.

THEOREM 4: *Let G be a planar oriented graph and M its incidence matrix. If $\mathbf{x}_1, \ldots, \mathbf{x}_f$ correspond to the bounded faces of the graph, then $\{\mathbf{x}_1, \ldots, \mathbf{x}_f\}$ is a basis of $\mathcal{N}(M)$.*

COROLLARY 5: *Let A be an incomplete reciprocal matrix. If G_A is planar and has no bounded faces, then there exists a consistent completion of A.*

4 A protocol to assess consistency

We provide a protocol that can be easily implemented in a decision support tool and/or followed by a facilitator in charge of a decision problem when assessing the consistency of an incomplete judgment given by a stakeholder.

Given the reciprocal incomplete matrix A, build matrix M_A and vector $\mathbf{b}_A$, and determine the solvability of $M_A^T \mathbf{w} = \mathbf{b}_A$ (Theorem 1):

(a) Solvable: A can be consistently completed, and Theorem 1 gives the possible completions.

(b) Unsolvable: A cannot be consistently completed. In this case, by using least squares theory, the optimal solution of $M_A^T\mathbf{w} = \mathbf{b}_A$ can be used to find a completion of A that is close to be consistent.

Build the graph G_A. The main facts are:

(a) If $2k \geq n^2 3n + 2p$, then the completion is possible (Theorem 2).

(b) If $m > 0$ and $p = 1$, then the completion is unique (G_A is connected).

Calculate the Moore-Penrose inverse of matrix M_A, $M_A^\dagger$, and consider that the completion is possible if and only if $M_A^T(M_A^\dagger)^T\mathbf{b}_A = \mathbf{b}_A$. Then:

1. If the completion is unique, find the completion from $\mathbf{w} = (M_A^\dagger)^T\mathbf{b}_A$ and Theorem 1.
2. Otherwise, find the completions from $\mathbf{w} = (M_A^\dagger)^T\mathbf{b}_A + [I - (M_A^\dagger)^T M_A^T]\mathbf{y}$ for arbitrary $y \in \mathbb{R}^n$ and Theorem 1.

If G_A is planar and there are no bounded faces, then there exists a consistent completion of A. Otherwise, find the cycles of G_A. Then

1. There is a consistent completion of A if and only if $\mathbf{b}_A^T\mathbf{x} = 0$ for any $\mathbf{x} \in \mathcal{N}(M_A)$.
2. If there is not a consistent completion of A, then by forcing $\mathbf{b}_A^T\mathbf{x} = 0$ for any $\mathbf{x} \in \mathcal{N}(M_A)$, we can modify A to get a possible completion.

References

[1] Benítez J., Delgado-Galván X., Izquierdo J., Pérez-García R., Achieving matrix consistency in AHP through linearization, *Appl. Math. Modelling* 35: 4449–4457, 2011.

[2] Benítez J., Delgado-Galván X., Izquierdo J., Pérez-García R., An approach to AHP decision in a dynamic context, *Decision Support Systems* 53: 499–506, 2012.

[3] Saaty T.L., A scaling method for priorities in hierarchical structures, *J. of Math. Psychol.*, 15: 234–281, 1977.

[4] Saaty T.L., The Analytic Network Process. Pittsburgh, RWS Pub, 2001.

Dynamic Prediction of Failures. A Comparison of Methodologies for a Wind Turbine

S. Carlos[†] [*], A. Sánchez[‡] I. Martón[†], S. Martorell[†]

([†]) Departament d'Enginyeria Química i Nuclear.

([‡]) Departament d'Estadística i Investigació Operativa Aplicades i Qualitat

Universitat Politècnica de València.

November 26, 2013

1 Introduction

Energy production systems are becoming increasingly complex and require new methods to diagnose and anticipate unexpected failures in order to avoid revenue losses. Nowadays, Condition Based Maintenance (CMB) is becoming more demanded to plan the maintenance activities. CBM is based on collecting information about the equipment working condition, related to the system degradation, to prevent its failure and to determine the optimal maintenance. So, to plan an efficient CBM strategy it is necessary to perform a prognosis on the degradation level. The prognosis methods can be classified as: model-based and data-driven methods. Data-driven methods make use of available monitored data to train learning algorithms to forecast the equipment failures [1]. In this work, principal components analysis (PCA) combined with partial least squares (PLS) and dynamic neural networks are used to detect the failure of a Spanish commercial wind turbine farm.

[*]e-mail: scarlos@iqn.upv.es

2 Principal components-Partial least squares

PCA is based on a linear transformation that produces new uncorrelated variables, named components, from the original correlated measured variables [1]. The projection of X down on a subspace by means of the projection matrix, P', gives the object coordinates in the plane, T, and E are the residuals. In matrix form, PCA is expressed as:

$$X = TP' + E. \tag{1}$$

PLS is a PCA extension which uses the measured data, X, to predict changes in the output variables, Y [2], which is also decomposed as:

$$Y = UC' + F, \tag{2}$$

where U and C are the scores and loading matrices of Y, respectively, and F is the residual matrix. U, has a relationship with the score matrix of X, T, which can be represented as:

$$U = TB + R, \tag{3}$$

where B and R are the regression coefficients and the residual matrices, respectively. Here the PLS model is computed using the Non-linear Iterative Partial Least Squares (NIPALS) algorithm [2].

3 Dynamic Neural networks

A common linear dynamic model is the ARX [3]. The ARX response can be expressed as:

$$\begin{aligned} y(t) &= q^{-d}\left(b_0 u(t) + b_1 u(t-1) + \cdots + b_m u(t-m)\right) \\ &- a_1 y(t-1) - a_2 y(t-2) - \cdots - a_n y(t-n) + e(t), \end{aligned}$$

which depends on the response on previous time steps and the input in m time steps. A similar structure can be implemented using Neural Networks [3][4]. The resulting dynamic model is called NARX.

4 Case of application

The objective of this study is focused on detecting the failures in the gearbox of a wind turbine following the gearbox oil temperature, T_{oil}, provided by SCADA system [5],[6]. To reconstruct T_{oil} at time t the input variables used are wind velocity at t and $(t-1)$ and T_{oil} at $(t-1)$ and $(t-2)$. PCA provides three principal components, so the predicted value of T_{oil} is given by:

$$\hat{Toil}(t) = K_1 T1(t) + K_2 T2(t) + K_3 T3(t)$$

where K_1, K_2, K_3 are constants determined by the PLS method and $T1$, $T2$ and $T3$ are the principal components. The model has been obtained with data of a non failed wind turbine and used to reconstruct the failed behaviour. As shown in Figure 1, a good prediction is obtained for normal behaviour reconstruction, but for the failed wind turbine the error between data and predicted values is larger, what is needed to set an alarm. In fact, as the difference is observed only at the final time steps it makes difficult to establish an alarm based on these data.

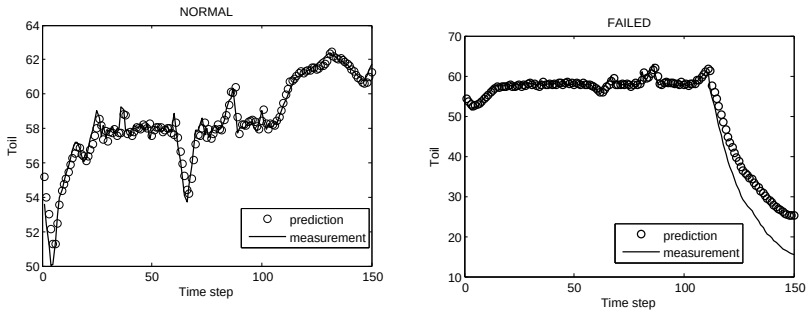

Figure 1: PLS reconstruction

It is considered a NARX model based on an three layered multilayer perceptron using as input data wind velocity measurements at time t and $(t-1)$ and gearbox oil temperature at $(t-1)$ and $(t-2)$. Thus, T_{oil} prediction is given by

$$\hat{Toil}(t) = f(v(t), v(t-1), Toil(t-1), Toil(t-2)),$$

where the $f()$, is approximated by the multilayer perceptron. As shown in Figure 2, normal behaviour prediction is quite good, and for the failed wind

turbine the error is larger what is necessary to detect the failure and set an alarm. When comparing PCA-PLS and NARX models, it is observed that failure is earlier detected by the NARX, see Figure 1 and Figure 2, what is an advantage for practical use, as the repairing task can be launched earlier and the time until wind turbine operation is reduced.

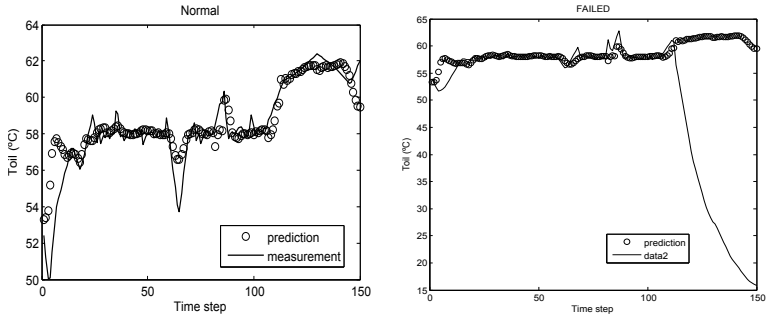

Figure 2: NARX model reconstruction

5 Conclusions

SCADA data are available in wind farms and can be used to perform CBM to improve maintenance planning. PCA-PLS detects the failure but the physical meaning of the dominant principal components may be lost. The NARX model constructed provides good results to set the alarms as the failure is detected just when it is produced while PCA-PLS technique presents a delay in detecting the failure.

References

[1] Wold S.; Esbensen K.; Geladi P. *Chemometrics Intell. Lab. Syst.* 1987, 2, 37-52.

[2] Geladi P.; Kowalsky R.B.; *Anal. Chim. Acta.* 1986, 185, 1-17.

[3] Ljung L.; T. Glad. *Modelling of Dynamic Systems*; Information and Systems Science series; Prentice Hall: Englewwod Cliffs, NJ, 1994.

[4] Norgaard M.; Ravn O.; Poulsen N.K.; Handsen L.K. *Neural Networks for modelling and control of dynamic systems: A practitioner's handbook*; Springer: London, UK, 2000.

[5] Garcia M.C.; Sanz-Bobi M.A.; Del Pico J. *Comput. Ind.* 2006, 57, 552-568.

[6] Yang W.; Court R.; Jiang J.; *Renew. Energy* 2013, 53, 365-376.

Mathematical modeling of advertising using fractional order derivatives

Benito Chen-Charpentier* ,*
Gilberto González-Parra†,
and Abraham J. Arenas‡

(*) University of Texas at Arlington,

Department of Mathematics, UTA, TX 76019, USA.

(†) Universidad de los Andes,

Grupo de Matemática Multidisciplinar, Fac. de Ingeniería, Mérida, Venezuela.

(‡)Universidad de Córdoba,

Departamento de Matemáticas y Estadística, Colombia.

September 30, 2013

1 Introduction

Advertising is a common communication form that can be used to induce consumers to take some actions with respect to products or services [**?**, **?**]. There are many ways to attempt to change consumer behavior such as advertising messages using mass media such as newspapers, magazines, television and radio. Advertising tries to convince consumers to buy a certain product by first creating a need for the product in general and then by creating a differentiation among products to get consumers to buy a particular brand [**?**, **?**]. The study of advertising strategies is important in order to boost the sales and improve the firm's profit. Thus, it is important to construct an appropriate dynamic advertising model to characterize the time-dependent sales which depend on consumer population.

*e-mail:bmchen@uta.edu

Generally, the differential form models consider that the change of a state variable depends instantaneously on the values of the states variables. However, in many cases the changes do not depend on the actual values of the state variables exclusively. Instead they may depend on the value of the states variables at different previous times. Thus, we present here a advertising fractional order model to include the effect of previous values of the state variables. This model is studied in order to understand in a better way the effect of two different type of advertising on the population dynamics. This model is based on a diffusion process and the advertising is divided on increasing awareness and changing predisposition to buy. For simplicity these types will be denoted here as awareness and trial advertising [**?**].

For certain applications the use of fractional derivatives is justified since they provide a better model than integer order derivative models do since they provide a powerful instrument for incorporation of memory and hereditary properties of the systems as opposed to the integer order models, where such effects are neglected or difficult to incorporate. The memory effect is due to the fact that fractional derivatives are non-local. The next state of a fractional system depends not only upon its current state but also upon all of its historical states. In order to deal with fractional derivatives we rely on the Caputo operator and on an accurate predictor-corrector to numerically approximate the fractional derivatives [**?**].

2 Financial fractional differential model

Here we present the definition of fractional derivatives in the sense of Caputo. Suppose that the function $y(\tau)$ satisfies some smoothness conditions in every finite interval $(0, t)$ with $t \leq T$. Then the Caputo definition for fractional derivative is given by:

$$ {}_0^C D_t^\alpha y(t) := \frac{1}{\Gamma(m-\alpha)} \int_0^t (t-\tau)^{-\alpha-1+m} \frac{d^m}{d\tau^m} y(\tau) d\tau \quad m-1 < \alpha < m, \quad (1) $$

where α is the order of the derivative and the initial conditions given by,

$$ y^{(\nu-1)}(0) = b_\nu, \qquad m-1 < \alpha < m, \;\; \nu = 1, 2, ..., m. \qquad (2) $$

The advertising model deals with an introduction of a new product in a market with size population $N(t)$. The population is divided in three

categories, $x(t)$ the number of individuals unaware of the existence of the product, $y(t)$ the number who know about the product but have not yet purchased it, and $z(t)$ the number of people who have purchased the product. It follows that $x(t) + y(t) + z(t) = N(t)$.

In regard to advertising, it has been proposed that it can be broken down to its two components: (1) awareness (denoted by u) which informs consumers about the product and thus transfers them from the unaware group $x(t)$ into the potential group $y(t)$, and (2) trial advertising (denoted by ν) which persuades consumers to purchase the product and transfers them from the potential consumers group $y(t)$ into the current customers group $z(t)$ [**?**]. The flows of consumers in the advertising fractional order model can be represented analytically using the first-order Caputo derivatives of order α by the following nonlinear system,

$$\begin{aligned}
{}_0^C D_t^\alpha x(t) =& - u^\alpha x(t) - k^\alpha x(t)(N(t) - x(t))/N(t), \\
{}_0^C D_t^\alpha y(t) =& u^\alpha x(t) + k^\alpha x(t)(N(t) - x(t))/N(t) - (a^\alpha + \nu^\alpha) y(t) + \delta^\alpha z(t), \\
{}_0^C D_t^\alpha z(t) =& (a^\alpha + \nu^\alpha) y(t) - \delta^\alpha z(t),
\end{aligned} \tag{3}$$

where k is the contact rate, a is the trial (first purchase) rate, and δ is the switching rate, i.e., the rate at which current customers are purchasing rival brands.

3 Numerical simulations

We perform a numerical simulation of the integer and fractional advertising models in order to observe the effect of the memory on the advertising process. We simulate several years in order to observe transient and steady states. In Figure 1, it can be observed the dynamics of the unaware $x(t)$ and the potential $y(t)$ populations. It can be seen that the changes of the populations in the advertising fractional order model are slower in comparison to the integer model due to the memory effect (it is easier to maintain the status quo). The simulation of this scenario is performed using a total population of $N = 1000$, awareness rate $u = 0.01$, advertising trial rate $\nu = 0.05$, effective contact rate between unaware and aware subpopulations $k = 0.01$, first purchase rate $a = 0.02$ and a switching rate $\delta = 0.2$. Initial conditions are assumed to simulate the introduction of a new product, i.e.

$x(0) = N, y(0) = 0$ and $z(0) = 0$. The parameter α affects the speed of the dynamics and therefore how fast the people changes form one group to another due to the advertising effect.

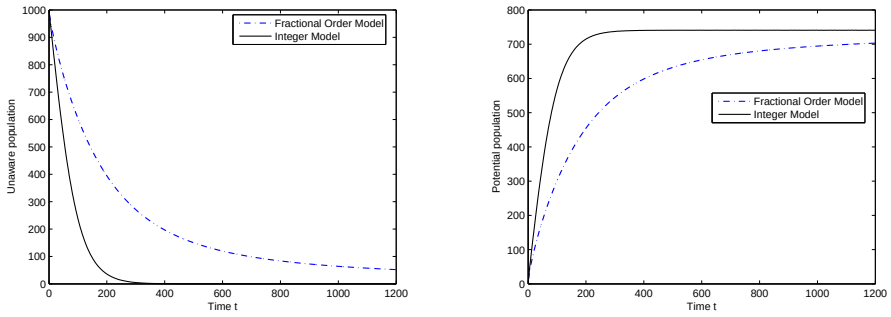

Figure 1: Numerical solution of the solution of the advertising integer and fractional order models using predictor-corrector method with a time step size $\Delta t = 0.01$ and a fractional order $\alpha = 0.7$.

It can be concluded that fractional models have the potential to describe more complex dynamics than the integer models and can include easily the memory effect present in many real world phenomena. Thus, new models using fractional models for advertising are promising because they implicitly include memory which is important in persuading a population to continue or take some new action. This is also true in political and ideological advertising.

Derivative-free iterative methods for determining orbits of artificial satellites*

Carlos Andreu, Noelia Cambil, Alicia Cordero, and Juan R. Torregrosa

Instituto de Matemáticas Multidisciplinar,

Universitat Politècnica de València,

caranesandreu@gmail.com, nctnoelia@gmail.com, acordero@mat.upv.es, jrtorre@mat.upv.es

November 30, 2013

1 Introduction

Many applied problems in different fields of science and technology require to find the solution of a nonlinear equation $f(x) = 0$, where $f : I \subset \mathbb{R} \to \mathbb{R}$ is a scalar function on an open interval I: in particular, the numerical solution of nonlinear equations and systems are needed in the study of dynamical models of chemical reactors [1], or in radioactive transfer [2]. Moreover, many of numerical applications use high precision in their computations; in [3], high-precision calculations are used to solve interpolation problems in Astronomy; in [4] the authors describe the use of arbitrary precision computations to improve the results obtained in climate simulations; the results of these numerical experiments show that the high order methods associated with a multiprecision arithmetic floating point are very useful, because it yields a clear reduction in iterations.

Throughout this paper we consider multipoint iterative methods to find a simple root ξ of a nonlinear equation $f(x) = 0$, where $f : I \subseteq \mathbb{R} \to \mathbb{R}$ for an open interval I. Newton's method is probably the most widely used iterative scheme. Many modified schemes of Newton's method have been proposed to improve the local order of convergence and the efficiency index over the last years. The efficiency index, introduced by Ostrowski in [5] as $I = p^{1/d}$, where p is the order of

*This research was supported by Ministerio de Ciencia y Tecnología MTM2011-28636-C02-02

convergence and d the number of functional evaluations per step, establishes the effectiveness of the iterative method. In this sense, Kung and Traub conjectured in [6] that a multipoint iterative scheme without memory, requiring $d+1$ functional evaluations per iteration, has order of convergence at most 2^d. Multipoint schemes which achieve this bound are called optimal methods.

We propose a derivative-free optimal eighth-order family of iterative methods for solving nonlinear equations. We obtain this family of optimal eight-order schemes by using weight functions procedure, with functions of one variable which are quotients of the nonelinear function evaluated in the previous steps, or quotients of divided differences of order one. In the numerical section we solve the classical problem of preliminary orbit determination, by using some modifications of the scheme designed by Danchick in [7], and comparing them with the classical Danchick' and Gauss's methods.

In Section 2 we describe our family of iterative methods and we present the convergence result. In the numerical section, we compare the proposed methods with other ones, by replacing them into the Danchick's algorithm, for solving the problem of the orbital determination. We finish the work with some conclusions an the references used in it.

2 A new family of Steffensen-type methods with optimal order of convergence

We design a three-step family of Steffensen-type methods, using weight functions technique. To develop it, we compose Steffensen's method with itself twice, but using different divided differences in each step. For reaching the optimal order, we use in the second step a weight function whose variable is a quotient of two values of f in different steps and in the third step a weight function whose variable is the quotient between two divided difference of order 1. The iterative expression of our family is:

$$\begin{aligned} y_k &= x_k - \frac{f(x_k)}{f[z_k, x_k]}, \\ w_k &= y_k - H(\mu)\frac{f(y_k)}{f[y_k, z_k]}, \quad \mu = \frac{f(y_k)}{f(z_k)} \\ x_{k+1} &= w_k - G(\eta)\frac{f(w_k)}{f[w_k, y_k]}, \quad \eta = \frac{f[w_k, y_k]}{f[w_k, z_k]} \end{aligned} \tag{1}$$

where $z_k = x_k + f(x_k)^3$, $f[\cdot,\cdot]$ denotes divided difference of first order and $H(\mu)$ and $G(\eta)$ are real functions.

In this scheme, the election of the exponent of $f(x_k)$ in the expression of z_k is key to obtain the order of convergence eighth. In fact, following the ideas shown in [8], if we take in (1) $z_k = x_k + f(x_k)$ or $z_k = x_k + f(x_k)^2$ the order eight is not reached. On the other hand, the next result holds also if $z_k = x_k + \gamma f(x_k)^n$, for $n \geq 3$ and any value of parameter γ, $\gamma \neq 0$.

Theorem 1 *Let $x^* \in I$ be a simple zero of a sufficiently differentiable function $f : I \subseteq \mathbb{R} \to \mathbb{R}$ in a open interval I. If x_0 is close enough to x^* and being H and G any sufficiently differentiable real functions satisfying the following conditions: $H(0) = 0$, $H'(0) = 1$, $G(1) = 1$, $G'(1) = 0$, $G''(1) = 2$ and $G'''(1) = -12$; then the iterative methods of family (1) have optimal eighth order of convergence, whose error equation is:*

$$e_{k+1} = \frac{1}{2}C_2((-6 + H_2)C_2^2 + 2C_3)(f'(x^*)^3C_2^2 - 4C_2^4 + C_3^2 - C_2C_4)e_k^8 + O[e_k^9],$$

where $e_k = x_k - x^*$ and $C_k = \dfrac{1}{k!}\dfrac{f^{(k)}(x^*)}{f'(x^*)}$, $k = 2, 3, ...$

3 Numerical results

The classical method of Gauss starts from two position vectors, denoted by $\vec{r}_1$ and $\vec{r}_2$, of the satellite in its orbit and the time instants in which they were obtained. This method is based on the rate y between the triangle and the ellipse sector defined by the two position vectors (see Figure 1a). The complete explanation about Gauss' equations and his method can be found in [10].

The original Gauss' scheme use the fixed point method and has a restriction when the angle formed by the two position vectors is greater than $\pi/4$, since in this case the areas of the triangle and the ellipse sector are not similar. For this reason, Danchick in [7] modified Gauss' method solving separately by means of Newton's method the Gaussian equations, depending on the value of the true anomalies. As a direct consequence of this alternative procedure, he was able to increase the separation of observation instants to values close to π radians. In order to enhance the Danchick's initial scheme, we replace the Newton's method in the two ways of proceed by higher-order methods, including some members of our family.

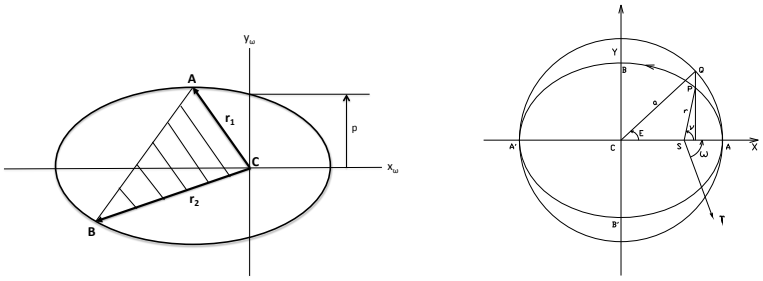

(a) Ratio sector-triangle y (b) Size, shape and anomalies

Figure 1: Some aspects of the orbital plane

The schemes that we will use to compare the original and the proposed schemes, whose results can see in the next tables, are:

Method	**Iterative expression**
Classical Gauss (FPoint) [10]	$x_{k+1} = g(x_k)$
Danchick-Newton [7]	$x_{k+1} = x_k - \dfrac{f(x_k)}{f'(x_k)}$
Steffensen (DS) [11]	$z_k^+ = x_k + f(x_k),$ $x_{k+1} = x_k - \dfrac{f^2(x_k)}{f(z_k^+) - f(x_k)}.$
DSR	$z_k^- = x_k - f(x_k)$ $x_{k+1} = x_k - \dfrac{f^2(x_k)}{f(z_k^-) - f(x_k)},$
Traub (DT) [11]	$y_k = x_k - \dfrac{f(x_k)}{f'(x_k)},$ $x_{k+1} = y_k - \dfrac{f(y_k)}{f'(x_k)}.$
DTS	$y_k = x_k - \dfrac{f^2(x_k)}{f(z_k^+) - f(x_k)},$ $x_{k+1} = y_k - \dfrac{f(x_k)f(y_k)}{f(z_k^+) - f(x_k)}.$
DTSR	$y_k = x_k - \dfrac{f^2(x_k)}{f(z_k^-) - f(x_k)},$ $x_{k+1} = y_k - \dfrac{f(x_k)f(y_k)}{f(x_k) - f(z_k^-)}.$
MO	Chosen weight functions: $H(\mu) = 1 + \mu,$ $G(\eta) = 1/4 + (-3/4 + \eta)^2 - 2(-1 + \eta)^3 + \eta.$

In order to compare the different schemes we use some indicators widely used such as the number of iterations *iter* and the Approximated Computational Order of Convergence ρ defined in (see [9]) as:

$$p \approx \ \rho = \frac{\ln(|x_{k+1} - x_k|/|x_k - x_{k-1}|)}{\ln(|x_k - x_{k-1}|/|x_{k-1} - x_{k-2}|)}.$$

From ρ we design two new parameters: the approximated index of efficiency denoted by $\tilde{I} = \rho^{1/d}$ and what we call the approximated computational index calculated as $\tilde{I}_c = \rho^{1/op}$, where d is the number of functional evaluations and op is number of products and quotients realized per step. Finally, $error_{parameter}$ is the exact error of each orbital element.

The numerical results have been calculated with Mathematica 8.0, using Variable Precision Arithmetics with 1000 digits and the stopping criterium $|x_{k+1} - x_k| < 10^{-100}$. To test these methods, we will calculate the orbital elements which appears in the reference orbit VI extracted of [10].

	FPoint	Danchick	DS	DSR	DT	DTS	DTSR	MO
$iter$	–	–	–	–	–	–	–	4
ρ	–	–	–	–	–	–	–	8.0010
$\tilde{I}$	–	–	–	–	–	–	–	1.5528
$\tilde{I}_c$	–	–	–	–	–	–	–	1.1221
$error_a$	–	–	–	–	–	–	–	1.7358e-202
$error_e$	–	–	–	–	–	–	–	3.6984e-202
$error_i$	–	–	–	–	–	–	–	1.2487e-202
$error_\omega$	–	–	–	–	–	–	–	8.0140e-200
$error_\Omega$	–	–	–	–	–	–	–	2.4857e-251
$Time$	–	–	–	–	–	–	–	0.00121789

Table 1: Results of Reference Orbit VI $|\nu_2 - \nu_1| = 59.0148^\circ$, $y_0 = 0.46$

To determine the orbital elements we must take into account that the difference of true anomalies is above forty-five degrees, for this reason fixed point, can not reach the solution. In Table 1, we can see that MO method is the only one able to give the solution with a small error, being the number of iterations and the computational time specially low, although we are using a very good initial estimation $y_0 = 0.46$. Like the other methods did not reach the solution, we decided to increase the tolerance to a value of 10^{-10} and reduce the number of digits to 250, to verify that our method kept the good results reached with tighter tolerance.

	FPoint	Danchick	DS	DSR	DT	DTS	DTSR	MO
$iter$	–	3	7	5	2	2	4	3
ρ	–	1.996	2.007	2.018	2.097	2.097	2.972	8.001
$\tilde{I}$	–	1.254	1.193	1.280	0.914	1.225	1.488	1.553
$\tilde{I}_c$	–	1.597	1.193	1.198	1.448	0.914	1.2251	1.109
$error_a$	–	5.51e-10	1.72e-12	1.19e-09	3.28e-10	3.28e-10	1.33e-14	1.74e-202
$error_e$	–	1.71e-10	5.31e-13	3.68e-10	1.02e-10	1.02e-10	2.27e-15	3.70e-202
$error_i$	–	1.65e-11	5.10e-14	3.55e-11	9.80e-12	9.80e-12	1.72e-16	1.25e-202
$error_\omega$	–	1.06e-08	3.27e-11	2.28e-08	6.29e-09	6.29e-09	1.11e-13	8.01e-200
$error_\Omega$	–	2.48e-251	2.48e-251	2.48e-251	2.48e-251	2.48e-251	2.48e-251	2.48e-251
$Time$	–	0.00287	0.01875	0.01085	0.00183	0.01479	0.00763	0.00093

Table 2: Results of Reference Orbit VI, $|\nu_2 - \nu_1| = 59.0148^\circ$, $y_0 = 0.46$

As we can see in Table 2, in spite of DT and DTS need only two iterations to give us the solution, if we look at the error of the orbital parameters we can see that, with only one iteration more, MO gives us the least error in the shortest computational time and we conclude that the overall good results in our method MO are maintained, so that our method has proved to be very stable, robust and efficient.

4 Conclusions

In this work, we have designed a new family of Steffensen-type methods of optimal eighth-order by using weight functions procedures. We have also used the Danchick's method, based on the preliminary orbit determination provided by Gauss, and we have enhanced it by replacing Newton's method by the proposed ones, maintaining the range of the difference of the true anomalies to values close to π and reducing considerably the number of iterations along with reduced computing time and an error committed much lower than in the rest of methods.

References

[1] D.D. Bruns, J.E. Bailey. Nonlinear feedback control for operating a non-isothermal CSTR near an unstable steady state, *Chemical Engineering Science*, 32: 257–264, 1977.

[2] J.A. Ezquerro, J.M. Gutiérrez, M.A. Hernández, M.A. Salanova. Chebyshev-like methods and quadratic equations, *Revue d'Analyse Numérique et de Théorie de l'Approximation*, 28: 23–35, 1999.

[3] Y. Zhang, P. Huang. High-precision Time-interval Measurement Techniques and Methods, *Progress in Astronomy*, 24: 1–15, 2006.

[4] Y. He, C. Ding. Using accurate arithmetics to improve numerical reproducibility and stability in parallel applications, *Journal of Supercomputing*, 18: 259–277, 2001.

[5] A.M. Ostrowski. Solutions of equations and systems of equations, *Academic Press, New York-London*, 1966.

[6] H. T. Kung, J. F. Traub. Optimal order of one-point and multi-pointiteration, *Journal Assoc. Comput. Math*, 21: 643–651, 1974.

[7] R. Danchick. Gauss meets Newton again: How to make Gauss orbit determination from two position vectors more efficient and robust with Newton-Raphson iterations, *Applied Mathematics and Computation*, 195: 364-375, 2008.

[8] A. Cordero, J. R. Torregrosa. A technique to design derivative-free methods for nonlinear equations, *Proceedings of the 13th International Conference on Computational and Mathematical Methods in Science and Engineering, CMMSE 2013*, ISBN: 978-84-616-2723-3, 24-27 June, 2013.

[9] A. Cordero, J.R. Torregrosa. Variants of Newton's Method using fifth-order quadrature formulas, *Applied Mathematics and Computation* 190: 686-698, 2007.

[10] Pedro Ramon Escobal, Methods of Orbit Determination. Krieger Publishing Company, 1975.

[11] J.F. Traub, Iterative methods for the solution of equations. New York, Chelsea Publishing Company, 1982.

On the computation of the hyperbolic sine and cosine matrix functions*

E. Defez* †, J. Sastre◇, J. Ibáñez‡, J. Peinado‡ and M. M. Tung*

(*) Instituto de Matemática Multidisciplinar,

(◇) Instituto de Telecomunicaciones y Aplicaciones Multimedia,

(‡) Instituto de Instrumentación para Imagen Molecular,

Universidad Politécnica de Valencia,

Camino de Vera s/n, 46022, Valencia, Spain.

November 30, 2013

1 Introduction

Coupled partial differential systems are frequently found in many different fields of science and technology: magnetohydrodynamic flows, biochemistry, elastic and inelastic contact problems of solids, etc., see [1, 2, 3, 4]. Exact solutions for a wide class of these important problems [5] are given in terms of matrix functions, in particular, in terms of the hyperbolic cosine and sine of a matrix, respectively defined by

$$\cosh(Ay) = \frac{e^{Ay} + e^{-Ay}}{2}\ ,\ \sinh(Ay) = \frac{e^{Ay} - e^{-Ay}}{2}\ ,\ A \in \mathbb{C}^{r\times r}. \qquad (1)$$

For the numerical solution of these problems, analytic-numerical approximations are most suitably obtained by using the hyperbolic matrix functions

*Acknowledgments. This work has been supported by the *Generalitat Valenciana* GV/2013/035 and the Universitat Politècnica de Valéncia Grant PAID-06-011-2020.

†e-mail:edefez@imm.upv.es

$\sinh(A)$ and $\cosh(A)$, see [5]. It is well known that the computation of both functions can be reduced to the cosine of a matrix due to the identities

$$\cosh(A) = \cos(iA), \quad \sinh(A) = i\cos\left(A - \frac{i\pi}{2}I\right).$$

Thus, the matrix cosine can in principle be calculated [6, 7]. This has the disadvantage, however, to require complex arithmetic even though the matrix A is real, which contributes substantially to the computational overhead. Furthermore, it is possible to reduce the computation of $\sinh(A)$ to the computation of $\cosh(A)$ by the relation

$$\sinh(A) = -i\cosh\left(-A - \frac{\pi}{2}iI\right). \tag{2}$$

Obviously, formula (2) also requires complex arithmetic although matrix A is real. Direct calculation through the exponential matrix using (1) is also costly.

In this work we propose a method to evaluate both matrix functions, $\sinh(A)$ and $\cosh(A)$ simultaneously and by avoiding complex arithmetic whenever possible.

This work is organized as follows. Section 2 summarizes previous results of Hermite matrix polynomials and includes a new Hermite series expansion of the matrix hyperbolic sine and cosine. Section 3 deals with the Hermite matrix polynomial series expansion of $\cosh(At)$ and $\sinh(At)$ for an arbitrary matrix as well as with its finite truncated series with a previously fixed accuracy in a bounded domain. An algorithm for this method is given. Section 4 deals with a numerical example in order to investigate the accuracy of the newly proposed method. An algorithm and test are given in section 5. Finally, the conclusions are presented in section 6.

Throughout this work $[x]$ denotes the integer part of x. The matrices I_r and $\theta_{r\times r}$ in $\mathbb{C}^{r\times r}$ denote the matrix identity and the null matrix of order r, respectively. Following [8], for a matrix A in $\mathbb{C}^{r\times r}$, its infinite-norm will be denoted by $\|A\|_\infty$ and its 2-norm will be denoted by $\|A\|_2$.

2 Previous results on Hermite matrix polynomials

For the sake of clarity in the presentation of the following results, we recall some properties of Hermite matrix polynomials which have been established in [9] and [10]. From (3.4) of [10] the $n-$th Hermite matrix polynomial is defined by

$$H_n\left(x, \frac{1}{2}A^2\right) = n! \sum_{k=0}^{\left[\frac{n}{2}\right]} \frac{(-1)^k (xA)^{n-2k}}{k!(n-2k)!} \ ,$$

for an arbitrary matrix A in $\mathbb{C}^{r\times r}$. Taking into account the three-term recurrence relationship (3.12) of [10, p. 26], it follows that

$$\left.\begin{array}{c} H_n\left(x, \frac{1}{2}A^2\right) = xAH_{n-1}\left(x, \frac{1}{2}A^2\right) - 2(n-1)H_{n-2}\left(x, \frac{1}{2}A^2\right) \quad , \quad n \geq 1 \\ H_{-1}(x, \frac{1}{2}A^2) = \theta_{r\times r} \quad , \quad H_0(x, \frac{1}{2}A^2) = I_r \end{array}\right] , \tag{3}$$

and from its generating function in (3.1) and (3.2) [10, p. 24] one gets

$$e^{xtA-t^2 I} = \sum_{n\geq 0} \frac{1}{n!} H_n\left(x, \frac{1}{2}A^2\right) t^n, \quad |t| < \infty, \tag{4}$$

where $x, t \in \mathbb{C}$. Then, after taking $y = tx$ and $\lambda = 1/t$ in (4) it follows that

$$e^{Ay} = e^{\frac{1}{\lambda^2}} \sum_{n\geq 0} \frac{1}{\lambda^n n!} H_n\left(\lambda y, \frac{1}{2}A^2\right), \ \lambda \in \mathbb{C}, \ \ y \in \mathbb{C}, \ \ A \in \mathbb{C}^{r\times r} \ . \tag{5}$$

Next, we wish to determine the series expansion in terms of Hermite matrix polynomials for the matrix hyperbolic cosine $\cosh(Ay)$. Given an arbitrary matrix $A \in \mathbb{C}^{r\times r}$, with (1) and using (5) in combination with [10, p. 25], it follows that

$$H_n(-x, A) = (-1)^n H_n(x, A) \, .$$

Thus, one obtains the following, required expression:

$$\cosh(Ay) \ = e^{\frac{1}{\lambda^2}} \sum_{n\geq 0} \frac{1}{\lambda^{2n}(2n)!} H_{2n}\left(y\lambda, \frac{1}{2}A^2\right) \ . \tag{6}$$

Denoting by $CH_N(A,\lambda)$ the Nth partial sum of series (6) for $y=1$, one gets

$$CH_N(\lambda,A)=e^{\frac{1}{\lambda^2}}\sum_{n=0}^{N}\frac{1}{\lambda^{2n}(2n)!}H_{2n}\left(\lambda,\frac{1}{2}A^2\right)\approx\cosh(A),\ \lambda\in\mathbb{C},\quad A\in\mathbb{C}^{r\times r}. \tag{7}$$

Similarly, one derives the other expression being looked for:

$$\sinh(Ay)\ =e^{\frac{1}{\lambda^2}}\sum_{n\geq 0}\frac{1}{\lambda^{2n+1}(2n+1)!}H_{2n+1}\left(y\lambda,\frac{1}{2}A^2\right)\ . \tag{8}$$

Denoting by $SH_N(A,\lambda)$ the Nth partial sum of series (8) for $y=1$, one gets

$$SH_N(\lambda,A)=e^{\frac{1}{\lambda^2}}\sum_{n=0}^{N}\frac{1}{\lambda^{2n+1}(2n+1)!}H_{2n+1}\left(\lambda,\frac{1}{2}A^2\right)\approx\sinh(A),\lambda\in\mathbb{C},A\in\mathbb{C}^{r\times r}. \tag{9}$$

3 Accurate and error bounds for hyperbolic matrix cosine and sine approximation

Form reference [11] we have the bound $\left\|H_n\left(x,\frac{1}{2}A^2\right)\right\|_2\leq n!e^{\left(|x|\|A\|_2+1\right)}$, and thus

$$\left\|H_{2n}\left(\lambda,\frac{1}{2}A^2\right)\right\|_2\leq(2n)!e^{\left(|\lambda|\|A\|_2+1\right)}. \tag{10}$$

Taking the approximate value $CH_N(\lambda,A)$ given by (7) and taking into account (10) and $\lambda>1$, it follows that

$$\begin{aligned}\|\cosh(A)-CH_N(\lambda,A)\|_2 &\leq e^{\frac{1}{\lambda^2}}\sum_{n\geq N+1}\frac{1}{\lambda^{2n}(2n)!}\left\|H_{2n}\left(\lambda,\frac{1}{2}A^2\right)\right\|_2\\ &\leq e^{\left(\frac{1}{\lambda^2}+\lambda\|A\|_2+1\right)}\sum_{n\geq N+1}\frac{1}{\lambda^{2n}}\\ &= \frac{e^{\left(\frac{1}{\lambda^2}+\lambda\|A\|_2+1\right)}}{(\lambda^2-1)\,\lambda^{2N-1}}\ .\end{aligned}$$

Considering the previous expression, it is possible to arrive at the following error bound for approximation (7):

$$\|\cosh(A)-CH_N(\lambda,A)\|_2\leq\frac{e^{\left(\frac{1}{\lambda^2}+\lambda\|A\|_2+1\right)}}{(\lambda^2-1)\,\lambda^{2N-1}}. \tag{11}$$

Now, let $\varepsilon > 0$ be an *a priori* error bound. After using the estimate (11) and considering N to be the first positive integer with

$$N \geq \frac{\log\left(\frac{e^{\left(\frac{1}{\lambda^2}+\lambda\|A\|_2+1\right)}}{\varepsilon(\lambda^2-1)}\right)}{2\log(\lambda)} + \frac{1}{2}, \tag{12}$$

then Eq. (11) reduces to

$$\|\cosh(A) - CH_N(\lambda, A)\|_2 \ \leq \ \varepsilon \ .$$

On the other hand, from reference [11] we find the bound:

$$\left\| H_{2n+1}\left(\lambda, \frac{1}{2}A^2\right)\right\|_2 \leq (2n+1)! e^{\left(|\lambda|\|A\|_2+1\right)}. \tag{13}$$

Taking into account (8), $\lambda > 1$ and proceeding as above, we obtain the error bound for approximation (9):

$$\left\|\sinh(A) - SH_N(\lambda, A^2)\right\|_2 \leq \frac{e^{\left(\frac{1}{\lambda^2}+\lambda\|A\|_2+1\right)}}{(\lambda^2-1)\,\lambda^{2N}}. \tag{14}$$

Now, let $\varepsilon > 0$ be an *a priori* error bound. Using the previous inequality (14) and being N the first positive integer so that

$$N \geq \frac{\log\left(\frac{e^{\left(\frac{1}{\lambda^2}+\lambda\|A\|_2+1\right)}}{\varepsilon(\lambda^2-1)}\right)}{2\log(\lambda)}, \tag{15}$$

then Eq. (14) yields

$$\|\sinh(A) - SH_N(\lambda, A)\|_2 \ \leq \ \varepsilon \ .$$

4 A Numerical example

Let A be a matrix defined by

$$A \ = \ \begin{pmatrix} 1 & 0 & 0 & -1 \\ 1 & 1 & 0 & -1 \\ 1 & 1 & 2 & 0 \\ 0 & 0 & 0 & 1 \end{pmatrix} \ , \tag{16}$$

with $\sigma(A) = \{1, 2\}$. Matrix A is non-diagonalizable. Using the minimal theorem [12, p. 571], see also [9], the exact value of $\cosh(A)$ is

$$\cosh(A)$$

$$= \begin{pmatrix} (1/e+e)/2 & 0 & 0 & (1/e-e)/2 \\ (-1/e+e)/2 & (1/e+e)/2 & 0 & (1/e-3e)/4 \\ \frac{(-3e-\cosh(1)+4\cosh(2)+\sinh(1))}{2} & \frac{(-1+e)^2(1+e+e^2)}{2e^2} & \cosh(2) & \frac{(-6+e+13e^3-6e^4)}{4e^2} \\ 0 & 0 & 0 & (1/e+e)/2 \end{pmatrix}$$

$$\approx \begin{pmatrix} 1.5430806348152 & 0 & 0 & -1.1752011936438 \\ 1.1752011936438 & 1.5430806348152 & 0 & -1.9467415110514 \\ 3.2630289188930 & 2.2191150562684 & 3.7621956910836 & -2.3602012704661 \\ 0 & 0 & 0 & 1.5430806348152 \end{pmatrix}.$$

It is easy to check that $\|A\|_2 = 2.7763$. Choosing $\lambda = 10$ and $\varepsilon = 10^{-5}$, the estimate (12) requires to take $N = 9$:

$$\frac{\log\left(\frac{e^{\left(\frac{1}{\lambda^2}+\lambda\|A\|+1\right)}}{\varepsilon(\lambda^2-1)}\right)}{2\log(\lambda)} + \frac{1}{2} \approx 8.25015 \Longrightarrow N = 9.$$

Then, with $N = 9$ the associated approximation is

$$CH_9(10, A) = \begin{pmatrix} 1.5430806348152 & 0 & 0 & -1.1752011936438 \\ 1.1752011936438 & 1.5430806348152 & 0 & -1.9467415110514 \\ 3.2630289188927 & 2.2191150562682 & 3.7621956910835 & -2.3602012704657 \\ 0 & 0 & 0 & 1.5430806348152 \end{pmatrix},$$

so that

$$\|\cosh(A) - CH_9(10, A)\|_2 = 5.91319 \times 10^{-13}.$$

Note that the number of terms required to obtain a predetermined accuracy tends to be smaller than the one provided by (12). For instance, taking $N = 7$ one finds

$$CH_7(10, A) = \begin{pmatrix} 1.5430806348152 & 0 & 0 & -1.1752011936438 \\ 1.1752011936438 & 1.5430806348152 & 0 & -1.9467415110510 \\ 3.2630289155520 & 2.2191150545979 & 3.7621956894131 & -2.3602012654552 \\ 0 & 0 & 0 & 1.5430806348152 \end{pmatrix},$$

and

$$\|\cosh(A) - CH_7(10, A)\|_2 = 6.46938 \times 10^{-9}.$$

The specific choice of parameter λ can still be further refined. Figure 1 displays the graph for function

$$f(\lambda) = \frac{\log\left(\frac{e^{\left(\frac{1}{\lambda^2}+\lambda\|A\|_2+1\right)}}{10^{-5}(\lambda^2-1)}\right)}{2\log(\lambda)} + \frac{1}{2}$$

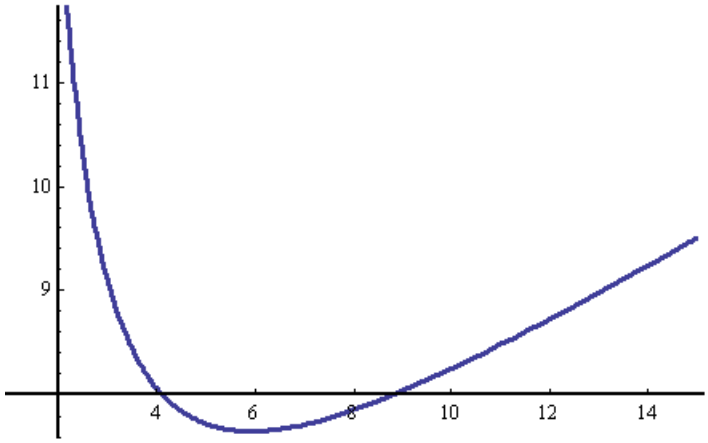

Figure 1: For $\varepsilon = 10^{-5}$ fixed and varying λ.

where $\varepsilon = 10^{-5}$ is chosen as the error bound and λ varies within the interval $(1, 15]$. This function possesses a minimum in the interval $[5, 7]$. By using numerical standard routines, we can compute that this minimum is reached at $\lambda = 5.91678$. Hence, one gets for the minimum $f(5.91678) = 7.6554$ and we take $N = 8$. Thus, for $N = 8, \lambda = 5.91678$, one gets

$$\|\cosh(A) - CH_8(5.91678, A)\|_2 = 7.25647 \times 10^{-12} .$$

This figure illustrates how the error norm depends on parameter λ. It becomes evident that an adequate choice of λ may provide results with higher accuracy.

On the other hand let us consider hyperbolic matrix sine

$$\sinh(A) = \begin{pmatrix} (-1/e+e)/2 & 0 & 0 & -\left(1+e^2\right)/2e \\ (1/e+e)/2 & (-1/e+e)/2 & 0 & -\dfrac{1+3e^2}{4e} \\ \dfrac{-2+e-3e^3+2e^4}{2e^2} & \dfrac{-1+e-e^3+e^4}{2e^2} & \sinh(2) & \dfrac{6-e+13e^3-6e^4}{4e^2} \\ 0 & 0 & 0 & (-1/e+e)/2 \end{pmatrix}$$

$$\approx \begin{pmatrix} 1.1752011936438 & 0 & 0 & -1.5430806348152 \\ 1.5430806348152 & 1.1752011936438 & 0 & -2.1306812316371 \\ 3.3602377935912 & 2.4516592142032 & 3.6268604078470 & -2.1381351413420 \\ 0 & 0 & 0 & 1.1752011936438 \end{pmatrix}.$$

For the same values $N = 8, \lambda = 5.91678$ we obtain the following approximation:

$$SH_8(5.91678, A)$$

$$= \begin{pmatrix} 1.1752011936438016 & 0 & 0 & -1.543080634815244 \\ 1.543080634815244 & 1.1752011936438016 & 0 & -2.130681231637144 \\ 3.360237793590955 & 2.4516592142030995 & 3.6268604078469004 & -2.138135141341666 \\ 0 & 0 & 0 & 1.1752011936438016 \end{pmatrix},$$

with an error

$$\|\sinh(A) - SH_8(5.91678, A)\|_2 = 4.56819 \times 10^{-13}.$$

5 Algorithm and test

Starting with expressions (7) and (9), it is possible to compute simultaneously the hyperbolic matrix cosine and sine using algorithm 1. We have determined the optimal value of λ, *i.e.*, the minimal of

$$\frac{e^{\left(\frac{1}{\lambda^2}+\lambda M+1\right)}}{\left(\lambda^2-1\right)\lambda^{2N-1}} \tag{17}$$

for each value of N and $M \in \mathbb{N}$, $1 \leq M \leq 100$. Since the minimal value of formula (17) in the limit $M \to \infty$ is obtained for $\lambda \to 1$, we have selected $\lambda = 1$ for sufficiently large $M \geq 100$.

The MATLAB implementation of this algorithm has been compared to the built-in Matlab function `funm`. For testing 100 diagonalizable matrices

of dimension r equal to 512 were used. These matrices were generated as $A = QDQ$, where $Q = H/\sqrt{512}$, with H a Hadamard matrix of dimension 512. All diagonal matrices D were randomly generated, with a 2-norm varying between 1 and 100. The exact hyperbolic cosine of A was computed by $\cosh(A) = Q\cosh(D)Q$ with 32 digits of precision. The error approximation was determined by using the infinite-norm of the difference.

We used an Apple Macintosh iMac (mid 2011) with a quadcore i5-2400S 2.5 GHz processor and 12GB of RAM. All the tests were carried out using MATLAB R2012a and OS X 10.6.8.

For the 100 benchmark tests our proposed Hermite algorithm has an improved error behaviour in 98 cases and is only less efficient in 2 times (see Figure 2). The total time average Te for all 100 executions of the algorithm is $Te = 9.407$ seconds, opposed to the built-in MATLAB routine `funm` with $Te = 11.371$ seconds. Similar results are obtained with the matrix hyperbolic sine, see Figure 3.

6 Conclusions.

In this work, for further optimization we have presented a modification of the algorithm proposed in [9] for computing matrix cosine and sine based on the polynomial expansion of Hermite matrices. The numerical experiments show that the MATLAB implementation of the new algorithm has lower execution times and higher accuracy than the MATLAB function `funm`. Also, the new algorithm allows for the simultaneous evaluation of the hyperbolic matrix sine and cosine. The algorithm depends on the parameter λ, whose impact on the numerical efficiency is currently studied. Moreover, pending work focuses on the optimal scaling of the matrix and the study of the evaluation [13] of the approximations (7) and (9). Further work in progress is the parallel implementation of these new algorithms on distributed memory platforms by using the message passing paradigm, MPI and BLACS for communications, and PBLAS and ScaLAPACK [14] for computations.

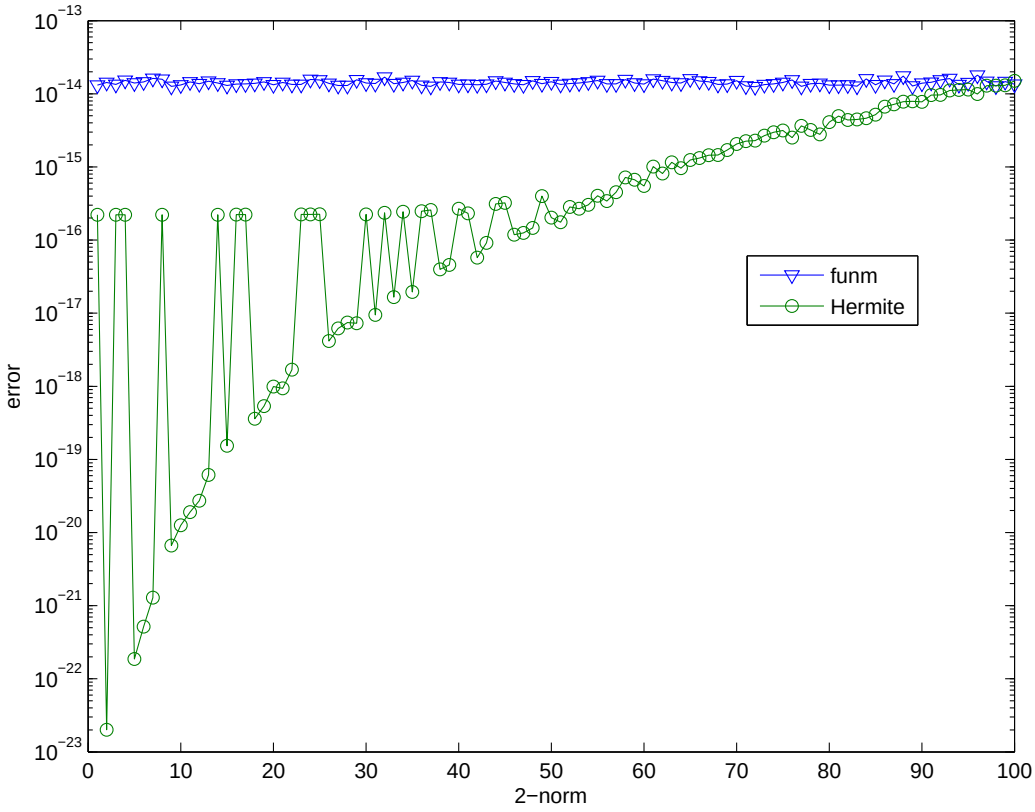

Figure 2: Error comparing MATLAB `funm` with Hermite hyperbolic matrix cosine approximation for $r = 512$, $\lambda = 2$.

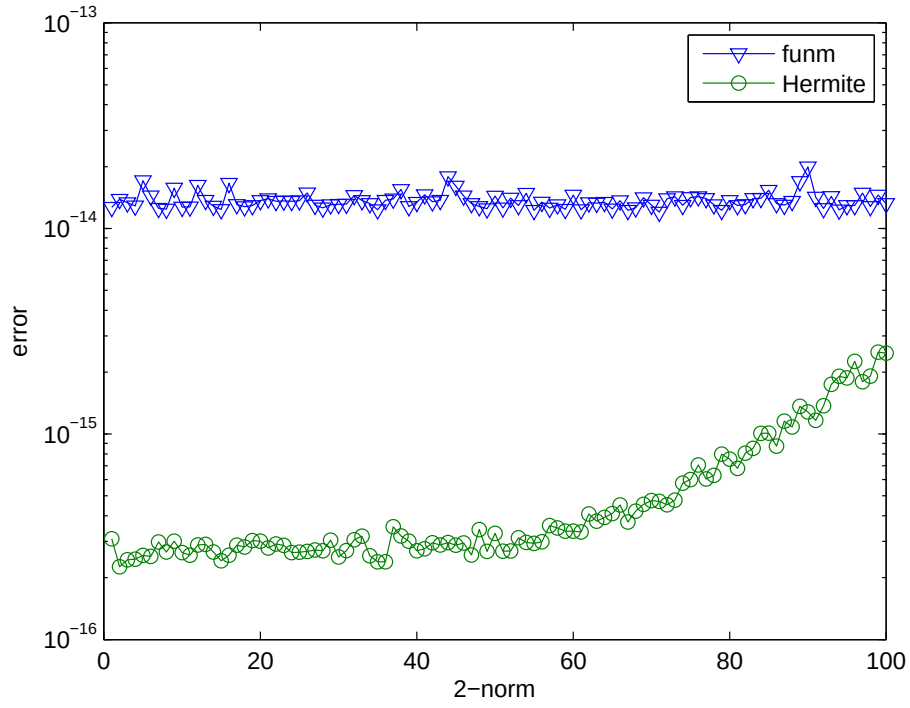

Figure 3: Error comparing MATLAB `funm` with Hermite hyperbolic matrix sine approximation for $r = 512$, $\lambda = 2$.

Algorithm 1 Computes hyperbolic sine and cosine of a matrix by means of Hermite approximants.

Function $[C, S] = sinhcoshher(A, N)$
Inputs: Matrix $A \in \mathbb{R}^{r\times r}$; $2N+1$ is the order of the Hermite approximation ($N \in \mathbb{N}$) of hyperbolic sine/cosine matrix function; parameter $\lambda \in \mathbb{R}$
Output: Matrices $C = \cosh(A) \in \mathbb{R}^{r\times r}$ and $S = \sinh(A) \in \mathbb{R}^{r\times r}$

1: $M = \lfloor \|A\|_2 \rfloor$
2: Select the optimal value of λ depending on N and M
3: $H_0 = I_r$
4: $H_1 = \lambda A$
5: $C = H_0$
6: $S = H_1/\lambda$
7: $\alpha = 1/\lambda$
8: **for** $n = 2 : 2N+1$ **do**
9: $\quad H = \lambda A H_1 - 2(n-1)H_0$
10: $\quad H_0 = H_1;$
11: $\quad H_1 = H$
12: $\quad \alpha = \alpha/(\lambda n)$
13: $\quad$ **if** $\mod(n, 2) == 0$ **then**
14: $\quad\quad C = C + \alpha H$
15: $\quad$ **else**
16: $\quad\quad S = S + \alpha H$
17: $\quad$ **end if**
18: **end for**
19: $C = e^{1/\lambda^2} C$
20: $S = e^{1/\lambda^2} S$

References

[1] M. Sezgin. Magnetohydrodynamics flows in a rectangular duct. *International Journal for Numerical Methods in Fluids*, 7(7): 697–718, 1987.

[2] A. King and C. Chou. Mathematical modeling simulation and experimental testing of biochemical systems crash response. *Journal of Biomechanics*, 9: 301–317, 1976.

[3] L. Jódar, E. Navarro and J.A. Martín. Exact and analytic-numerical solutions of strongly coupled mixed diffusion problems. *Proceedings of the Edinburgh Mathematical Society*, 43: 269–293, 2000.

[4] V. Soler, E. Defez, M.V. Ferrer, J. Camacho. On Exact Series Solution of Strongly Coupled Mixed Parabolic Problems. *Abstract and Applied Analysis*, vol. 2013, Article ID 524514, doi:10.1155/2013/524514, 2013.

[5] L. Jódar, E. Navarro, A.E. Posso and M.C. Casabán. Constructive solution of strongly coupled continuous hyperbolic mixed problems. *Applied Numerical Mathematics*, 47 (3–4): 477–492, 2003.

[6] E. Defez, J. Sastre, J.J. Ibáñez and Pedro A. Ruiz. Computing matrix functions solving coupled differential models. *Mathematical and Computer Modelling*, 50(5–6):831–839, 2009.

[7] E. Defez, J. Sastre, J.J. Ibáñez and Pedro A. Ruiz. Computing matrix functions arising in engineering models with orthogonal matrix polynomials. *Mathematical and Computer Modelling*, 57(7–8):1738–1743, 2013.

[8] G.H. Golub and C.F. Van Loan. Matrix computations (Second Edition). Baltimore, The Johns Hopkins University Press, 1989.

[9] E. Defez and L. Jódar. Some Applications of Hermite matrix polynomials series expansions. *Journal of Computational and Applied Mathematics*, 99: 105–117, 1998.

[10] L. Jódar and R. Company. Hermite matrix polynomials and second order matrix differential equations. *Journal Approximation Theory Application*, 12(2): 20–30, 1996.

[11] E. Defez, M.M. Tung and J. Sastre. Improvement on the bound of Hermite matrix polynomials. *Linear Algebra and its Applications*, 434: 1910–1919, 2011.

[12] N. Dunford and J. Schwartz, Linear Operators, Part I. New York, Interscience, 1957.

[13] M.S. Paterson and L.J. Stockmeyer. On the number of nonscalar multiplications necessary to evaluate polynomials. *SIAM Journal on Computing*, 2(1): 60–66, 1973.

[14] L.S. Blackford, J. Choi, A. Cleary, E. D'Azevedo, J. Demmel, I. Dhillon, J. Dongarra, S. Hammarling, G. Henry, A. Petitet, K. Stanley, D. Walker and R.C. Whaley, ScaLAPACK Users' Guide. Philadelphia, SIAM, 1997.

Numerical valuation of infinite activity Lévy option pricing models

M. Fakharany*, R. Company and L. Jódar

Instituto de Matemática Multidisciplinar, Universitat Politècnica de València, Camino de Vera s/n, 46022 Valencia, Spain

1 Introduction

The hypothesis that asset prices behave according to the geometric Brownian motion when one derives the option prices is inconsistent with market data [1]. This drawback has been overcome using Lévy process models allowing the calibration of the model to the option market data and the reproduction of a wide variety of implied volatility skews/smiles.

One of the most relevant and versatile Lévy models is the one proposed by Carr, Geman, Madan and Yor, the so called CGMY model [2] that is considered a prototype of the general class of models with jumps and enjoys widespread applicability. The CGMY model allows diffusions and jumps of both finite and infinite activity. The CGMY Lévy density is given by

$$\nu(y) = \begin{cases} \frac{\mathbf{C}e^{-\mathbf{G}|y|}}{|y|^{1+\mathbf{Y}}}, & y < 0, \\ \\ \frac{\mathbf{C}e^{-\mathbf{M}|y|}}{|y|^{1+\mathbf{Y}}}, & y > 0, \end{cases} \tag{1}$$

where $\mathbf{C} > 0$, $\mathbf{G} \geq 0$, $\mathbf{M} \geq 0$, and $\mathbf{Y} < 2$. The parameter $\mathbf{Y}$ allows to control the fine structure of asset return distribution. For $\mathbf{Y} < 0$, the Lévy process is of finite activity, i.e., the measure is finite, $\int \nu(y)dy < \infty$. For $0 \leq \mathbf{Y} \leq 1$,

*Corresponding author. Email: fakharany@aucegypt.edu

it is of infinity activity but finite variance, i.e., $\int_{|y|<1} y\nu(y)dy < \infty$. Finally, for $1 < \mathbf{Y} < 2$, both the activity and variation are infinite.

Our objective is to construct a stable and conditionally consistent numerical scheme that guarantees positive solutions for the PIDE of the option price CGMY model which is given by

$$\frac{\partial V}{\partial \tau} = \frac{\sigma^2}{2} S^2 \frac{\partial^2 V}{\partial S^2} + (r-q) S \frac{\partial V}{\partial S} - rV$$

$$+ \int_{-\infty}^{+\infty} \nu(y) \big[V(Se^y, \tau) - V(S,\tau) - S(e^y - 1) \frac{\partial V}{\partial S} \big] dy, \ S \in (0,\infty), \ \tau \in (0,T], \tag{2}$$

$$V(S,0) = f(S) = \max(S-E, 0), \qquad S \in (0,\infty), \tag{3}$$

with measure $\nu(y)$ given by (1). Here $V(S,\tau)$ is the option price depending on the underlying asset S, the time to maturity is $\tau = T - t$, σ is the volatility parameter, r and q are the risk-free interest, the continuous dividend paid by the asset respectively and E is the strike price.

2 Transformation of the PIDE problem

First we remove the singularity of the kernel of the integral term of PIDE (2). Let $\varepsilon > 0$ and let us split the real line into two regions $R_1 = [-\varepsilon, \varepsilon]$ and $R_2 = (-\infty, \varepsilon) \cup (\varepsilon, \infty)$. For the term $V(Se^y, \tau)$ in R_1, taking Taylor expansion for $z = Se^y$ about $z = S$ then the integral part takes the following form

$$I(V) = \frac{\sigma^2(\varepsilon)}{2} S^2 \frac{\partial^2 V}{\partial S^2} - \gamma(\varepsilon) S \frac{\partial V}{\partial S} - \lambda(\varepsilon) V(S,\tau) + \int_{R_2} \nu(y) V(Se^y, \tau) dy + \mathcal{O}(\varepsilon^{3-Y}), \tag{4}$$

where the integrals

$$\sigma^2(\varepsilon) = \int_{-\varepsilon}^{\varepsilon} \nu(y)(e^y - 1)^2 dy, \ \gamma(\varepsilon) = \int_{R_2} \nu(y)(e^y - 1) dy, \ \lambda(\varepsilon) = \int_{R_2} \nu(y) dy. \tag{5}$$

Next step, we remove the convection and reaction terms of (2) by using the following transformation

$$x = \exp[(r - q - \gamma(\varepsilon))\tau] S, \ U(x,\tau) = \exp[(r + \lambda(\varepsilon))\tau] V(S,\tau). \tag{6}$$

Hence(2) is approximated to the following form

$$\frac{\partial U}{\partial \tau} = \frac{\hat{\sigma}^2}{2} x^2 \frac{\partial^2 U}{\partial x^2} + J(U),\ x \in (0, +\infty),\ \tau \in (0, T], \tag{7}$$

$$U(x, 0) = f(x) = \max(x - E, 0),\ x \in (0, +\infty), \tag{8}$$

where

$$\hat{\sigma}^2 = \hat{\sigma}^2(\varepsilon) = \sigma^2 + \sigma^2(\varepsilon),\ \text{and}\ J(U) = \int_0^\infty g(x, \phi) U(\phi, \tau) d\phi, \tag{9}$$

where the new kernel $g(x, \phi)$ takes the form,

$$g(x, \phi) = \begin{cases} \frac{\nu(\ln(\phi/x))}{\phi}, & 0 < \phi \leq x e^{-\varepsilon}, \\ 0, & x e^{-\varepsilon} < \phi < x e^{\varepsilon}, \\ \frac{\nu(\ln(\phi/x))}{\phi}, & \phi \geq x e^{\varepsilon}. \end{cases} \tag{10}$$

In order to evaluate the integral (9) without truncation, let us introduce a parameter $A > 0$ splitting $[0, \infty)$ into $[0, A] \cup [A, \infty)$. The unbounded integral part related to $x > A$ is transformed to a finite one by means of the change $z = \frac{A}{\phi}$.

3 Numerical Scheme Construction

A forward in time finite difference scheme is constructed. Meanwhile, the unbounded domain for the spacial variable is divided into two intervals, $[0, A]$ and $[A, \infty)$. In the interval $[0, A]$, we establish a $N-$uniform mesh partition. The domain $[A, \infty)$ is transformed into $(0, 1]$ by $z = \frac{A}{\phi}$. A $M-$uniform mesh partition in $(0, 1]$ with stepsize δ such that $M\delta = 1$, results in a non-uniform mesh into $[A, \infty)$. Consequently, the unbounded domain follows a double discretization technique [3]. On the other hand the second derivative of U with respect to the spatial variable x has been discretized using what so-called Patankar-trick [4]. Meanwhile, the integral part is approximated using four-points integration formula of open type [5, pp. 92-93]. Based on the double discretization and Patankar-trick, a difference scheme has been established to obtain a numerical solution for the option price. It worth mention that this difference scheme provides unconditionally positive solutions, also these solutions are strongly stable but conditionally consistent with the PIDE (7).

4 Numerical Examples

In this section, we illustrate with several examples the behavior of the option price obtained by this scheme using Matlab.

Example 1. Consider the vanilla call option problem (2)-(3) under CGMY process with parameters $T = 1,\ E = 20,\ A = 3E,\ \sigma = 0.2,\ r = 0.01,\ q = 0,\ \mathbf{C} = 1,\ \mathbf{G} = 20,\ \mathbf{M} = 30,\ \mathbf{Y} = 1.6\ \varepsilon = 0.12,\ h = 0.3,\ \delta = 0.2,\ k = 0.05.$ Figure (1.a) exhibits the variation of the option price V as a function of the underlying asset and time t.
The next example illustrates that the consistency condition $k = \mathcal{O}(h^{2+\epsilon})$, cannot be ignored.

Example 2. Here in this example the parameters have been selected as follows $T = 1,\ E = 10,\ A = 3E,\ \sigma = 0.25,\ r = 0.01,\ q = 0,\ \mathbf{C} = 1,\ \mathbf{G} = 25,\ \mathbf{M} = 25,\ \mathbf{Y} = 1.65,\ \varepsilon = 0.15,\ h = 0.25,\ \delta = 0.1$, for several values of k such that $k = h^{2.5}$, $h^{1.5}$ and h. Figure (1.b) shows that the consistency condition holds for $k = h^{2.5}$, while for the other two values, it is broken and the values of the option price become unreliable.

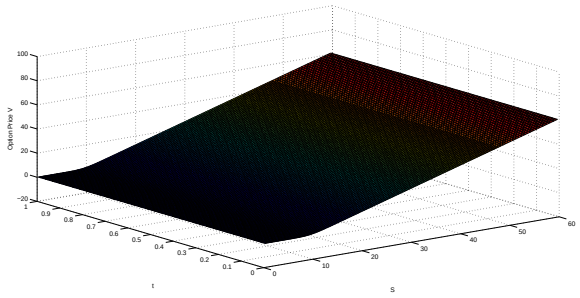

(1.a) The option price V as a function of S and t.

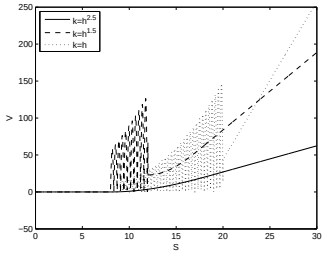

(1.b) The effect of consistency condition on V

References

[1] J. Y. Campbell, A. W. Lo, and A. C. MacKinlay, *The Econometrics of Financial Markets*, Princeton University Press, Princeton, NJ, USA, 1997.

[2] P. Carr, H. Geman, D. B. Madan, and M.Yor, *The fine structure of asset returns: An empirical investigation*, Journal of Business 75 (2002), pp. 305–332.

[3] M. C. Casabán, R. Company, L. Jódar, and J. V. Romero, *Double discretization difference schemes for partial integro-differential option pricing jump diffusion models*, Abstract and Applied Analysis 2012 (2012), pp. 1–20.

[4] S.V. Patankar, *Numerical Heat Transfer and Fluid Flow*, McGraw-Hill, New York, 1980.

[5] P. J. Davis, P. Rabinowitz, *Methods of Numerical Integration*, Second Edition, Academic Press, New York, USA, 1984.

Modelling the Evolution of Non Muscle Invasive Bladder Carcinoma using Frowgraphs

C. Santamaría[*] [*], B. García–Mora[*], G. Rubio[*] and D. Ramos[†]

(*) Instituto Universitario de Matemática Multidisciplinar,

Building 8G Access C, 2nd Floor. Universitat Politècnica de València.

Camino de Vera s/n, 46022. València (Spain),

(†) Hospital Universitari i Politècnic La Fe de València (Spain).

November 15, 2013

1 Introduction

Mathematical Flowgraph models represent Multistate Stochastic Processes (MSP) in which *nodes* are system states and directed *links* are the transitions between them. They provide time-to-event distributions and also for intermediate events to the final state, such as for example, *recurrences*, *progressions* or death in the evolution of a disease. Flowgraph models were developed to model semi–Markov processes and there are many applications in the engineering framework [1]. Recently they have expanded their applications in the field of medicine.

The objective is to discuss the application of this methodology to the evolution of bladder carcinoma. Transitional Cell Carcinoma (*TCC*) is the 11th most common cancer worldwide, accounting for 3–4% of all malignancies. Approximately 75-85% of patients present a *superficial TCC*, which can be managed with a surgical endoscope technique, that is, the transurethral resection (*TUR*). This generally has a favorable prognosis, although *recurrence* rates are 30-80% and *progression* to muscle invasive tumor is 1-45%. We are interested in predicting the risk of *recurrences* and tumor *progression* (see Figure 1a).

[*]e-mail: crisanna@imm.upv.es

2 The Flowgraph Model

The distribution, $F(.)$ on $[0, \infty[$, of the time until the absorption state in a Markov process with one absorbing state, is a *Phase–Type Distribution (PH)* given by

$$F(t) = 1 - \alpha \exp(Tt)\mathbf{e},\ t \geq 0 \tag{1}$$

where (α, α_{m+1}) is an initial probability vector and T is a matrix of order *m* representing transition rates of the m transient states. T^0 represents the absorbing rates from the transient states and $\mathbf{e} = (1, 1, \ldots, 1)^{'} \in \mathbb{R}^{m\times 1}$. The Laplace Transform of a *(PH)*-distribution is given by

$$L(s) = \alpha_{m+1} + \alpha(sI - T)^{-1}T^0,\ \text{for } Re(s) > 0 \tag{2}$$

The *Erlang Distribution* is a particular case of the *(PH)* distribution. The representation of order *r* of the Erlang distribution denoted by $E[r, \mu]$ is

$$\alpha = (1, 0, \ldots, 0)_{1\times r} \qquad T = \begin{pmatrix} -\mu & \mu & & & \\ & -\mu & \mu & & \\ & & \ddots & \ddots & \\ & & & -\mu & \mu \\ & & & & -\mu \end{pmatrix}_{r\times r} \tag{3}$$

The initial vector indicates that the lifetime begins in the first phase, and matrix T indicates that only transitions from one phase to the following are allowed. We will specifically deal with a linear combination of three Erlang proposed in [2]:

$$G(t) = p_1F_1(t) + p_2F_2(t) + p_3F_3(t), \tag{4}$$

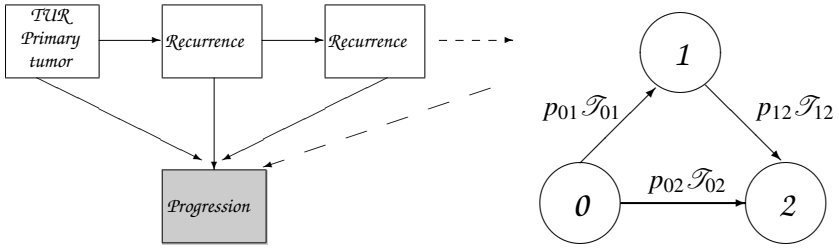

Figure 1: Multi–state Stochastic Process examples: a) Evolution of the bladder cancer; b) Transmittances for the Flowgraph model in bladder carcinoma.

with $p_1 + p_2 + p_3 = 1$, $p_i > 0$, $i = 1, 2, 3$. The three Erlang distributions are denoted by $E[r_1, \mu_1]$, $E[r_2, \mu_2]$, $E[r_3, \mu_3]$, with $\mu_i > 0$ and r_i a positive integer, $i = 1, 2, 3$. If $r_1 = 1$, $r_2 = 3$, $r_3 = 5$ the representation as *phase-type* distribution of G is (α, T) where

$$\alpha = (p_1 \quad p_2 \quad 0 \quad 0 \quad p_3 \quad 0 \quad 0 \quad 0 \quad 0) \tag{5}$$

$$T = \begin{pmatrix} -\mu_1 & 0 & 0 & 0 & 0 & 0 & 0 & 0 & 0 \\ 0 & -\mu_2 & \mu_2 & 0 & 0 & 0 & 0 & 0 & 0 \\ 0 & 0 & -\mu_2 & \mu_2 & 0 & 0 & 0 & 0 & 0 \\ 0 & 0 & 0 & -\mu_2 & 0 & 0 & 0 & 0 & 0 \\ 0 & 0 & 0 & 0 & -\mu_3 & \mu_3 & 0 & 0 & 0 \\ 0 & 0 & 0 & 0 & 0 & -\mu_3 & \mu_3 & 0 & 0 \\ 0 & 0 & 0 & 0 & 0 & 0 & -\mu_3 & \mu_3 & 0 \\ 0 & 0 & 0 & 0 & 0 & 0 & 0 & -\mu_3 & \mu_3 \\ 0 & 0 & 0 & 0 & 0 & 0 & 0 & 0 & -\mu_3 \end{pmatrix} \tag{6}$$

3 Results

We determine the empirical, K_{ij}, and parametric distributions, G_{ij}, for each transition $i \to j$ according to the procedure described above. The results indicated that the selected linear combination of three Erlang distributions presents a good approximation to the empirical distribution.

As we want to calculate the first passage distribution of transition from state 0 to state 2, we start computing the *transmittance* of the three transitions in the graph (see Figure 1b), which is the product $p_{ij}\mathcal{T}_{ij}$. Note the Laplace transform (2) for each F_{ij} is computed with the vector α and matrix T in the mixture of three Erlang distributions (5)-(6). On the other hand, the estimation of the probabilities p_{ij} is based on the sample data: $p_{01} = 0.3967742$, $p_{02} = 0.02507837$ and $p_{12} = 0.03252033$.

Having calculated a *transmittance* for each transition $i \to j$, the objective is now to reduce the flowgraph model to a *single transmittance* for the first passage between the states 0 and 2. In our case, the possible path from state 0 to state 2 is $0 \to 2$ and, at the same time, $0 \to 1 \to 2$. For this we use two Manson's rules [3]:

- The transmittance of transitions *in series* is the product of the series transmittances. In our case is the path $0 \to 1 \to 2$. This means that

$$\mathcal{T}_{02}(s) = p_{01}\mathcal{T}_{01}(s)p_{12}\mathcal{T}_{12}(s) = 0.4\mathcal{T}_{01}(s)0.03\mathcal{T}_{12}(s) = 0.012\mathcal{T}_{01}(s)\mathcal{T}_{12}(s)$$

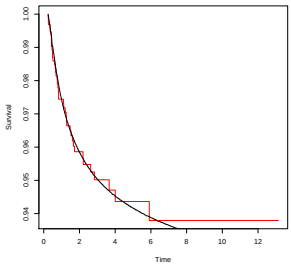

Figure 2: Survival function model for progression (*smooth line*) and empirical survival function for progression (*step function*). Time in years.

- The transmittance of transitions *in parallel* is the sum of the parallel transmittances.

  $$\mathcal{T}_{02}*(s) = p_{01}\mathcal{T}_{01}(s)p_{12}\mathcal{T}_{12}(s)+p_{02}\mathcal{T}_{02}(s) = 0.012\mathcal{T}_{01}(s)\mathcal{T}_{12}(s)+0.03\mathcal{T}_{02}(s)$$

  $\mathcal{T}_{02}*$ refers to the first passage from the state 0 to state 2, irrespective of the path.

Now we require the *inversion* of the Laplace transform $\mathcal{T}_{02}*(s)$ by means of a variant of the inversion algorithm EULER. In this way we can obtain the survival function with regard to *progression* jointly with the empirical survival function (Figure 2). We have obtained a parametric model to predict the probability of being free of *progression* at a given time.

References

[1] A. V. Huzurbazar and B. Williams. Incorporating covariates in flowgraph models: Applications to recurrent event data. *Thecnometrics*, 52:198–208, 2010.

[2] R. Pérez-Ocón and M. C. Segovia. Modeling lifetimes using phase-type distributions. In 3rd edition Taylor and Francis, editor, *Risk, Reliability and Societal Safety, Proceedings of the European Safety and Reliability Conference 2007 (ESREL 2007)*, 2007.

[3] S. J. Manson. Feedback theory-some properties of signal flowgraphs. In *ProcIRE*, 1953.

Data Mining and post-processing tools to extract comprehensible patterns from Venezuelan Financial Assets

D. Conti

Dep. of Operations Research, Universidad de Los Andes, Mérida, Venezuela

Consorzio Milano Ricerche, Milano, Italia

K. Gibert*

Dep. of Statistics and Operation Research, Universitat Politècnica de Catalunya-BarcelonaTech, Spain

Knowledge Engineering and Machine Learning Group, UPC, (Barcelona-Tech),Spain

October 20, 2013

1 Introduction

During the last years, mining of financial data is taking a remarkable importance to complement classical techniques used in financial fields [11], [10] describe underlying processes involved in these data. It is well known that Knowledge Discovery in Databases (KDD) provides a framework to support analysis and decision-making regarding complex phenomena [3]. One of the most popular KDD methods is Clustering [9].

In this paper, clustering techniques are used to find patterns on financial data related to assets of Venezuelan Stock Exchange (Bolsa de Valores de Caracas), which is a particularly complex market, where classical modelling techniques have shown poor performance [1] [4] [8]. Understandability of the provided model is discussed and compared with association rules mining results, as this is one of the first data mining techniques applied in the financial domain[11].

2 Case Study and previous work

This work is a collaboration between Bolsa de Valores de Caracas (Venezuela), Universidad de los Andes (Venezuela) and Universitat Polìtècnica de Catalunya-BarcelonaTech (Spain).

*e-mail: karina.gibert@upc.edu

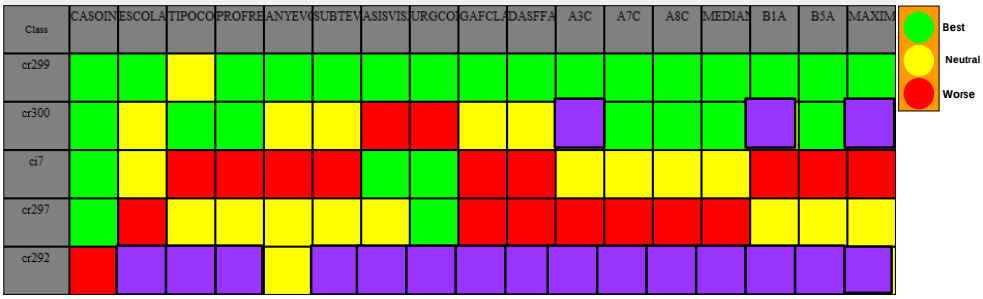

Figure 1: TLP describing the 5 clusters found.

As said before, data mining techniques are applied to find patterns on data provided by Bolsa de Valores de Caracas. The data refers the weekly variations in the price of 4 financial assets from Venezuela Stock Exchange (Bolsa de Valores de Caracas) considered relevant for the Venezuelan index (IGBC) and the two major indexes related to this market (Dow Jones-USA and BOVESPA-Brazil). Collected data corresponds to the period from January 1998 to April 2008. In particular, clustering techniques are used to find multivariate patterns describing the relationships among the venezuelan assets and both the internal and international indexes. A clustering in 5 classes is found.

3 Understanding patterns

It is well known that from a practical point of view, there is an important gap between the raw data mining results (including clusters) and effective decision-making activities [7]. Indeed, performing a clustering over a set of data requires an important process of understanding the underlying genesis of the clusters to be able to find the right decision/action to be associated to every cluster. Till now, only few works can be found addressing these issues.

TheTraffic Light Panel (TLP), introduced by Gibert in [6], is a symbolic postprocessing of the clustering results oriented to help the expert to better understand the clusters and to be able to identify domain concepts referred to the discovered classes. TLP was conceived to support the cluster's conceptualization, as a first bridge between clustering and effective decision-making. TLP proved to be extremely useful and well-accepted by domain experts in real applications from several domains, like mental health[6], health policy, water management[5], tourism or financial assets. In a previous work the TLP has been proved as a reliable goodness-of-clustering indicator[2].

The resulting TLP shows 5 clear patterns giving a realistic picture of the behaviour of the Venezuelan stock market (see Fig 1).

The patterns are directly understood by the experts, just looking at the TLP, as the color-coding is highly symbolic and do not requires extra explanation for non-technical users. A set of independent experts validated the results.

4 Discussion and Conclusions

In this work, the association rules analysis is compared with the process of clustering postponed by TLP use. It seems that using clustering provides some advantages: On the one hand, data can be analyzed in its original form, as no a priori discretization is required for the clustering. On the other hand, the association rules mining provides a set of 144 rules with minimum support 0.05 and minimum confidence 0.6 relating no more than 5 items among them, whereas the patterns provided by the clustering involve the whole set of available variables giving a more perspective and less fragmented picture of the Venezuelan stock market.

The patterns provided by the Clustering followed by TLP approach, identify both most frequent and most particular situations and provides a good insight on the behavior of the Venezuelan stock market where, the national index IGBC frequently evolves independently from Brazil and NY (all clusters except c359, the smallest one), and some internal assets can have less influence than expected to the national index (BPV).

Currently, temporal relationships among the discovered patterns are modelled to provide a qualitative framework to describe the dynamics of the process.

Acknowledgements

Authors wants to thank the Gerencia de Comunicación de la Bolsa de Balores de Caracas, Venezuela for its collaboration in the research. Also, Maria Elena Naranjo and Albany Sanchez for their collaboration in preprocessing and association rules mining. This research has been partially supported by the project AGAUR-2009-SGR 1365

References

[1] Conti D, Bencomo M, RodrÃguez A, Optimal investment portfolio determination by using non linear programming, Ciencia & Ingenieria, 26(2), 43-50, 2005

[2] Conti D, Gibert K (2012) The use of Traffic Lights Panel as a Goodness-of-Clustering Indicator: An Application to Financial Assets. In Artificial Intelligence Research and Development. Frontiers in Artificial Intelligence and Applications 248: 19-28 IOSPress

[3] Fayyad U, et al 1996: From Data Mining to Knowledge Discovery: An overview. In Advances in Knowledge Discovery and Data Mining. AAAI/MIT Press.

[4] Fu T, Chung F, Luk R, Ng C, 2007: Stock time series pattern matching: Template-based vs. rule-based approaches, Engineering Applications of Artificial Intelligence, 20(3),347-364

[5] Gibert K, D. Conti, D. Vrecko 2012 Assisting the end-user in the interpretation of profiles for decision support. An application to wastewater treatment plants: Environmental Engineering and Management Journal 11(5): 931-944

[6] Gibert K, A. García-Rudolph, G. Rodríguez-Silva 2008: The role of KDD Support-Interpretation tools in the conceptualization of medical profiles: An application to neurorehabilitation. Acta Informatica Medica 16(4) 178-182

[7] Gibert K, Rodríguez-Silva G, Annicchiarico R 2013: Post-processing: bridging the gap between modelling and effective decision-support. The Profile Assessment Grid in Human Behaviour. Mathematical and Computer Modelling 57(7-8): 1633-1639, Elsevier

[8] Hajizadeh E, Ardakani H, Jamal S, 2010: Application of data mining techniques in stock markets:A survey, Journal of Economics and International Finance Vol. 2(7), pp. 109-118.

[9] www.kdnuggets.com

[10] Kovalerchuk, B., Vityaev, E. 2010: Data Mining for Financial Applications. In: O. Maimon, L. Rokach (Eds.): The Data Mining and Knowledge Discovery Handbook. Springer 2005, pp. 1203-1224. Second edition

[11] Wiegend A., 1997 Data Mining in Finance. Report from the Post-NNCM-96 Wksh. on Teaching Computer Intensive Methods for Financial Modelling and Data Analysis, Proc. 4th NNCM-96 pp 399-411

Jump-diffusion term structure models: some results

L. Gómez-Valle *and J. Martínez-Rodríguez †

Departamento de Economía Aplicada, Facultad de CC. EE. y EE. Universidad de Valladolid, Avenida del Valle de Esgueva 6, 47011 Valladolid, Spain.‡

October 10, 2010

1 Introduction

In recent years there has been a growing body of literature that explicitly accounts for the presence of discontinuous jump components in many financial models (e.g.., see [1], [3], [4], [5]). For interest rates, jump-diffusion processes are particularly meaningful since the interest rate is an important economic variable, which is, to some extent, controlled by the government as an instrument for its financial policy. Discontinuous movements in interest rates are caused by several market phenomena such as money market interventions by the Federal Reserve. Moreover, empirical evidence suggests that interest rates exhibit substantial skewness and kurtosis, and therefore jump-diffusion interest rate models are more appropriate. However the relative scarcity of empirical work on models of discontinuous interest rates is most likely related to far less tractable mathematics involved in these models

The aim of this paper is to show a different approach for estimating the risk-neutral drift of a jump-diffusion interest rate stochastic process by means

*e-mail: lourdes@eco.uva.es

†e-mail: julia@eco.uva.es

‡This work was supported in part by the project VA191U13 of the Junta de Castilla y León and the GIR Optimización Dinámica, Finanzas Matemáticas y Utilidad Recursiva of the Universidad de Valladolid. J. Martínez-Rodríguez was also supported in part by the project of the Ministerio de Ciencia e Innovación MTM2011-25138.

of the slope of the yield curve in a term structure model. We will call this new approach GNEJ, General Nonparametric Estimation for Jumps. One advantage of this approach consists in the fact that the drift and the market price of risk associated to the brownian motion are jointly estimated and do not need to be individually specified and estimated. Finally, we apply this approach to US Treasury Bill data.

2 The term structure model

In this section, we briefly summarize a jump-diffusion term structure model with only one state variable. Let $(\Omega, \mathcal{F}, \mathcal{P})$ be a probability space equipped with a filtration $\mathcal{F}$ satisfying the usual conditions. The price of interest rate securities is driven by the instantaneous interest rate, which follows a mixed jump-diffusion stochastic process of the type:

$$dr(t) = \mu(r(t))dt + \sigma(r(t))dW(t) + J(r(t), Y(t))dN(t)(\lambda(t)), \tag{1}$$

where $\mu(r(t))$ is the drift, $\sigma(r(t))$ the volatility, $J(r(t), Y(t))$ is a function of the magnitude of the jump, $Y(t)$ which is a random variable, $dW(t)$ is the increment of a standard Wiener process and $N(t)$ represents a Poisson process with intensity $\lambda(t)$. Moreover, $dW(t)$ is assumed to be independent of $dN(t)$, which means that the diffusion component and the jump component of the short-term interest rates are independent of each other. We assume that jump size and jump arrival times are uncorrelated with the diffusion part of the process. We assume that μ, σ, λ, J satisfy enough technical regularity conditions: [6]. Under the above assumptions, the price at time t of a zero coupon bond maturing at time T, with $t \leq T$, can be expressed as $P(t, r; T)$. The bond is assumed to have a maturity value of one unit, i.e.

$$P(T, r; T) = 1. \tag{2}$$

We also assume that an equivalent martingale measure exists and all processes and expectations are understood as those under the equivalent martingale measures. The arbitrage-free pricing partial integro-differential equation is a follows:

$$\begin{aligned} P_t(t,r) &+ \left(\mu(t,r) - \theta^W(t,r)\sigma(t,r)\right) P_r(t,r) + \frac{1}{2}\sigma^2(t,r)P_{rr}(t,r) - rP(t,r) \\ &+ E_Y[P(t, r+J) - P(t,r)]\,\lambda(t)\theta^N(t,r) = 0, \end{aligned} \tag{3}$$

where θ^W and θ^N are the market prices of risk of Wiener and jump process, respectively.

3 Estimation technique

In this section, we prove a result which relates the risk-neutral drift of the model directly with data in the markets. Therefore, we propose an alternative approach to estimating more efficiently the coefficients of the partial integro-differential equation directly from data in the markets. For the estimation of these coefficients we obtain the following result.

Theorem 3.1 *Let $P(t,r;T)$ be solution to (3) subject to (2), and $r(t)$ follows a mixed jump-diffusion stochastic process given by (1), then*

$$\frac{\partial R}{\partial T}|_{T=t} = \frac{1}{2}\left((\mu(t,r) - \sigma(t,r)\theta^W(t,r)) + \theta^N(t,r)E_Y[J(r,Y)]\right). \qquad (4)$$

An analogous result, although for an diffusion process without jumps, is also shown in [2].

This theorem can be very useful. According to (4) the risk-neutral interest rate drift, which is the basis for the general asset pricing theory, is equal to the slope of the yield curve close to maturity. In order to implement Theorem 3.1 we rely on numerical differentiation to approximate the slope at the boundary of the time domain. Then, we use zero-coupon bond prices at points that are inside the time interval. Therefore, this allows us to estimate the drift of the risk-neutral interest rates which are unobservable.

4 Empirical analysis

In this section, we implement the GNEJ approach with US interest rate data and nonparametric kernel methods to reexamine the pricing of zero-coupon bonds in jump-diffusion models. We compare the results obtained with the GNEJ approach to the moment equations approach proposed by [3].

Daily data were obtained form the Federal Reserve h.15 database. The sample period covers from January 1971 to February 2013. First, we obtain the yield curves using the GNEJ approach and nonparametric kernel methods. Moreover, we assume two different jump size distributions: exponential and normal, which are very common in the interest rate literature. In order

Table 1: The RMSE of the yield curves for different maturity times

	6 months	1 year	2 years
GNEJ (Exponential)	$2.616e-3$	$4.610e-3$	$7.031e-3$
GNEJ (Normal)	$2.592e-3$	$4.514e-3$	$6.931e-3$
Johannes (2004)	$5.130e-3$	$9.222e-3$	$1.469e-2$

to estimate the risk-neutral drift of the interest rates we use (4) and a second order forward difference formula. Then, we also obtain the yield curves but with the approach proposed by [3] in order to make comparisons.

Table 1 shows the RMSE with the GNEJ approach and the model proposed by [3]. Notice that errors are considerably higher with [3] than with the GNEJ approach with both jump size distributions. They are even about twice as high for all the maturity range. Therefore GNEJ approach is efficient.

References

[1] S.R. Das, *The surprise element: Jumps in interest rates*, J. Econometrics. 106 (2002), pp. 27–65.

[2] L. Gómez-Valle and J. Martínez-Rodríguez, *Modelling the term structure of interest rates: An efficient nonparametric approach*, J Bank and Financ. 32 (2008), pp. 614–623.

[3] M. Johannes, *The statistical and economic role of jumps in continuous-time interet rate models*, J. Financ. 59 (2004), pp. 227–259.

[4] C. Mancini and R. Reno, *Threshold estimation of jump-diffusion models and interest rate modeling*, J. Econometrics. 160 (2011), pp. 77–92.

[5] S.K. Nawalkha, N. Beliaeva, and G.M. Soto, *Dynamic Term Structure Modeling*, John Wiley & Sons, Inc. 2007.

[6] B. Øksendal and A. Sulem, *Applied Stochastic Control of Jump Diffusions*, Springer-Verlag, Berlin, Heidelberg, 2005.

Using the energy rating software for mathematical modelling of the costs of construction and energy in a simulated home

M. J. Ruá*,[*] and N. Guadalajara†

(*) Universitat Jaume I, Castellón de la Plana, Spain

(†) Centro de Ingeniería Económica, Universitat Politècnica de València, Spain

1. Introduction

The building industry is becoming very important in sustainable development. The recently developed policies in European Union directives on energy and their transposition to Spanish regulations make the Energy Performance Certification process for buildings mandatory. Two software tools have been developed in Spain to carry out this process: on the one hand, Lider v.01, for compliance with minimum energy demand limits; on the other hand, Calener-VYP, v1.0 (version for residential buildings) to obtain the energy performance (energy efficiency label as specified in RD 47/2007) and the CO_2 emissions of the simulated dwelling .

These software programmes were developed by the Thermotechnics Group of the School of Industrial Engineers at the University of Seville for the Institute for Energy Diversification and Saving (IDAE) of the Spanish Ministry of Industry, Tourism and Trade. Software Lider v1.0 and Calener-VYP v.01 are the Spanish versions of DOE-2.2. This is the most commonly used simulation engine for this purpose that offers a detailed description of the building.

Firstly, the thermal envelope of the building has to be described in detail when using Lider. This is composed of all the enclosures that limit living spaces with the external environment (air, ground or another building) and all the internal partitions that limit habitable spaces with no habitable spaces which, in turn, come into contact with the external environment. A building modelled in Lider can be exported to the Calener-VYP programme, where the energy performance level is obtained after entering the facilities needed for heating, cooling, DHW and air-conditioning (Calener-GT is the programme for commercial buildings and it also considers lighting). New buildings are assigned an energy rate on a scale of five values indicated by letters A to G, with A being the best rating. According to RD 47/2007, new buildings are assigned a label that indicates their energy rate which corresponds to this scale. These ratings are based on annual emission values in kg of CO_2 and on the annual primary energy consumption in kWh depending on: type of building; thermal envelope; climatic zone; the municipality in which the building is located; heating and cooling facilities; minimum solar contribution to the domestic hot water (DHW) required in the municipality. New buildings that meet the CTE must have an E grade or above, while lower F and G grades can be used in existing buildings.

These software tools have been used in this paper to simulate energy performance in new semidetached houses after taking into account the thermal envelope of the building

*email: rua@uji.es

and facilities. This has been done in every climatic zone in Spain and for all the possible energy ratings, obtaining 50 configurations combining energy performance and the climatic features. These configurations present different combination of materials, constructive solutions and facilities. From every configuration, depreciation costs, maintenance costs, energy consumption cost, during the service life of a house, have been estimated (with 2010 prices). These have been considered as private costs.

2 Methodology

To obtain depreciation cost, the investment cost is calculated by drawing up an estimation or budget with the chosen configurations. Besides, an estimation of the service life of the different elements making up the building has been done [1-4]. This allows the cost per year to be estimated, being the depreciation cost. Prices are obtained from the Cype S.A. database for construction prices.

The maintenance cost is calculated from 45 maintenance routines, each with a different periodicity.

For the energy consumption cost, three types of energy have been considered for heating and hot water, which are electricity, natural gas, and biomass. Only electricity is used for cooling. The electricity and gas rates were obtained from the Spanish Official State Gazette (BOE 31.12.09). If official rates were absent, biomass prices including delivery were obtained as the market price averages from various suppliers.

On the other hand, the simulation software Calener allows obtaining an energy performance level or energy rating. This rate is directly linked with the CO_2 emissions per year and per square meter for the simulated building.

From the obtained data, mathematical models to express private costs components and CO_2 emissions were developed by a multiple regression analysis using ordinary least squares. The dependent variables are: annual depreciation cost per square meter, annual maintenance cost per square meter, annual energy consumption cost per square meter and annual CO_2 emissions per square meter. The explanatory variables are: energy performance level and the climatic zone, quantified by the average annual temperature

3. Results

According to the results, the average temperature significantly explains depreciation, maintenance, energy consumption and CO_2 emissions.

The depreciation cost model indicates that the depreciation cost will increase by 1.34, 2.40 and 3.26 €/m^2 for energy performances C, B and A, respectively. The maintenance costs model reveals that there are no differences for the various energy ratings. The initial cost of €16.93/m^2 lowers by €0.381/m^2 for each degree of increased temperature in the climatic zone. Temperature explains up to 49% of maintenance cost variability. Maintenance work differs only slightly between the ratings as many operations are the same; i.e., painting, fire prevention, audiovisual, or ventilation facilities, etc. The cost of energy model indicates that temperature and energy ratings C, B and A explain 79% of the value obtained. In this case, and as expected, the cost of energy consumption decreases in warmer areas.

Finally, CO_2 emissions model shows that all the variables together explain 86.6% of the variability of emissions and have negative coefficients. This means that warmer areas

have lower emissions and that these emissions decrease as the energy rating improves. The maximum emission is 61.55 kg per year for ratings D and E, which decreases at a rate of 1.862 kg for each degree of increased temperature; and is 11.96, 20.19 and 28.80 kg for ratings C, B and A, respectively.

Standardized residuals were analyzed in comparison to the established prognostic values to test the linearity and homoscedasticity of the models.

4. Conclusions

Basic mathematical models can be an excellent application to get conclusions from real data in architectural and technical contexts. According to this study, more energetically efficient dwellings imply higher costs for users. According to the model developed for CO_2 emissions, there is a clear decline in emissions as energy performance improves. From the economic or private viewpoint, a rational purchaser will buy more economic dwellings, and possibly less energy-efficient ones. However, energy savings and lower environmental pollution costs for society favour the promotion of energy-efficient dwellings.

References

[1] Davies H., and Wyatt D. Appropiate use or method for durability and service life prediction *Building Research and Information*, 32: 552-553, 2004.
[2] Johnstone I.M. Energy and mass flows of housing: a model and example *Building and Environment*, 36: 27-41, 2001a.
[3] Johnstone I.M. Energy and mass flows of housing: estimating mortality *Building and Environment*, 36: 43-51, 2001b.
[4] Rudbeck C. Service life of building envelope components: making it operational in economical assessment *Construction and Building Materials*, 16: 83-89, 2002.

Kernel Spectral Clustering for Identifying Vulnerable Areas of Biofilm Development in Drinking Water Distribution Systems

J.A. Gutiérrez-Pérez[†] [*], E. Ramos-Martínez[†], M. Herrera[‡]
J. Izquierdo[†], and R. Pérez-García[†]

([†]) Fluing–Institut for Multidisciplinary Mathematics (IMM), Universitat Politècnica de València,
C. de Vera s/n, 46022, Valencia (Spain),

([‡]) BATir–Université libre de Bruxelles,
Av. F. Roosevelt, 50 CP 194/2 B-1050 Brussels (Belgium).

November 30, 2013

1 Introduction

Biofilm develops in drinking water distribution systems (DWDSs) as layers of microorganisms bound by a matrix of organic polymers and attached to pipe walls. The presence of biofilm can decrease the water quality and increase operational problems in DWDSs. One of the main objectives in the quality control of DWDSs is the analysis of development of biofilm in the distribution network, discovering areas more prone to it. To achieve this aim we resorted to graph spectral methods and we introduce a methodology based on kernel spectral clustering [1] to divide the DWDS according to its vulnerability to a high biofilm development. An eigenvector selection based on entropy measures attempts to adapt the spectral clustering to the underlying data information better than the usual Ng-Jordan-Weiss (NJW) proposal [2]. Both the scale parameter of the Laplacian matrix and the weights of the

[*]e-mail:joagupre@upv.es

kernel combination, are tuned by a new approach based on multistart trust-regions. This alternative searches the best combination of parameters for achieving spectral clustering under some optimality condition.

2 Tuning kernel spectral clustering process

In the first instance, we define a kernel matrix K that captures the semantics inherent to the graph structure and where the spectral clustering takes place. The Table 1 shows the process steps.

Table 1: Kernel embedding process

1. Build the affinity matrix $A \in \mathbb{R}^{n \times n}$
defined by $A_{ij} = exp\left(-\frac{||x_i - x_j||^2}{2\sigma^2}\right)$ if $i \neq j$ and $A_{ii} = 0$.
2. Define D to be the degree diagonal matrix whose (i, i)-element
is the sum of the entries in A's ith row.
3. Build the Laplacian matrix $L = I - D^{-1/2}AD^{-1/2}$.
4. Embed into a kernel space the Laplacian and dissimilarity matrices
associated with the problem.
5. $K = w_{Lap}K_{Lap} + \sum_{i \in I} \omega_i K_i$

Each ω_i (step 5) allows to give different importance to each dissimilarity matrix, K_i $(i \in I)$, involved in the performance of K.

In summary, we have to choose the following key parts of the kernel spectral clustering: the σ parameter, the weights ω_i, $(i \in I)$ and ω_{Lap} associated with the Laplacian, and finally, the eigenvector selection.

To selecting possible values for σ, the proposal is to calculate a local scaling parameter for each data point x_i. Thus, the local scale, σ_i, can be estimated as $\sigma_i = d(x_i, x_k)$.

To find the eigenvector selection, we propose entropy measures [3]. We utilize $V \in \mathbb{R}^{n \times n}$ to denote the matrix consisting of all the eigenvectors of the kernel matrix K. Thus, the entropy of V is defined as follows:

$$E = -\sum_{v_i \in V} \sum_{v_j \in V} E_{ij} = -\sum_{v_i \in V} \sum_{v_j \in V} [s_{ij} log(s_{ij}) + (1 - s_{ij}) log(1 - s_{ij})] \quad (1)$$

where $Dist_{ij}$ is the distance between v_i and v_j, s_{ij} is the similarity between two points v_i and v_j, and is given by $s_{ij} = e^{-Dist_{ij}}$.

Moreover, we are interested in tuning weights and parameters within other optimization process (clustering in this case), so we propose to apply derivative-free optimization algorithms. The basic algorithm starts selecting m regions of the parametric space (trust-regions). These trust regions are specified with a center point and radius r. The rule for redefining these trust-regions depends on the average silhouette width (ASW) [4].

3 Case study

In order to apply the methodology exposed we considered a real case, the DWDS of the central area of Celaya, Mexico. The network is made out of 479 lines and 339 nodes and its total pipe length is 42.5 km. Besides the common hydraulic parameters (pipe length, pipe diameter, roughness, flow velocity, losses and friction factor) we have also introduced in the analysis the pipe age and pipe material. The better clustering configuration is selected by the criterion of maximum ASW, which reaches to 0.32.

Once applied the spectral clustering we obtained 3 well differentiated clusters (Figure 1). The two clusters associated with metal pipes, also correspond to the clusters with the oldest pipes. One cluster corresponds mostly to 50 years old cast iron pipes while the other to 40 years old galvanized iron pipes. Thus the first cluster would be the most prone to biofilm development. In contrast, the third cluster, integrated mostly by 30 years old asbestos cement pipes, would be the one with less risk of biofilm development when comparing it with the other clusters.

4 Conclusions and future work

This paper provides an innovative approach to knowing the relative trend to biofilm development in the different areas within a DWDS. The implementation of this instrument could facilitate and increase the effectiveness in biofilm control and mitigation policies by replacing and/or renewing the most vulnerable and problematic areas or pipes of the distribution system.

The kernel spectral clustering process has been tuned by a new methodology based on multistart trust-regions. This tuning method has been pro-

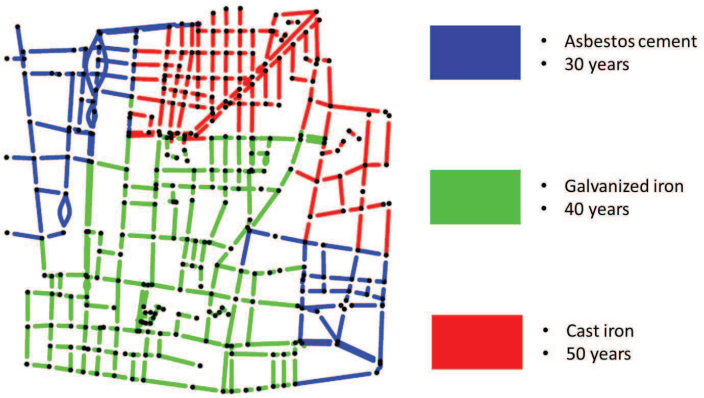

Figure 1: Obtained sectorization after kernel spectral clustering analysis

posed along with an interesting option for estimating the scale parameter of the Laplacian matrix by a k-nearest-neighbors approach and an eigenvector selection based on entropy measures with better detection ability than the usual NJW method.

Further research will be focused in a deeper understanding, from a more hydraulic point of view, if cluster homogeneity remains when the distribution system is repaired and new pipes of different materials are introduced within DWDS areas constructed long time ago.

References

[1] Herrera, M.; Canu, S.; Karatzoglou, A.; Prez-Garca, R.; Izquierdo, J., An approach to water supply clusters by semi-supervised learning. in: International Environmental Modelling and Software Society (iEMSs) 2010.

[2] Ng. A.; Jordan, M.; Weiss, Y. On spectral clustering: Analysis and an algorithm, *NIPS*. 2001, *14*, 849-856.

[3] Xiang, T.; Gong, S. G. Spectral clustering with eigenvector selection, *Pattern Recognition*. 2008, *41(3)*, 1012-1029.

[4] Rousseeuw, P. J. Silhouettes: a graphical aid to the interpretation and validation of cluster analysis, *Computational and Applied Mathematics*. 1987, *20*, 53-65.

A S.E.M. for analysis of factors associated with the choice of degrees at UPV

A. Antonio Hervas[♭] [*], B. Joan Guardia[†], C. Maribel Pero[†]
D. Roberto Capilla[‡] and E.Pedro Pablo Soriano[♮]

(*) Instituto de Matematica Multidisciplinar (IMM) (‡) Departamento de Ingenieria Electronica,

(♮) Universitat Politecnica de Valencia,

(†) Institut de Recerca en Cervell, Cognicio i Conducta (IR3C),

Universitat de Barcelona,

November 30, 2013

1 Introduction

The question of which factors determine a student's selection of university and degree course has been the subject of debate for some time. This issue has also been raised in Europe, where the universities have found that new students are highly motivated but are somewhat lacking in the necessary capacities. The European Access Network (EAN) (www.ean-edu.org) for example has been very active in this field. In the USA the tradition is very similar with the "slight" difference that recruitment systems are supposedly competitive, but are ultimately based on the financial resources of prospective students, very different from our policy of scholarships and student grants. In our system grants play a social role, while in the USA there is a policy of recruiting talent. Other studies, such as Capilla im http://riunet.upv.es/handle/10251/5767, [2] and [3], also see the demand for a university course as a very non-specific assessment of the "social value" given to the degree and also to the university. This more qualitative or more

[*]e-mail:ahervas@imm.upv.es

subjective perception is constructed from certain parameters which must be carefully analyzed.

The Spanish public university admittance system is a relatively simple one. Those students who have successfully passed high school and also a common university entrance exam, known as the Prueba de Acceso a la Universidad (PAU), can apply for a place at any university in the public system. The access grades of students considered for admittance consist of a weighted linear combination of the average grade of all high school subjects and the average marks of subjects taken in the PAU. The system of access grades means that all students seeking a place at a public university can be ranked from the highest rating to the lowest and that places can be systematically assigned according to the preferences of the students. This ensures that no student gets a place in the public system with a lower entrance grade than another student who would not have been admitted to the same degree course.

The main objective of this work is to verify a multivariate model based on the principles of the structural equations model (SEM), which analyzes the impact of the different variables and factors identified by the bibliography as linked to the decision process on university degree courses, in the Universitat Politecnica de Valencia (UPV) The study was carried out on various cohorts of freshmen students enrolled for the first time in the Spanish university system in the academic years 2010-2011 and 2011 - 2012 and formed part of a larger project which analyzed the decision process in other areas of knowledge.

2 The structural model

The structural relationships used in the analysis were based on the structural model (SEM) proposed by Guardia et al in [4], which obtained good fits of the structural model shown in the figure below as applied to a psychology degree course.

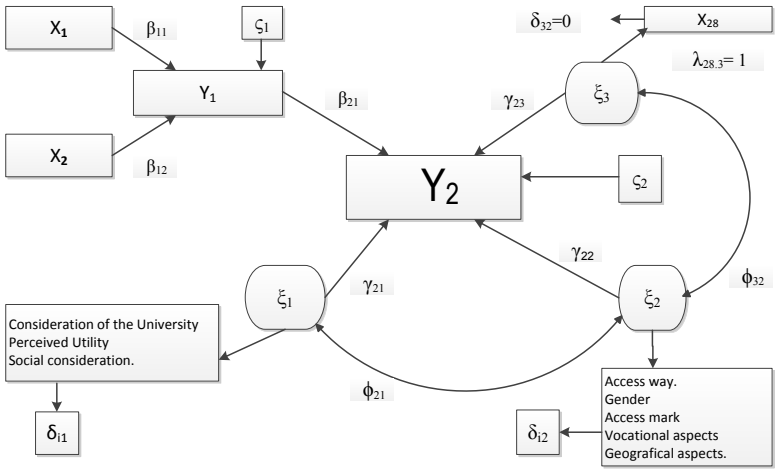

The structural equations that can be specified from figure are as follows:

$$Y_1 = \beta_{11}X_1 + \beta_{12}X_2 + \zeta_1 Y_2 = \beta_{21}Y_1 + \gamma_{21}\xi_1 + \gamma_{22}\xi_2 + \gamma_{23}\xi 3 + \zeta_2. \quad (1)$$

we considered the following statistical assumptions for quantitative variables $E(X_i) = E(Y_i) = E(\xi_i) = 0$ and $Var(X_i) = Var(Y_i) = Var(\xi_i) = 1$. Consequently, all quantitative variables were transformed by reduction and standardization, and similarly $E(\epsilon_i\varepsilon_j) = E(\delta_i\delta_j) = E(\eta\varepsilon) = E(\xi\delta) = E(\zeta_i\zeta_j) = 0$; assuming initially that the errors of measurement were uncorrelated with each other, as in the case of the observable and latent variables. Four accidental samples were obtained (n = 2244) composed of undergraduate students doing different degree courses at the UPV. The UPV sample consisted of 265 students enrolled in Social Science degree programs (12%), 189 in experimental sciences and health (8%), and the rest (80%) were engaged in engineering studies, the fundamental faculty at the UPV. In engineering, the percentage of women is much lower than usual, ranging from 15% to 30%. This paper is focused exclusively on engineering students (n = 1790). Ages ranged from 18 to 21 in all samples, so that there was wide homogeneity in the distribution (M = 18.77; SD = 0.38). The students tended to come from the technical areas of the Baccalaureate (98% from Science and Technology

and the residual 2% from other branches). The cut-off mark ranged from 5 to 12.96 , reaching M = 8.12 and SD = 1.52, but with a very skewed distribution towards the tail on the right. Each student was administered the questionnaire proposed in (http://riunet.upv.es/handle/10251/30128) which showed good values for reliability and validity. The questionnaire variables related to access was divided into two second order factors (social and individual) defined by six primary factors: Consideration of the University; Perceived Utility and Social Considerations as social factors. The primary factors were: Vocational Aspects; Influence of Geographical Location for the individual factor, including the Access Grade, Method of Access and Gender. In the initial study, Cronbach's α values ranged between .84 and .95 for all factors. The factorial validity analysis carried out with confirmatory factor analysis also showed a good fit that confirmed the structure of the factors described ($\chi^2 = 1234.74; p = .18$). In addition to the variables included in the questionnaire, data were obtained from institutional variables, i.e. cut-off marks, places offered in the academic years considered, numbers of students enrolled in each degree course, etc.

3 Conclusions

The first issue to highlight has to do with the adjustment values of the models analyzed; while the fit of the 2 statistic was not particularly good, we consider that the general model proposed to explain the demand for the students' first choice in engineering studies at the UPV under the Spanish public system could be a suitable model. This conclusion is based on the fact both in the case of the overall adjustment of the UPV total and in the adjustment for the different engineering courses, the adjustment rates are good, since the values of GFI, AGFI, BBNFI, BBNNFI, or IFC indices are over .90 and in some cases more than .95. The SRMR values are lower than .011 and SRMSE values are below .005. These indices are acceptable when they are superior to .90 , also the $\chi^2/dfratio < 2$ indicates an excellent fit, $\chi^2/df < 3$ a good fit, and in our case for all the models fitted these ratio are lower than 3.

It can also be pointed out that in general the hypothesized parameters in the model are statistically significant in all cases, which is another argument in favor of the proposed model's ability to explain the demand for the first choice of university degree courses. All the estimated values are statistically significant with a confidence level of 95%.

References

[1] Murphy,P.E. and McGarrity,R.A. Marketing Universities:A Survey of Student Recruitment Activities. *College and University*,53,3,249-6.1978.

[2] Huang, Sh. and Fang, N. Predicting student academic performance in an enginnering dynamics course: A comparison for four types of predictive mathematical models. *Computers & Education*, 61, 133-145.2013.

[3] Veenstra, C.P.; Dey, E.L. and Herrin, G.D. . Is modeling of freshman engineering succes different from modeling of non-engineering succes? *Journal of Engineering Education*, 467- 479.2008.

[4] Guardia, J.; Pero, M.; Hervas, A.; Capilla, R.; Soriano, P,P. & Porras, M. Factores asociados con la decision de cursar estudios universitarios de Psicologia. Una aproximacion mediante modelos de ecuaciones estructurales. *Anuario de Psicologia*, 42 (1), 87-104.2012.

Semi-automatic segmentation of IVUS images for the diagnosis of cardiac allograft vasculopathy

D. Ginestar[†], J. L. Hueso[†] [*], J. Riera[†], I. Sánchez-Lázaro[‡]

([†]) Instituto Universitario de Matemática Multidisciplinar,

Universitat Politècnica de València.

([‡]) Hospital La Fe Universitari i Politècnic.

November 30, 2013

1 Introduction

Cardiac allograft vasculopathy (CAV) is the major cause of late death in patients undergoing heart transplantation. It is manifested by a unique and unusually accelerated form of coronary disease affecting both intramyocardial and epicardial coronary arteries and veins [1].

The most validated method for the diagnosis of CAV is intravascular ultrasound imaging (IVUS), a relatively new medical tool that consists of placing a catheter with a sensor inside the artery. This sensor rotates as it emits pulses of ultrasound. When it receives the echoes the tissues return, it generates an image like the one shown in the figures bellow.

Automatic processing of large IVUS data sets represents an important challenge due to ultrasound speckle, catheter artefacts or calcification shadows. Moreover, a typical IVUS acquisition contains several hundred of images making nonautomatic analysis of the data long, fastidious and subject to intraobserver and interobserver variabilities. These could be serious constraints against the clinical usage of IVUS.

[*]e-mail: jlhueso@mat.upv.es

Usual techniques addressing segmentation of vessel borders rely on a single local image descriptors of edges. Energy minimization contour-based techniques either guide a snake towards the target structures or minimize a cost function. A common inconvenience of segmentation based on contour detection is that it requires some kind of image filtering to avoid fake responses. Recent approaches use either a probabilistic framework or classification strategies to better characterize coronary structures. Here a simple supervised method for the IVUS images segmentation is proposed that is mainly based on two steps, first the intima border is detected by preprocessing the image to enhance the contours information and a snake is used to determine the border. This determines a region of interest and, in this region, a classifier is used to distinguish between the lumen and the plaque. To use the method it is necessary the segmentation by an expert of the first IVUS image and the following images are segmented automatically.

2 Vessel segmentation

IVUS images are quite noisy, so a noise reduction filtering has been considered. Particularly, a median filter is used.

To find the main edges present in the image a Canny's filter has been applied [2]. A typical output of the Canny's filter applied to an IVUS image is shown in Figure 1.a), where part of the media-adventitia border is recovered.

A snake model is used to close the contour of the vessel. The model used is a parametric active contours [3], which synthesizes parametric curves within an image domain and allows them to move toward the edges drawn by internal and external forces.

The particular snake used in this work is based on the gradient vector flow (GVF) field [3]. Figure 1.b) shows an example of snake that adjusts the vessel contour.

Once the the intima border has been obtained the inner part of the vessel is considered as a region of interest. The pixels of this region are classified in in two groups or categories corresponding to the lumen and the plaque, using a linear discriminant analysis classifier.

The result of the classification is a binary image, the mask, which must be smoothed in order to obtain likely shapes for the lumen and plaque. The final result determines the plaque and lumen zones in the vessel, which are measured in order to obtain a quantitative information. By performing these

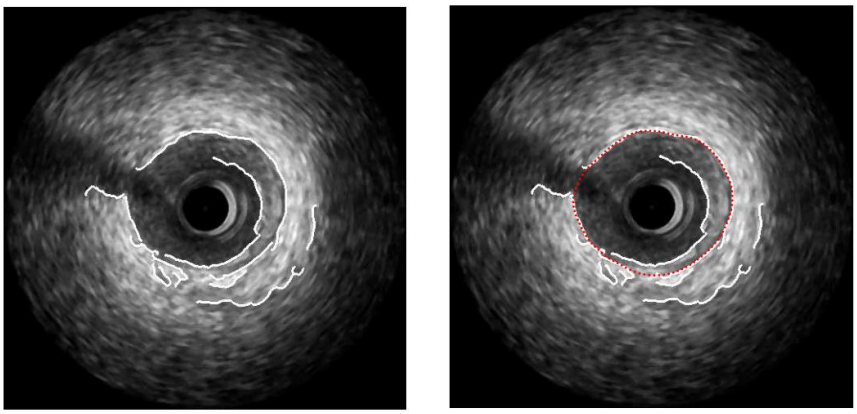

Figure 1: a) Borders obtained by Canny's method. b) Snake closing the contour.

operations on successive frames of the IVUS sequence, one can estimate the volume of the plaque along the vessel, which is of interest for the diagnosis of CAV.

3 Ivus analysis

The IVUS images were acquired using a iLab(R) (Boston Scientific Corp., Natick, MA, USA) with a catheter model Atlantis. The ultrasound frequency was 40MHz and the catheter pull-out speed was 0.5 mm/s. A sequence of 23 IVUS images was manually segmented by an expert who drew by hand the vessel and plaque contours and used a software to measure them. We have performed our analysis on the same sequence and have compared qualitative and quantitatively the results. Figure 2 shows the segmentations of two frames by the expert and by our software. In order to assess the performance of our software, we have compared the vessel and lumen areas of the analyzed sequence.

The differences of both measurements are normally distributed, specially the vessel area differences. The t-test reveals no significant differences between the expert and the software measurements. In order to visually assess the suitability of the software measurements, we present the Bland-Altman plots for the vessel and lumen areas obtained in both ways. In the diagram

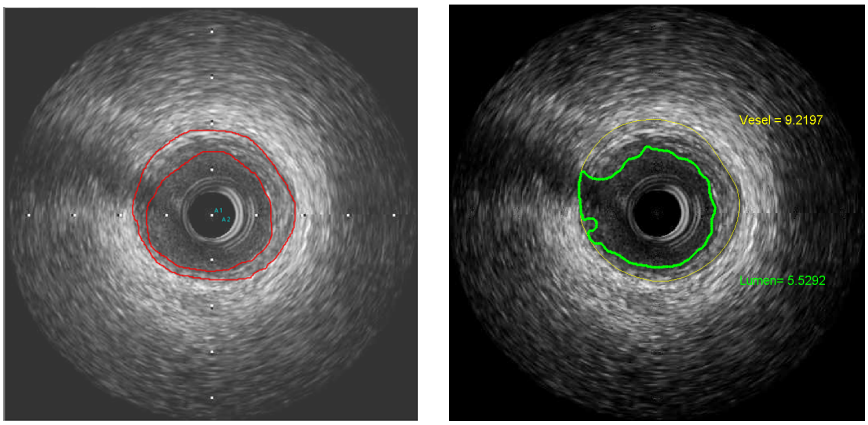

Figure 2: Left: expert segmentation. Right: software segmentation

corresponding to the vessel areas, shown in Figure 3, it can be observed that the deviation is bigger for high values of the average, which correspond to frames where the vase section is not well defined. The differences lie between the lines corresponding to the mean value plus or minus 1.96 times the standard deviation (the 95% confidence interval), except for two outliers.

4 Conclusions

We have presented a semi-automatic procedure for segmenting IVUS images of the coronary artery that is of interest in the diagnosis of cardiac allograft vasculopathy. The procedure has two phases. In the first phase, the vessel contour is detected. In the second phase, the interior of the vessel is segmented, identifying and measuring the lumen and the plaque. With the result of successive segmentations, a volumetric estimation of the vessel occupations is obtained, which is of interest for the diagnosis.

The procedure has to be supervised from time to time, in order to avoid an erroneous detection of the vessel, which would cause meaningless results in the segmentation phase. The variations in intensity or contrast in the images can also require and adjustment in the classification criteria. The minimization of these limitations will be the object of our future work in the area.

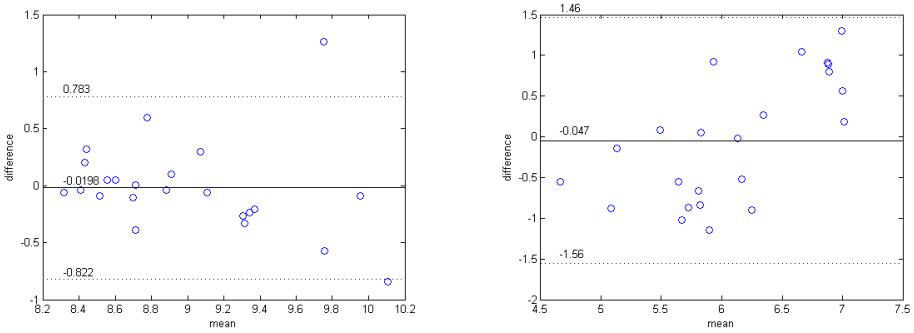

Figure 3: Bland-Altman diagram for the vessel (left) and lumen area (right) measurements.

5 Acknowledgements

This research was supported by Ministerio de Ciencia y Tecnología MTM2011-28636-C02-02 and by Vicerrectorado de Investigación, Universitat Politècnica de València PAID-SP-2012-0498.

References

[1] M. Weis, W. von Scheidt, Cardiac Allograft Vasculopathy. A Review, *Circulation*, 96: 2069–2077, 1997.

[2] J. Canny, A Computational Approach to Edge Detection, *IEEE Transactions on Pattern Analysis and Machine Intelligence*,Vol. PAMI-8(6): 679–698, 1986.

[3] C. Xu, J.L. Prince, Snakes, Shapes, and Gradient Vector Flow, *IEEE Transactions on Image Processing*, 7(3): 359–369, 1998.

[4] L. Cohen, On active contour models and balloons. *Computer Vision, Graphics, and Image Processing: Image Understanding*, 53(2): 211–218, 1991.

[5] R.O. Duda, P.E. Hart, D.G. Stork, Pattern Classification. 2nd Edition. John Wiley & Sons, Inc. New York, 2001.

Analysis of noise for the Sparse Givens method in CT medical image reconstruction

A. Iborra[†,*], M. J. Rodríguez-Álvarez[‡], A. Soriano[‡], F. Sánchez[‡], M. D. Roselló[†], P. Bellido[‡], P. Conde[‡], E. Crespo[‡], A. J. González[‡], L. Hernández[‡], F. Martos[‡], L. Moliner[‡], J. P. Rigla[‡], M. Seimetz[‡], L. F. Vidal[‡], and J. M. Benlloch[‡]

([†]) Instituto de Matemática Multidisciplinar (IM2),

Universitat Politècnica de València, Camino de Vera s/n E 46022 Valencia (Spain).

([‡]) Instituto de Instrumentación para Imagen Molecular (I3M),

Universitat Politècnica de València, Camino de Vera s/n E 46022 Valencia (Spain).

November 26, 2013

1 Introduction

Computed Tomography (CT) systems can be modeled as linear systems of equations $Ax = b$ [1], where $A \in \mathbb{R}^{m \times n}$ represents the CT system response (mainly geometry and detector efficiency) [2], $x \in \mathbb{R}^n$ represents the unknown object scanned and $b \in \mathbb{R}^m$ represents CT measurement. Each one of the n elements of $x \in \mathbb{R}^n$ is called *voxel* where n is limited by the spatial resolution of the system. m depends on the number of projections and pixels in the detector. In general, model parameters generate systems such that $m \geq n$ and therefore these systems do not always have an exact solution. QR decomposition can be used to solve these kind of systems because its solution x satisfies $\min \|r\|_2 = \min \|Ax - b\|_2$ [3].

In practice what it is obtained when a measure is carried out with a CT is $\hat{b} = b + \delta b$ which is a perturbation of the expected CT measurement,

[*]e-mail: amibcar@upv.es

according to the CT system response represented in A. In this way we obtain a reconstructed image $\hat{x} = x + \delta x$ which is a perturbation of the real scanned object.

The size of perturbation on the reconstructed image $\frac{\|\delta x\|_2}{\|x\|_2}$ and the size of perturbation on the CT measurement $\frac{\|\delta b\|_2}{\|b\|_2}$ are related by the condition number bound $\frac{\|\delta x\|_2}{\|x\|_2} \leq \kappa(A)\frac{\|\delta b\|_2}{\|b\|_2}$ [4]. The size of perturbation on the reconstructed image $\frac{\|\delta x\|_2}{\|x\|_2}$ is equivalent to its relative error $\frac{\|x-\hat{x}\|_2}{\|x\|_2}$. Therefore it is possible to rewrite this bound in terms of the relative error of x

$$\frac{\|x - \hat{x}\|_2}{\|x\|_2} \leq \kappa(A)\frac{\|\delta b\|_2}{\|b\|_2} \tag{1}$$

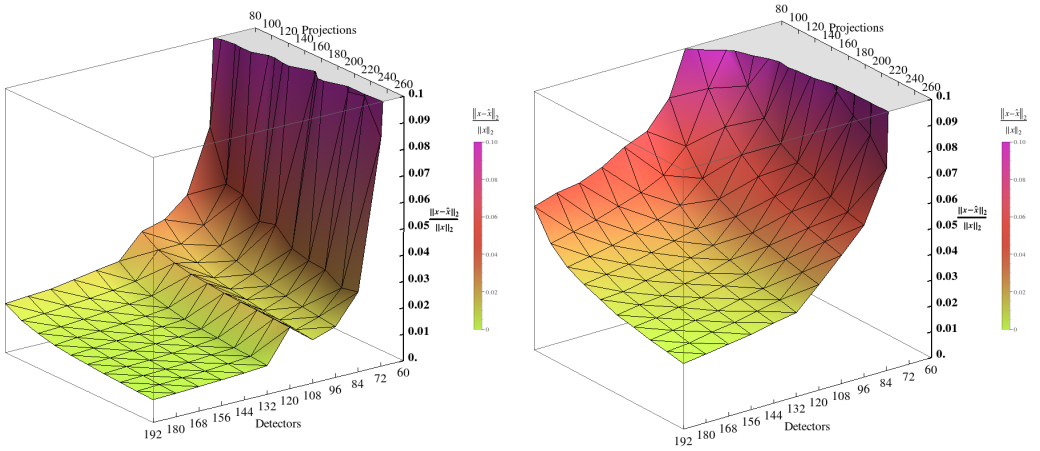

(a) 1% measurement perturbation. (b) 3% measurement perturbation.

Figure 1: Mean relative errors for image reconstructions with different levels of CT measurement perturbations.

2 Results and Conclusions

In order to determine the relationship between the relative reconstruction errors and the different CT model (of Albira μCT described in [5]) parameters, the same phantom (a PMMA cylinder with inserts of different materials which model adipose tissue, organs tissue and soft bone) was reconstructed

with projections varying from 80 to 260. The detector pixels varied from 60×60 to 192×192 and CT measurement perturbations varied from 1% to 10%. The CT measurement perturbation has a random component, so each combination of the above parameters has been repeated ten times. Mean relative errors of phantom image reconstructions, for each combination of parameters with 1% and 3% measurement perturbation are shown in figure (1).

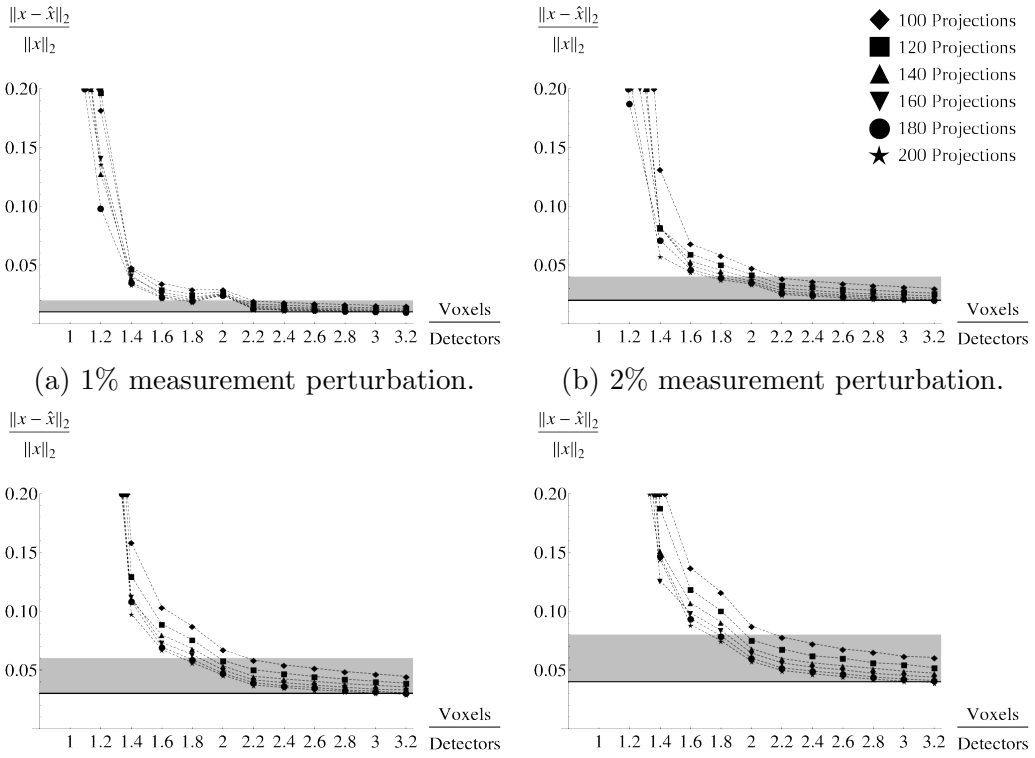

(a) 1% measurement perturbation.

(b) 2% measurement perturbation.

(c) 3% measurement perturbation.

(d) 4% measurement perturbation.

Figure 2: Mean relative errors of reconstructions for different $\frac{voxelsize}{detectorsize}$ ratios and number of projections. A horizontal line shows the level of CT measurement perturbation in each case and the shaded area represents the relative errors below the bound (1) derived from $\kappa_2(A) = 2$.

Figure (2) shows the mean relative errors of some of the reconstructions and the bound (1) derived from $\kappa_2(A) = 2$. A $\kappa_2(A)$ value of unity will represent the *ideal* situation where the error in the measurement transates

exactly to the same amount in the reconstructed image. The mean errors that are at least twice the measurement perturbation are left under this bound. For values of $\frac{Voxels}{Detectors}$ above 2.2, the system matrix has a condition number such that its mean of relative errors stays below this bound.

Similar results have been obtained with the rest of system configurations and perturbed measurements. It may therefore be concluded that if the system matrix is built with a relation $\frac{Voxels}{Detectors} \geq 2.2$ its condition number will be low and the noise in the reconstructed image will be similar to the perturbation in the CT measurement.

The quality of CT image reconstruction based on QR decomposition by Givens rotations does not mainly depend on the number of projections of the CT measurements. This allows reconstructions to be modeled with a high number of pixels on the detector, which is widely exceeded in modern CT systems, and a low number of projections, which reduces the CT scanning time and radiation dose received by the patient.

References

[1] María-José Rodríguez-Álvarez, Filomeno Sánchez, Antonio Soriano and Amadeo Iborra. Sparse Givens resolution of large system of linear equations: Applications to image reconstruction. *Mathematical and Computer Modelling*, 52(7–8):1258–1264, 2010.

[2] Yao, Weiguang and Leszczynsky, Konrad. Analytically derived weighting factors for transmission tomography cone beam projections. *Physics in Medicine and Biology*, 54(3):513–533, 2009.

[3] Gene H. Golub and Charles F. Van Loan, Matrix Computations. JHU Press, 1996.

[4] David S. Watkins, Fundamentals of Matrix Computations. John Wiley and Sons. Inc., 2002.

[5] F. Sánchez and A. Orero and A. Soriano and C. Correcher and P. Conde and A. González and L. Hernández and L. Moliner and M. J. Rodríguez-Álvarez and L. F. Vidal and J. M. Benlloch and S. E. Chapman and W. M. Leevy. ALBIRA: A small animal PET/SPECT/CT imaging system. *Medical Physics*, 40(5):051906, 2013.

Water demand simplifications used to build mathematical models for hydraulic simulations

J. Izquierdo[‡] [*], E. Campbell[‡], I. Montalvo[⋆], R. Pérez–García[‡] and D. Ayala-Cabrera[‡]

(‡) FluIng-IMM, Universitat Politècnica de València,

C. de Vera s/n, Edif 5C, 46022 Valencia, Spain,

(⋆) 3SConsult GmbH, Karlsruhe, Germany.

November 15, 2013

1 Introduction

Mathematical/numerical models are applied in all the areas of hydraulics – including urban hydraulics [1, 2]. Currently, with the generalized use of geographic information systems, models containing even hundreds of thousands of pipes and nodes are being built [3]. Mathematical modeling of water distribution networks (WDNs) uses simplifications aimed to optimize the development and use of the models. One of these simplifications is the grouping of the consumptions associated with interior points of a line in one or both ends of the line. These points concentrate all the existing consuming points (users) within the line.

This paper analyzes the error that may derive from the effect of using the widespread 50% rule, which allocates half of the in-line demand to each line end. We analyze to what extent this simplification is acceptable. Also, we obtain formulae that enable to distribute inner line demand between the line ends with minimal error.

[*]e-mail: jizquier@upv.es

2 Is the 50% allocation rule adequate?

Let us consider the case of a single line associated with some internal consumption under steady state condition. The characteristics of the line are: length: L; diameter: D; upstream head (boundary condition at the upstream node): H_0; line resistance: K; and inflow: Q_{in}.

Scenarios of consumption in the line are associated with two characteristics: total demand in the line with regard to inflow, and specific distribution of the demand along the line.

Let us assume that the flow consumed within the line (total in-line demand) represents a percentage of the line inflow. If this fraction is represented by F_Q, $0 < F_Q \leq 1$, the actual demand in the line is given by the expression $Q_d = F_Q Q_{in}$.

Let F_{Qd} be the factor that allocates a part of the line distributed demand, Q_d, to its upstream end. Thus, the demand assigned to this upstream node is $Q_0 = F_{Qd} Q_d$. As a result, $Q_l = Q_{in} - Q_0$ is the flowrate through the line. Then, the expression of H_C, where subindex '$_C$' stands for 'calculated', for a given value of F_{Qd}, is

$$H_C\left(F_{Qd}; x\right) = H_0 - K Q_l^2 x. \tag{1}$$

The HGL obtained is, thus, a straight line that connects the point $(0, H_0)$ with the point $(L, H_C\left(F_{Qd}; L\right))$. This last value corresponds to the calculated head at L, the downstream node.

To state the problem in its more general form, let us now consider a demand distribution on the line whose accumulated demand is given by a function $Q\left(x\right) = Q_d q\left(x\right)$, where $q\left(x\right)$ is the accumulated demand ratio, a function increasing monotonically from 0 to 1. While H_C is calculated as in (1), H_R, the subindex '$_R$' standing for 'real' distribution of piezometric head along the line as real demands are used to compare values, is calculated by integrating the loss $\Delta H = -K\left(Q_{in} - Q\left(x\right)\right)^2 \Delta x$ through the line [0, L]:

$$H_R\left(F_Q; q\left(x\right); x\right) = H_0 - \int_0^x K\left(Q_{in} - Q\left(u\right)\right)^2 \mathrm{d}u. \tag{2}$$

Observe that this function is monotonically decreasing and concave upwards.

Example 1. $q\left(x\right) = x/L$, for the case of continuous uniform demand. ▲

Using (2) and the expression (1) for H_C in L, the equation $H_C = H_R$ in L gives

$$F_{Qd}\left(F_Q\right)=\frac{1}{F_Q}\left(1-\sqrt{\frac{1}{L}\int_0^L\left(1-F_Q q\left(x\right)\right)^2\mathrm{d}x}\right).$$

The general solution for the problem in hand when an arbitrary demand through the line is considered may only be solved after having a specific expression for $q\left(x\right)$. As a consequence, to pinpoint the new aspects that may arise when considering arbitrary demands, we will restrict ourselves to considering the case of discrete demands on a finite number of points of the pipe, as in real life happens.

Let us consider $q\left(x\right)=\sum_{k=1}^{n}d_k\delta\left(x-x_k\right)$, where d_k are the demands at points x_k, with $0<x_1<x_2<\ldots<x_{n-1}<x_n<L$, such that $\sum_{k=1}^{n}d_k=Q_d$. $\delta\left(\cdot\right)$ is the Dirac delta.

Example 2. $q\left(x\right)=\frac{1}{n}\sum_{k=1}^{n}\delta\left(x-\frac{k}{n+1}L\right)$ in the case of uniform demand at n equally distributed points in the pipe. ▲

In the general case, H_R is calculated by

$$H_R\left(F_Q,L\right)=H_0-Kx_1Q_{in}^2-K\left(x_2-x_1\right)\left(Q_{in}-d_1\right)^2-\cdots \tag{3}$$
$$-K\left(x_3-x_2\right)\left(Q_{in}-\left(d_1+d_2\right)\right)^2-k\left(x_n-x_{n-1}\right)\left(Q_{in}-\sum_{k=1}^{n-1}d_k\right)^2-\cdots$$
$$-K\left(L-x_n\right)\left(Q_{in}-\sum_{k=1}^{n}d_k\right)^2.$$

By denoting

$$\mu_i=\frac{d_i}{Q_d},\mu_0=0,\lambda_i=\frac{x_i}{L},\lambda_0=0,\lambda_{n+1}=1,\ \text{for}\ i=1,\ldots,n, \tag{4}$$

this expression can be written

$$H_R\left(F_Q,L\right)=H_0-KLQ_{in}^2\sum_{k=0}^{n}\left(\lambda_{k+1}-\lambda_k\right)\left(1-F_Q\sum_{j=0}^{k}\mu_j\right)^2.$$

Then, by equating again $H_C = H_R$ at L gives

$$F_{Qd}\left(F_Q, \lambda, \mu\right) = \frac{1}{F_Q}\left(1 - \sqrt{\sum_{k=0}^{n}\left(\lambda_{k+1} - \lambda_k\right)\left(1 - F_Q \sum_{j=0}^{k} \mu_j\right)^2}\right). \qquad (5)$$

This expression can be easily calculated using, for example a worksheet.

3 Conclusions

This contribution focuses on the study of the influence that the concentration of a distributed demand in a line on the line ends represents in modeling steady state conditions in WDNs. By using a practical approach, we show the importance of the relation between the total inflow and the flow that is extracted due to the load of demands in the line. The distribution of the consumptions along the line also greatly influences the validity of the model. After assessing the error that may derive from using the generalized 50% rule, we obtain the general formula (5) that enables to distribute arbitrary inner line demand between the line ends with zero error at the downstream end of the line.

References

[1] Izquierdo, J.; Pérez, R.; Iglesias, P.L. Mathematical Models and Methods in the Water Industry, *Math Comp Mod*. 2004, *39*, 1353-1374.

[2] Izquierdo, J.; Montalvo, I.; Pérez-García, R.; Matías, A. On the Complexities of the Design of Water Distribution Networks, *Math Probl Eng*. 2012, Article ID 947961.

[3] Savić, D.A.; Banyard, J.K. *Water Distribution Systems*, ICE Publishing, London, UK, 2011.

A model to set fare zones for maximizing benefits of a subway line

J. Alberto Conejero* ⁎, Cristina. Jordán † ⁑ and Esther Sanabria-Codesal‡ ‡

(*) IInstituto Universitario de Matemática Pura y Aplicada,

Universitat Politècnica de València.

E-46022 Valencia, Spain,

(†) Instituto Universitario de Matemática Multidisciplinar.

Universitat Politècnica de València.

E-46022 Valencia, Spain,

(‡) Depto. Matemática Aplicada. Universitat Politècnica de València.

E-46022 Valencia, Spain

November 1st, 2013

Suppose that we have a subway line where we know the location of all the stops, the amount of people traveling between every pair of stops, and the benefit that can be obtained from each one of these travels attending to the amount of zones visited by each passenger on each trip. An interest problem is to show how to split the n stops into k zones in order to maximize the benefit obtained by the sale of tickets. The case $n = k$ has a trivial solution since the maximum benefit would be obtained when we set a unique stop at every zone. So that, the cases of interests will be the ones with $n > k$.

Let us consider the n stops, namely $\{s_1, s_2, \ldots, s_n\}$. These stops are assumed to be ordered in the line, namely $s_1 \prec s_2 \prec s_3, \ldots, \prec s_n$, being s_1 the first one and s_n the last one. Every single stop s_i is located at one of

*e-mail: aconejero@upv.es

†e-mail: cjordan@mat.upv.es

‡e-mail: esanabri@mat.upv.es

the k zones, and we denote this zone by z_i, with $1 \leq i \leq n$. We assume the following statements about the distribution of stops into zones:

Assumptions on the distribution of stops into zones.

1. $z_1 = 1$ and $z_n = k$, i.e. the first and the last city of the line are located at the first and at the last zone, respectively.

2. for every $1 < i < k$ there exists some $1 < j < n$ such that $z_j = i$, i.e. we have at least one stop at every zone, and

3. for every $1 \leq i \leq n-1$, either $z_{i+1} = z_i$ or $z_{i+1} = z_i + 1$, i.e. two consecutive stops in the line must be in the same zone or in contiguous zones.

This last observation can be used for defining the vertices and arcs of a directed tree with root that models our problem.

Taking into account these considerations, not all possible distributions of stops into zones can have sense. An *admissible distribution* of n stops into k zones will be denoted by a k-tuple of the form $[y_1, y_2, \ldots, y_k]$ where $y_1 + y_2 + \ldots + y_k = n$ and $y_i \geq 1$ for all $1 \leq i \leq k$. This k-tuple is used for representing that stops $s_1, \ldots, s_{y_1}$ are in zone 1, stops $s_{y_1+1}, \ldots, s_{y_1+y_2}$ are in zone 2, and so on. We finally have that the stops $s_{y_1+\ldots+y_{k-1}+1}, \ldots, s_{y_1+\ldots+y_k}$ are located in zone k.

We will start with the first stop s_1 and, by order, we keep adding the other stops taking into account assumptions $(A1)$ and $(A3)$. By the assumptions, not all possible distributions will be admissible. Moreover, in the process of generating admissible distributions of zones we will deal with eventually null subsequences of $[y_1, y_2, \ldots, y_k]$, that is, $[y_1, y_2, \ldots, y_{k'}, 0, \ldots, 0]$ with $y_1 + y_2 + \ldots + y_{k'} < n$ and $y_i \geq 1$ for all $1 \leq i \leq k'$. We refer to them as *partial admissible distributions*.

In Figure 1 we have a tree with all admissible and partial admissible distributions for the case of 3 zones and 4 stops. We see that this is a directed tree with root. In this tree the root is the partial admissible distribution $[1, 0, 0, 0]$. All the admissible distributions are located at some of the leaves of the tree, that is $[2, 1, 1, 1], [1, 2, 1, 1], [1, 1, 2, 1]$, and $[1, 1, 1, 2]$.

Once we have defined the corresponding tree of the case, we assign weights to the arcs in order that if we sum all the arcs needed to connect the vertex $[1, 0, 0, 0]$ with a certain admissible distribution by a path, then the sum of

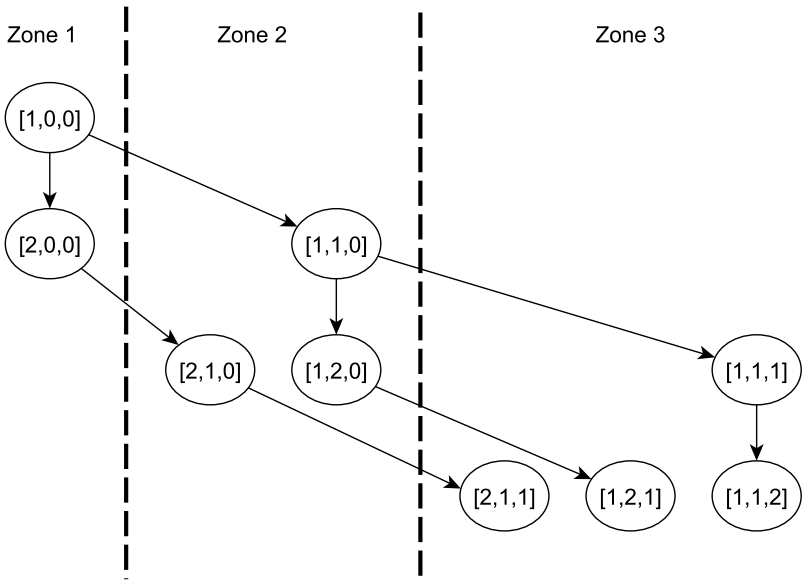

Figure 1: Graph for 3 zones and 4 stops.

the weights of such a path is equal to the total benefit that can be obtained by the sale of tickets.

For solving our problem we have to find the path of maximum weight from $[1, 0, 0, 0]$ to one of the leaves. After redefining the weights in order that our problem can be rephrased as a problem of finding a shortest path, we can apply Dijkstra's algorithm for solving it. Further information concerning graphs and algorithms for solving the shortest path problem can be found on [1, 3, 4].

The complete exposition of these results can be found in [2].

Acknowledgement We would like to thank RENFE for providing us data of the flow of passengers of the commuter trains of the Valencia region.

References

[1] R.K. Ahuja, T.L. Magnanti & J.B. Orli, Network flows. Theory, Algorithms and Applications. Prentice Hall, 1993.

[2] J.A. Conejero, C. Jordán, and E. Sanabria-Codesal. A mathematical model for setting subway fare zones. Preprint, 2013.

[3] A. Dolan and J. Aldous, Networks and algorithms: An introductory approach. England, Wiley, 1993.

[4] J.R. Evans and E. Minieka, Optimization algorithms for networks and graphs. USA, Dekker, 1992.

A formal model to identify patterns of movement in sets of moving objects

F. Moreno* ,* J. Guzmán *, and S. Gómez*

(*) Universidad Nacional de Colombia, Sede Medellín,

Bloque M8A

November 30, 2013

1 Introduction

Diverse movement patterns are identifiable when a set of moving entities is studied, e.g., a flock of birds [1] and a school of fish [2]. One of these patterns is known as a V-formation for it is shaped like the letter V. Another movement pattern is known as a circular formation for it is shaped like a circle.

Informally, a set of entities presents a V-formation if the entities are located on one of their two characteristic lines. The lines meet in a position where there is just one entity considered the entity leader [3]. On the other hand, circular formations are a set of entities grouped around a common center in which the distance from these individuals to the center is less than a given threshold.

This extended abstract is organized as follows. In Section 2, we present a method to detect V-formations. In Section 3, we present a method to detect circular formations. Then, in Section 4 we present a method to detect outliers in V-formations and in circular formations, i.e., formations which despite having some entities that do not tend to be grouped with the rest of the members are considered part of a V-formation or a circular formation.

*e-mail:fjmoreno@unal.edu.co

In Section 5, we present experiments, and finally, in Section 6 we conclude our extended abstract.

2 V-formations

In this section we present the basic definitions and the mathematic model to identify V-formations.

Let $F =< e_1, e_2, \ldots, e_n >$ be a list of moving entities in a point in time t. $e_k \in F$ is the entity leader, $1 < k < n$. F is a V-formation if:

i) Entities $e_i, 1 \leq i \leq k$, tend to form a straight line l_1.

ii) Entities $e_j, k \leq j \leq n$, tend to form a straight line l_2.

iii) Straight lines l_1 and l_2 converge in position $(xpos(e_k, t), ypos(e_k, t))$. *xpos* and *ypos* are function that return the coordinates of an entity at t.

iv) $\angle ap_t > 0$ (the smallest angle defined by straight lines l_1 and l_2).

Regarding conditions i) and ii), to establish if a set of entities tend to form a straight line, we use Pearson correlation coefficient r. Regarding condition iv), $\angle ap_t$ is calculated as follows: we obtain straight lines l_1 and l_2 of the formation, and we find the smallest angle among them as follows: a is the angle of the entity leader towards l_1, b the angle of the entity leader towards l_2, and $w =\mid a–b \mid$, then $\angle ap_t = w$ if $w \leq \pi$ and $\angle ap_t = 2\pi$-w, otherwise .

3 Circular formations

In this section we present the basic definitions and the mathematic model to identify circular formations.

The centroid (x_c, y_c) of a set of points $\{(x_1, y_1), (x_2, y_2), \ldots, (x_n, y_n)\}$ is obtained as follows. x_c is the average of the sum of ordinates and y_c is the average of the sum of abscissas.

We say that a set of moving entities exhibits a circular formation at a point in time t if

i) Distance d from each entity to the centroid is less than distance R (radius).

ii) The minimum number of members of the formation is N_{min}.

4 Outliers

For a V-formation an outlier is an entity that is far from its characteristic lines; and for a circular formation, it is an entity found beyond the radius of the formation. There are many methods to detect outliers in different domains. We have developed an algorithm, which we do not present here for space reasons, that receives a set of m entities (*lineMembers* array) which form the characteristic straight line of a formation at a point in time t. The algorithm determines if when we remove a maximum number of entities from the given set, the Pearson coefficient surpasses a given μ_p threshold. Then, the algorithm receives the minimum value of Pearson coefficient μ_p which must be met, and the maximum percentage of the entities (*percentageOutliers*) that may be removed from a set of entities. This percentage is calculated with regard to the total number of m entities. We have also proposed a slight modification to our algorithm to identify outliers in circular formations.

5 Experiments

For our experiments, we worked with NetLogo, it enables us to explore the relation between the behavior at the micro level of individuals and patterns at the macro level of groups. To generate V-formations in NetLogo, we used the model given in [4], which was conceived specifically for this goal. To generate circular formations, we used the model given in [5], which generates random formations of individuals in NetLogo.

Experimental results are shown on Table 1. 100 runs were done both to generate V-formations and circular formations. The time for each run was 200 ticks (a *tick* is a time measurement unit in Netlogo and at normal velocity equals 0.5 seconds).

6 Conclusions

In this extended abstract we propose two formal models: a) a model to identify V-formations with outliers and b) a model to identify circular formations

Table 1: Results of the identification of V-formations (on the left) and circular formations (on the right) in Netlogo.

	V-formations		**Circular formations**
Total number of formations identified in the 100 runs	318	Total number of formations identified in the 100 runs	332
Average number of formations identified in each run (200 ticks)	3	Average number of formations identified in each run (1200 ticks)	3
Average number of individuals in each formation	4	Average number of individuals in each formation	13
Average number of outliers	1	Average number of outliers	2

Source: authors' own presentation.

with outliers.

Both models considered the location of the entities to determine if they form this type of formation. The rules of our model for V-formations are flexible, for they allow V-formations which are not necessarily aligned as it usually happens in the real world. Furthermore, we considered the possible presence of entity outliers both in V-formations and in circular formations, i.e., members of the formation which may be far from it during some periods. Results in Netlogo showed that our models identified this type of formations in an environment where they are generated.

7 Acknowledgments

This extended abstract presents preliminary results of the project "Apoyo al Grupo de Sistemas Inteligentes Web-SINTELWEB with Quipú code 205010011129, developed at the Universidad Nacional de Colombia, Sede Medelln.

References

[1] Dodge, Somayeh, Robert Weibel, and Anna-Katharina Lautenschtz. Towards a taxonomy of movement patterns. *Information visualization*, Volume(7):240–252, 2008.

[2] Reynolds, Craig W. Flocks, herds and schools: A distributed behavioral model. *ACM SIGGRAPH Computer Graphics*, Volume(21):25–34, 1987.

[3] Cattivelli, Federico, and Ali H. Sayed. Self-organization in bird flight formations using diffusion adaptation. *Computational Advances in Multi-Sensor Adaptive Processing (CAMSAP)*, Volume(3rd):49–52, 2009.

[4] Nathan, Andre, and Valmir C. Barbosa. V-like formations in flocks of artificial birds *Artificial life*, Volume(14.2):179–188, 2008.

[5] Wilensky, Uri, and William Rand. Making models match: Replicating an agent-based model. *Journal of Artificial Societies and Social Simulation*, Volume(10.4):2, 2009.

A Mathematical model to forecast the female consumption of non-surgical plastic procedures in Spain

M. Alkasadi[†], E. De la Poza[‡] [*], L. Jódar[†]

(†)Instituto Universitario de Matemática Multidisciplinar,

(‡)Facultad de Administración y Dirección de Empresas,

Universitat Politècnica de València,

(†) (‡)Universitat Politècnica de València,Camino de Vera s/n. 46022,

Valencia, Spain.

1 Introduction

The attractiveness of physical appearance and stereotyped female body image makes that procedures such as augmentation or reduction of breasts, anti-aging surgeries, rejuvenation and/or look for an ideal body pattern are becoming natural practices as any other consumption good in Western societies [1] [2]; thus, gym practices combined with diet foods and drinks are usually correlated with the consumption of aesthetic surgical practices. Indeed, it is well known that a good image eases the professional promotion and social recognition [3][4][5][6].

In this study, we construct an epidemiological discrete mathematical model to forecast the population of female consumers of non-surgical plastic procedures (NSPP) in the next years in Spain. We deal with populations more than individuals[7]. Finally, public health recommendations and suggested.

[*]e-mail:elpopla@esp.upv.es

2 Mathematical model and results

The population of study is composed by the Spanish women who practice NSPP aged among the interval [16,60].
We classified the population into three categories according to their level of consumption of NSPP measured throughout the questionnaire developed for this purpose.

The three defined subpopulations were:

R_n: Rational women were those whose consumption was 0 or 1 NSPP at year n.

O_n: Over-consumer women whose level of consumption was 2 or 3 NSPP at year n.

D_n: Women who performed more than 3 NSPP at year n.

The individuals can only transit from one category or subpopulation to another. Thus, the R can transit to O; and O to D. Also, it is assumed a possible recovery transit from O to R or from D to O; both transits depend on the economic trends. The drivers that define the transits between subpopulation depend on economic (α_e) (β_e), emotional (α_r) nature [8], but also due to contagion, mimetic behaviour and human herding (γ_1) [9][10].

The dynamic of population can be described by the following equations:

$$P(n) = R(n) + O(n) + D(n). \tag{1}$$

$$\begin{aligned} R_{n+1} &= (1 + \alpha_b - \frac{d_i + \alpha_f}{3})R_n - \alpha_r R_n - \alpha_e(n)R_n - \gamma_1 R_n - E, \\ O_{n+1} &= (1 - \frac{d_i + \alpha_f}{3})O_n + \alpha_e(n)R_n + \alpha_r R_n - \beta_e(n)O_n + \gamma_1(R_n - O_n), \\ D_{n+1} &= (1 - \frac{d_i + \alpha_f}{3})D_n + \beta_e(n)O_n + \gamma_1 O_n. \end{aligned} \tag{2}$$

Thus, α_b expresses the Spanish women birth rate, d_i the biological death rate and α_f the system death rate(women going out of our age interval).

All parameters were estimated from different sources of information, own hypotheses and the survey designed and implemented in this study. We simulated two possible scenarios according to different annual levels of unemployment based on the economic forecast from [11] from 2011 until 2014, for pessimistic scenario, and from [12] for 2015 (the pessimistic scenario), and for the period [2016, 2018] was estimated by ourselves. The optimistic scenario is coming from [13] for the period [2011, 2018](See Figure 1).

Figure 1 shows how the subpopulation O evolves in the interval[4.86%, 5.12%] and D [0.884%, 0.8881%]for the pessimistic scenario. However, for the optimistic scenario O subpopulation trend ranges in the interval[4.86%, 5.16%]while D subpopulation evolves between [0.8849%, 0.8977%].
Then, we performed a sensitivity analysis of both models (pessimistic and optimistic) versus the contagious parameter C ranging in the interval [0.0049, 0.1], involved in the coefficient $\gamma_1 = 0.033 \times C$.
Results showed that both subpopulations O and D consumers evolve in accordance with the economy what confirms the robustness of our model.

3 Conclusions

The study of the consumption of this product in Spain shows its consumption by middle classes like other western countries as any other service employed to body care during last decade. However, the impact of the ferocious Spanish economic crisis slowed down suddenly its trend until the point where these services are just affordable by high-income women. The percentage of R subpopulation decline from [94.24%, 93.99%] during the period from 2012 until 2018 while the O subpopulation evolves from 4.86% to the interval [4.86%, 5.12%] for the case pessimistic and for the optimistic case the R decline from 94.24% to the interval [94.24%, 93.99%] and for O evolves from 4.86% for the interval [4.86%, 5.16%]. also, This study is interesting from the public health point of view since the practice of these procedures among dependent and over-consumers may lead to develop body dysmorphic disorder(BDD). Authorities should control the advertising/marketing through television and internet.

References

[1] M. H. Smirnova. A will to youth: the women's anti-aging elixir *Social Science & Medicine*, 75(7):1236-1243, 2012.

[2] B. Garnham. Designing 'older' rather than denying ageing: Problematizing anti -ageing discourse in relation to cosmetic surgery undertaken by older people *Journal of Aging studies*, 27(1):38-46, 2013.

[3] V. Swami, A. Arteche, T. Chamorro-Premuzic, A. Furnham, S. Stieger, T. Haubner, and M. Voracek. Looking good: Factors affecting the likelihood of having cosmetic surgery *European Journal of Plastic Surgery*, 30(5):211-218, 2008.

[4] V. Swami, R. Taylor, and C. Carvalho. Acceptance of cosmetic surgery and celebrity worship: Evidence of associations among female undergraduates *Journal of Personality and Individual Differences,* 47(8):869-872, 2009.

[5] C. N. Markey, and P. M. Markey. A correlational and experimental examination of reality television viewing and interest in cosmetic surgery *Journal of Body Image,* 7 (2):165-171, 2010.

[6] J. Maltby, and L. Day. Celebrity worship and incidence of elective cosmetic surgery: Evidence of a link among young adults *Journal of Adolescent Health,* 49(5):483- 489, 2011.

[7] C. R. MacCluer, Industrial Mathematics: Modeling in Industry,Science, and Covernment. Prentic Hall, Upper Saddle River, New Jersey ,USA, 2000.

[8] R. Duato,and L. Jódar. Mathematical modeling of the spread of divorce in Spain. *Mathematical and Computer Modelling,* 57(7-8):1732-1737, 2013.

[9] N. A. Christakis, and J. H. Fowler, Connected: The Surprising Power of Our Social Networks and How They Shape Our Lives. USA, Back Bay Books, Little Brown and Company, 2009.

[10] R. M. Raafat, N. Chater, and C. Frith. Herding in humans *Trends in Cognitive Sciences,* 13(10):420-428, 2009.

[11] The Organization for Economic Co-operation and Development (OECD), France, 2013, fhttp://www.oecd.org/eco/outlook/spaineconomicforecastsummary.htm.

[12] Cross Asset Research. Socite Gnrale (SG), France, 2013, https://publication.sgresearch.com/en/3/0/172963/125179.html?sid=5b4256d8671034005116a674000337f9.

[13] International Monetary Fund (IMF), USA , 2013, http://www.imf.org/external/pubs/ft/scr/2013/cr1354.pdf.

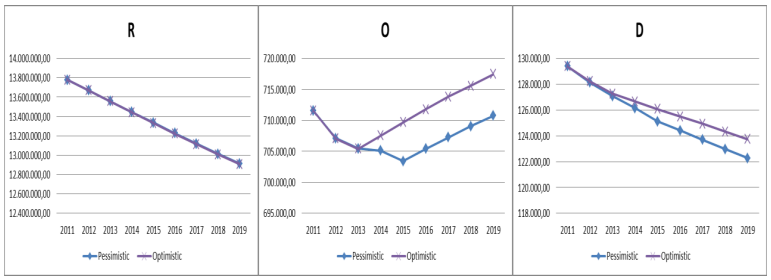

Figure 1: Shows subpopulations R, O and D during the period 2011-2018 by economic scenario.

Study of two different types of diesel injector nozzles by CFD: Internal flow comparison of microsac and VCO nozzle

F.J. Salvador[†,*], D. Jaramillo-Císcar[†], J.-V. Romero[‡] and M.-D. Roselló[‡]

(†) CMT-Motores Térmicos, Universitat Politècnica de València,

Camino de Vera s/n, Edificio 6D, 46022 Valencia, Spain,

(‡) Instituto de Matemática Multidisciplinar, Universitat Politècnica de València,

Camino de Vera s/n, Edificio 8G, 2°, 46022 Valencia, Spain

November 15, 2013

1 Introduction

The pollutant emissions and fuel consumption are one of the most important variables taken under study in modern Diesel engines, due to the new emission standards and fossil fuels prices. One of the key elements for the study of Diesel engines is the Diesel injector which will determine the air-fuel mixture and the combustion process.

Different types of Diesel injector nozzles can be found into commercial use, the two most important are the microSac nozzles and the VCO nozzles. Both types have been studied experimentally [4, 3] and computational [2, 5] separately, but the computational study of the internal flow and the comparison between both nozzles with the same geometrical characteristics has been not reported yet.

[*]e-mail: fsalvado@mot.upv.es, Telephone: 34-963879659, Fax: 34-963877659

The aim of this article is to compare the microSac and VCO internal flow. Two non-conical nozzles have been simulated: a microSac nozzle and a VCO, using a homogeneous equilibrium model (HEM) for the cavitation and a RANS approach (RNG k-ε) for take into account the turbulence effects. Different injection pressure, backpressure and needle lift have been considered to study the flow behaviour and the cavitation of each nozzle to catch cavitating and non-cavitating conditions.

The present paper has been divided into 5 sections. First of all, a brief description of the code used for reproduce cavitation phenomena is performed in section 2. The geometry characteristics for both nozzles that have been simulated are explained in section 3. The results of the study are presented in section 4 and finally, the main conclusions are drawn in section 5.

2 Cavitation modelling

Modern Diesel injector systems reach injection pressures until 200 MPa and the dimensions of the injection nozzles are about 1mm for the orifice length and 0.1–0.2 mm for the nozzle diameter. Under those conditions it can happen that the pressure falls below the saturation pressure and the fuel will cavitate, i.e., it will change from liquid to vapour state.

For describing the cavitation phenomena a homogenous equilibrium model [3] has been used in the present work. The code implemented in OpenFOAM, assumes that both liquid and vapour phases are in each cell completely mixed together and it considers a barotropic equation of state to relate the pressure with the density [1]. The compressibility on each cell depends on both phases.

The code has been validated and optimized improving the convergence and the accuracy of the results by choosing the right numerical schemes for the internal flow modelling in Diesel nozzles by Salvador et al. [6].

The turbulence is modelled using a RANS techniques. This method solves the Reynolds-averaged Navier Stokes (RANS) equations which models turbulent quantities, decomposing the fluid properties into an averaged and a fluctuating component. From previous studies the RNG k-ε model have been shown be the best option to model the turbulence.

3 Geometry and boundary conditions

The geometries that have been used in this study are multi-hole nozzles with 6 orifices. Due to the symmetry only 1 of the holes (60°) is used for the simulations. Two types of Diesel injector nozzles have been considered for the simulations: microSac nozzle and VCO nozzle. As far as the orifice geometry is concerned, it has been kept the same for both nozzles. The geometrical characteristics of both can be found in Table 1. Furthermore the simulations have been done at different needle lifts.

Nozzle	D_i [μm]	D_o [μm]	k-factor [-]	r [μm]	r/D_o [-]	L/D_o [-]
6-hole	170	170	0	13	0.074	5.71

Table 1: Nozzle's geometrical characteristics.

The difference between both types of nozzles is in the needle seat as can be observed in the Figure 1. In the VCO nozzle the orifice is fully covered when the needle downs, while that for the microSac nozzle the nozzles orifice remains connected with the sac when the needle downs.

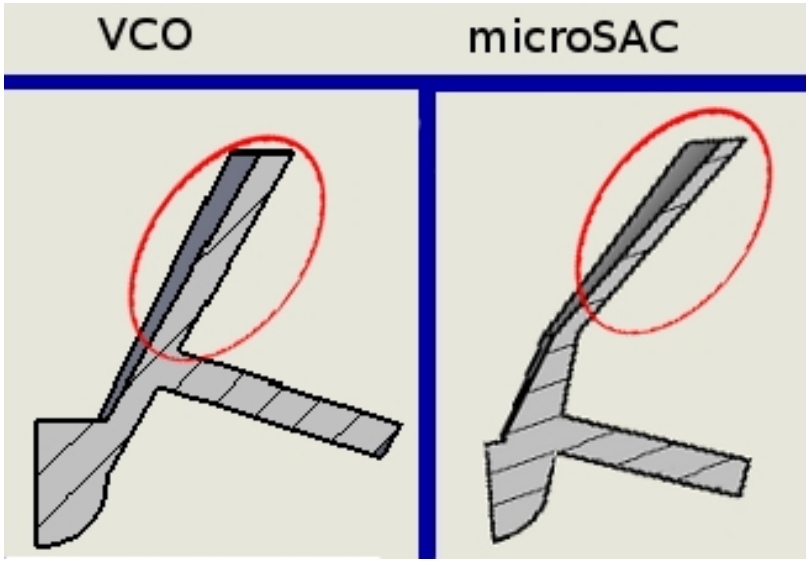

Figure 1: VCO nozzle and microSac nozzle.

For the simulations, a fixed pressure condition have been used at the entry while for the outlet, a mean pressure condition has been used. The mean pressure condition allows the existence of very low pressure regions as required for the presence of vapour inside the flow, while the mean pressure is kept at the desirable value.

For the walls a non-slip condition has been used for the velocity, while a zero-normal gradient for the pressure.

For the present study different values of backpressures for three different injection pressures have been studied: a low injection pressure of 30 MPa, a medium injection pressure of 80 MPa and a high injection pressure 160 MPa have been used. The text matrix used for the foreseen simulation are depicted in Table 2.

Injection Pressure [MPa]	Backpressure [MPa]	
30	microSac	3,5,7,9
	VCO	3,5,7,9,10,15,20
80	microSac	3,5,7,9,20
	VCO	3,5,7,9,10,20,30,40,50
160	microSac	3,5,7,9,10,20,30,40
	VCO	3,5,7,9,10,20,30,40,50, 60,70,80,90,100,110

Table 2: Boundary conditions.

4 Results

4.1 Full needle lift

Following the comparison of results for both nozzles at maximum needle lift of 250 micrometers are going to be presented.

4.1.1 Flow properties

In Figure 2, the results in terms of mass flow rate are compared as a function of the pressure as can be observed, the VCO nozzle injects less amount of fuel

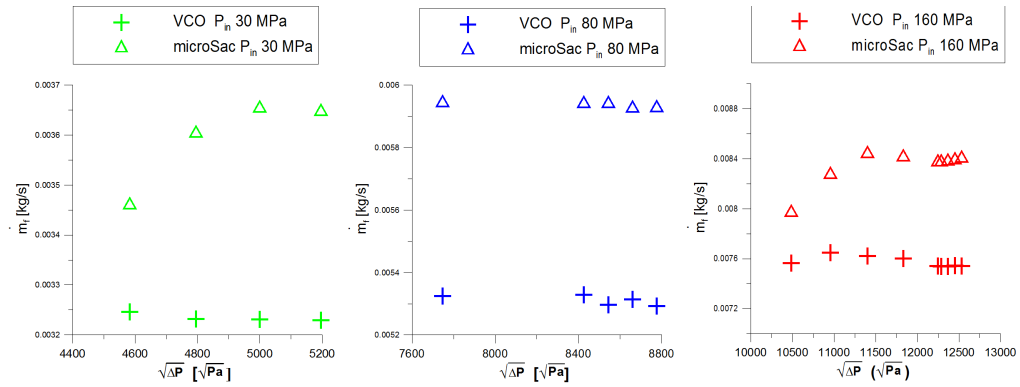

Figure 2: Comparison of mass flow.

for all the conditions and is more prone to cavitate (cavitation phenomena produce mass flow collapse [3]).

For the momentum flux, in Figure 3, it is observed the same behaviour, the values of the VCO nozzle are lower than microSac momentum flux values.

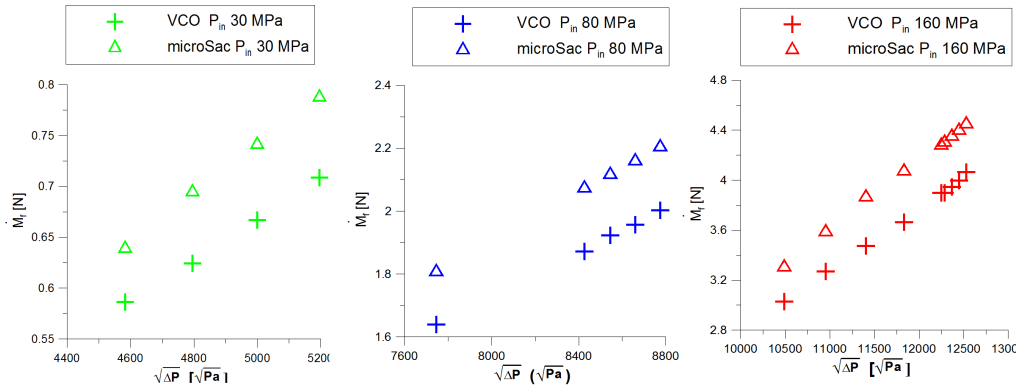

Figure 3: Momentum flux.

From the previous values of mass flow and momentum flux it is possible to calculate the effective velocity using the equation 1:

$$u_{\text{eff}} = \frac{\dot{m}_{\text{f}}}{\dot{M}_{\text{f}}} \tag{1}$$

The values of effective velocity are depicted in Figure 4. It can be observed

that although the mass flow and the momentum flux are lower for the VCO nozzle, the effective velocity at the outlet is higher for the VCO for low backpressure conditions (more cavitating conditions).

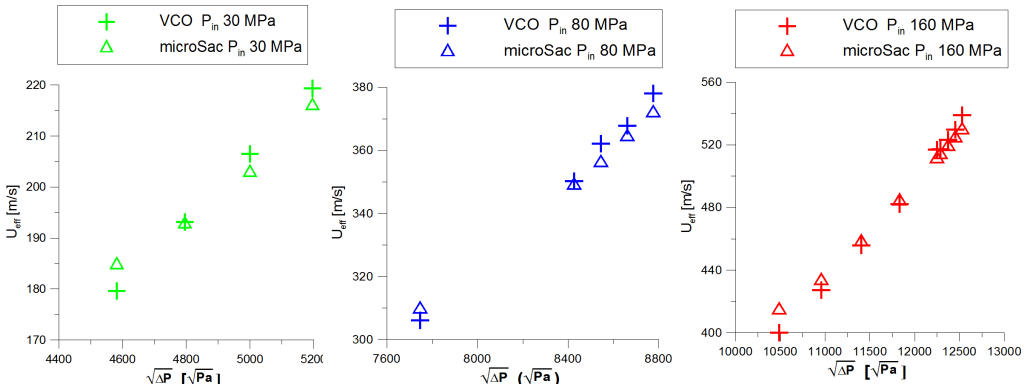

Figure 4: Effective velocity.

4.1.2 Cavitation pattern

Regards to the cavitation pattern, in Figure 5, it can be observed that for the VCO nozzle the cavitation pattern spreads only by the upper part of the nozzle orifice, while for the microSac nozzle at the entry of the orifice the cavitation spreads at the upper and the lower part of the nozzle hole.

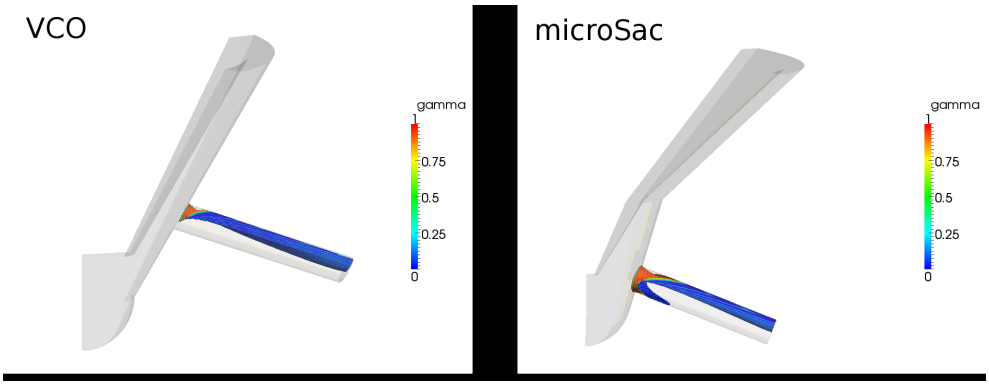

Figure 5: Cavitation pattern.

4.2 Partial needle lift

Following the comparison of results for both nozzles at partial needle lifts are going to be presented.

4.2.1 Mass flow rate - microSac at partial needle lift

Results of mass flow rate for both nozzles are depicted in Figure 6 for both nozzles. In that Figure, it can be observed that for the case of the microsSac nozzle, the mass flow rate does not change significantly until the needle lift is under 75 μm.

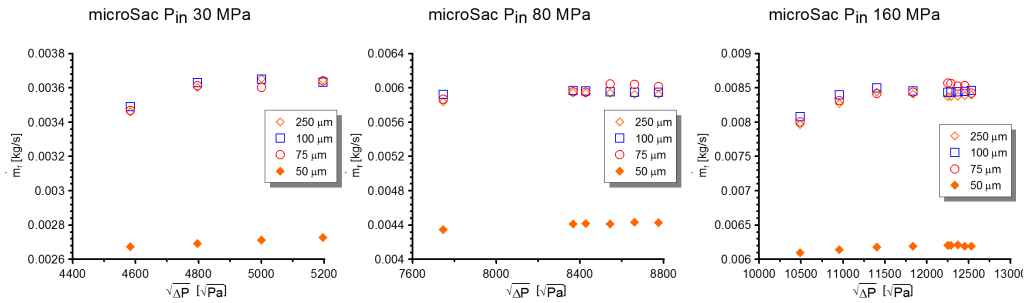

Figure 6: Mass flow - microSac

4.2.2 Mass flow rate - VCO at partial needle lift

In opposite to the microSac nozzle, for the VCO nozzle any change in the needle lift affects the mass flow rate as shown in Figure 7.

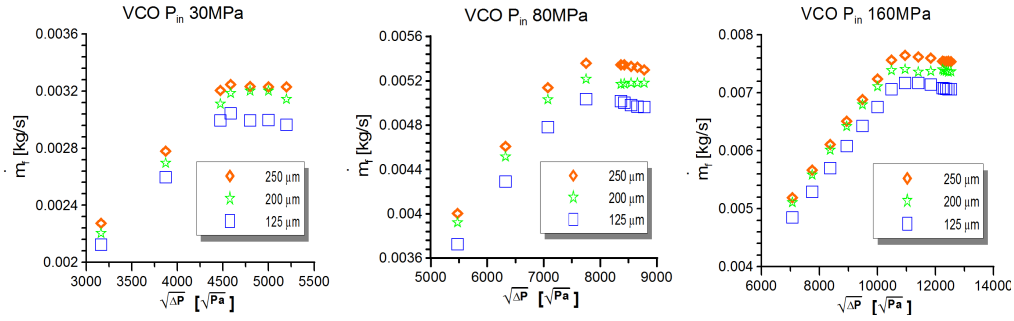

Figure 7: Mass flow - VCO.

5 Conclusions

The main conclusions from the present work for the studied geometries are the following:

- Mass flow and momentum flux are higher for the microSac nozzle.
- The VCO nozzle is more prone to cavitate, hence the effective velocity at low backpressure is higher for this nozzle.
- The type of seat for the needle of the microSac nozzle leads the flow properties to do not be affected until the needle lift is lower to 75 μm. Nevertheless, for the VCO nozzle the flow properties are affected by any change in the needle position.

Acknowledgements

This work was partly sponsored by "Vicerrectorado de Investigación, Desarrollo e Innovación" of the "Universitat Politècnica de València" in the frame of the project "Estudio de la influencia del uso de combustibles alternativos sobre el proceso de inyección mediante GRID computing (FUEL-GRID)", Reference SP20120396 and by "Ministerio de Economía y Competitividad" in the frame of the project "Comprensión de la influencia de combustibles no convencionales en el proceso de inyección y combustión tipo diesel", reference TRA2012-36932. This support is gratefully acknowledged by the authors.

The authors would like to thank the computer resources, technical expertise and assistance provided by the Universidad de Valencia in the use of the supercomputer "Tirant".

Nomenclature

D_i: inlet diameter
D_o: oulet diameter
k-factor: conicity factor
L: orifice lenght
$\dot{m}_\mathrm{f}$: mass flow/mass flux
$\dot{M}_\mathrm{f}$: momentum flux

P_{back}: back pressure
P_{inj}: injection pressure
r: curvature radius
u_{eff}: injection effective velocity
Greek symbols:
ΔP: pressure drop, $\Delta P = P_{\text{inj}} - P_{\text{back}}$

References

[1] F. P. Kärrholm. *Numerical Modelling of Diesel Spray Injection, Turbulence Interaction and Combustion*. PhD thesis, Chalmers University of Technology, 2008.

[2] M. Kubo, T. Araki, and S. Kimura. Internal flow analysis of nozzles for di diesel engines using a cavitation model. *JSAE Review*, 24(3):255–261, 2003.

[3] F. Payri, V. Bermúdez, R. Payri, and F. J. Salvador. The influence of cavitation on the internal flow and the spray characteristics in diesel injection nozzles. *Fuel*, 83:419–431, 2004.

[4] H. Roth, M. Gavaises, and Arcoumanis C. Cavitation initiation, its development and link with flow turbulence in diesel injector nozzles. SAE Paper 2002 01–0214.

[5] F. J. Salvador, J. V. Romero, M. D. Rosell, and J. Martínez-López. Validation of a code for modeling cavitation phenomena in diesel injector nozzles. *Mathematical and Computer Modelling*, 52:1123–1132, 2010.

[6] D. P. Schmidt, C. J. Rutland, and M. L. Corradini. A fully compressible two-dimensional model of high speed cavitationg nozzles. *Atomization and Sprays*, 9(3):255–276, 1999.

Forecasting Latin America's country risk scores by means of a dynamic diffusion model

R. Cervelló-Royo* *, J.-C. Cortés†, A. Sánchez-Sánchez†,
F.-J. Santonja‡, and R.-J. Villanueva†

(*) Department of Economics and Social Sciences, Universitat Politècnica de València, Spain,

(†) Instituto Universitario de Matemática Multidisciplinar, Universitat Politècnica de València, Spain,

(‡) Departamento de Estadística e Investigación Operativa, Universitat de València, Spain.

1 Introduction

Until the first half of 2011, the South and Central American economies expanded at a high pace. This growth was particularly strong in South America. In Central America growth has been subdued but also accelerated whereas Caribbean economies growth remained weak.

Country risk has become a topic of major concern for the international financial community over the last two decades. Country Risk Scores (CRS) are built in order to measure several factors, both quantitative and qualitative. Thus, CRS can represent a good indicator of the current situation of a country regarding measures of economic, political and financial risk in order to determine country risk ratings.

In order to model dynamically the CRS of each Latin America country, it should be considered both the endogenous effect of each country policies and the contagion effect among them.

The contagion is usually modelled using epidemiological and/or diffusion techniques. Let us study the dynamics of CRS using these mathematical techniques. Our objective is to predict the CRS trends over the next year, providing prediction tools for policy makers.

*e-mail: rocerro@esp.upv.es

2 Modelling

In finance, and especially in country risk assessment, it is useful to group the different countries sharing similar economic characteristics. Therefore, before constructing our diffusion mathematical model, we have performed a clustering analysis. The clustering technique allows us to gather the different countries into homogeneous groups. In order to deal with this task, we have used the Non-Hierarchical clustering (also called k-means clustering) [1, 2]. This method separates n observations into k clusters in which each observation belongs to the cluster with the nearest mean. We have grouped all the Latin American countries ($i = 1, \ldots, 18$) into four clusters considering the available data corresponding to the six categories C1-C6 introduced in the previous section.

The first cluster gathers Chile, the safest and most prosperous South American economy. The Second cluster gathers both South American and Central American economies which have done better in the last 10 years. The third cluster includes Central American, South American and Caribbean economies which have suffered a weaker growth in the last 10 years. The fourth cluster includes the considered less safe attractive investing South American and Central American economies due to its political-security and/or economic situation.

We are going to assume that the obtained clustering does not change over the time.

Once the clusters have been established, we propose a type-diffusion dynamic mathematical model to study the evolution of the CRS of each Latin American country. Type-diffusion dynamic models have demonstrated to be powerful tools to study a wide range of applied problems in different areas including Economics and its related fields [3, 4, 5]. Although very complex models have been proposed based on this approach, all of them are mainly based on the following pattern:

$$C_i'(t) = \alpha_i C_i(t) + \sum_{1 \le k, k(i) \le 4} \beta_{k(i),k} C_i(t) \left(\overline{C}_k(t) - C_i(t) \right), \ 1 \le i \le 18, \qquad (1)$$

where $C_i'(t)$ is the CRS of country i-th at the time instant t.

As we shall see in detail later, our model considers Ci(t) as a linear function which can be decomposed into two factors:

- α Measures the autonomous behaviour of each Latin American country.
- β Measures the transmission behaviour; that is to say, the contagion between each pair of Latin American countries.

The first one represents, through CRS, the autonomous economic behavior of each country and, the second one, the contagion effect for loss or gain of confidence both between and within clusters for each country. As we will see, in our case the resulting model based on 1 is nonlinear.

In order to reduce the number of parameters, we take advantage of previous clustering classification and we consider the β coefficient is the same for every country belonging to the same cluster and the average value $\overline{C}_k(t)$ as a balanced CRS indicator.

3 Prediction

This section is divided into two parts. The first one, is devoted to model parameters estimation and CRS deterministic punctual forecasting over the next few months. Since uncertainty and variability are the rules when dealing with modelling real problems, in the second subsection, we complete our predictions by means of confidence intervals obtained using Cross-Validation technique.

3.1 Parameter Estimation

As we have previously pointed out, this subsection is firstly addressed to estimate the parameters of model. This task has been performed by fitting the model in the mean square sense to the available data. Computations have been carried out with Mathematica 8.0 [6]. The system of differential equations is numerically solved by taking as initial conditions the CRS data of February 6, 2012 (corresponding to t = 0) (see Table 1 and Table 2).

3.2 Predictions

In order to complete the punctual prediction of CRS provided previously, it is more realistic to construct predictions by confidence intervals. To calculate these intervals, we used an adaptation of the statistical technique usually referred to as cross-validation or rotation estimation.

Country name	α_i		Country name	α_i
Chile	1.6844		Honduras	-0.0440
			Ecuador	-0.5731
			Nicaragua	-0.7551
			Dominican Rep.	-0.4340
			Trinidad Tobago	1.3411
Brazil	1.8554		Costa Rica	1.0763
Mexico	1.2784		Paraguay	-0.0203
Peru	1.1126		El Salvador	0.4658
Colombia	1.5382		Argentina	-0.4093
Uruguay	0.0696		Bolivia	-0.5837
Panama	1.2563		Venezuela	-0.4590

Table 1: Estimation of the autonomous model parameters, α_i, separated by clusters.

$\beta_{k(i),k}$	$k=1$	$k=2$	$k=3$	$k=4$
$k(i)=1,\ 1\leq i\leq 1$	0	0.01122	0.02525	0.01736
$k(i)=2,\ 2\leq i\leq 7$	0.05222	0.00007	0.04198	0.07828
$k(i)=3,\ 8\leq i\leq 12$	0.00047	0.00180	0.03809	0.04129
$k(i)=4,\ 13\leq i\leq 18$	0.00004	0.00283	0.04903	0.04771

Table 2: Estimated values of the contagion model parameters. The value of model parameter $\beta_{k(i),k}$ measures the contagion effect transmitted by the countries belonging to cluster k ($1 \leq k \leq 4$) on country i ($1 \leq i \leq 18$) belonging to cluster $k(i)$. Figures indicate that countries in clusters $k = 3, 4$ have a remarkable influence on the others, lower on Chile (columns 3 and 4). In addition, it can be observed that Chile (cluster 1) has a strong influence on countries which belong to cluster 2 (element (2, 1), which value is 0.01122).

The results showed that with the exception of Bolivia, Ecuador and Venezuela, the confidence intervals contain most of the data at the beginning of the period and some data points lie outside but close to the confidence interval.

4 Conclusions

Latin America's relative resilience to the more acute rise in risk seen in other regions during last years is offering investors new options for improving risk-return trade-offs. Country Risk Score (CRS) represents the level of confidence on each country and a measure of its economic health.

In this work, we present a diffusion model to study the dynamics of the Country Risk Score (CRS), for a total of 18 Latin American countries. As we can check in our results even over a one year horizon, Latin America might

held up fairly well, despite an average score loss driven by drops for Argentina and Venezuela and the region's strong dependence on the US Economy.

References

[1] G. Hamerly, C. Elkan, Alternatives to the k-means algorithm that find better clusterings. In: Proceedings of the 11th ACM International Conference on Information and Knowledge Management, 600-607, 2002.

[2] D. MacKay, Information Theory, Inference and Learning Algorithms, Cambridge University Press, 2003.

[3] R.T. Frambach, An integrated model of organizational adoption and diffusion of innovations, *European Journal of Marketing*, 27: 22–41, 1993.

[4] V. Mahajan, E. Muller, F.M. Bass, New product diffusion models in marketing: A review and directions for research, *The Journal of Marketing*, 54(1): 1–26, 1990.

[5] D. Zhang, A. Ntoko, Mathematical model of technology diffusion in developing countries, *Computational Methods in Decision-Making, Economics and Finance*, 526–539, 2002.

[6] *Mathematica*. Available: http://www.wolfram.com/products/mathematica [June 24, 2012].

Efficient iterative methods for nonlinear models *

Carlos Andreu, Noelia Cambil, Alicia Cordero, and Juan R. Torregrosa

Instituto de Matemáticas Multidisciplinar,
Universitat Politècnica de València,
caranesandreu@gmail.com, nctnoelia@gmail.com, acordero@mat.upv.es, jrtorre@mat.upv.es

November 30, 2013

1. Introduction

Solving nonlinear systems is a classical problem which has interesting applications in various branches of science and engineering. In this study, we describe new iterative methods to find a root α of a nonlinear system $F(x) = 0$, where $F : D \subseteq \mathbb{R}^n \to \mathbb{R}^n$ is a vectorial function on a convex set D.

In last decades, many researchers have proposed different iterative methods to improve Newton's one, which is still the most used scheme in practice. These variants of Newton's method have been designed by means of different techniques, providing in the most of cases multistep schemes.

Recently, for one-dimensional models, the weight-function procedure has been used to increase the order of convergence of known methods ([10]). This technique can be also used, with some restrictions, in the development of high order iterative methods for systems: see, for example the papers of Sharma et al. ([11, 12]) and Abad et al. [1], where the authors apply the designed method to the software improvement of the Global Positioning System.

A great way to design new schemes is the direct composition of known methods with a later treatment to reduce the number of functional evaluations (see [2, 3, 8, 13], for example). A variant of this technique is the so called Pseudocomposition, introduced in [6] and [7].

In the second section of this work, we introduce a class of sixth-order Newton-type methods by using the composition technique and matricial weight functions. The convergence results of this family have been obtained by means of the n-dimensional Taylor expansion of the involved functions, by using the notation introduced in [4]. The third section is devoted to analyze the efficiency of the proposed procedures applied on systems of different sizes, comparing our methods with the classical Newton', Traub' ([14]) and Jarratt's ([9]) schemes. We finish the paper with some conclusions and the references used in it.

*This research was supported by Ministerio de Ciencia y Tecnología MTM2011-28636-C02-02

2. The new class of methods and its convergence

In this section, we show our new family of three-step iterative methods. It has been designed from Newton's scheme composing with itself twice, once with 'frozen' function and other one with 'frozen' Jacobian matrix. By using matricial weight functions in the second and third step, we obtain that the methods of the proposed family have sixth-order of convergence, under certain conditions of function F and of weight functions. From an initial estimation $x^{(0)}$, the iterative expression of our family is:

$$\begin{aligned} y^{(k)} &= x^{(k)} - \left[F'(x^{(k)})\right]^{-1} F(x^{(k)}), \\ z^{(k)} &= y^{(k)} - H(\mu^{(k)}) \left[F'(y^{(k)})\right]^{-1} F(x^{(k)}), \\ x^{(k+1)} &= z^{(k)} - G(\mu^{(k)}) \left[F'(y^{(k)})\right]^{-1} F(z^{(k)}), \quad k = 0, 1, 2, \ldots \end{aligned} \tag{1}$$

where $\mu^{(k)} = \left[F'(y^{(k)})\right]^{-1} F'\left(x^{(k)}\right)$ and $H, G : \mathbb{R}^{n\times n} \to \mathbb{R}^{n\times n}$ are matricial functions.

In the following result we establish the convergence of (1). We can prove this theorem by using the Taylor's expansion of the different elements that appear in the iterative expression and many algebraic manipulations.

Theorem 1 *Let $\alpha \in D$ be a zero of a sufficiently differentiable function $F : D \subseteq \mathbb{R}^n \to \mathbb{R}^n$ in a convex set D with non-singular Jacobian in α and $x^{(0)}$ an initial approximation near to α. Let H and G be enough differentiable functions, which satisfy the following conditions: $H(I) = 0$, $H'(I) = \frac{1}{2}I$, $H''(I) = 0$, and $G(I) = I$, $G'(I) = 0$, $G''(I) = \frac{1}{2}I$; being I the identity matrix. Then, the elements of family described by (1) provides sixth-order of convergence, whose error equation is given by*

$$e^{(k+1)} = \left[-\frac{3}{2}C_3C_2C_3 + \frac{1}{4}C_2C_3^2 + 6C_3C_2^3 - C_2C_3C_2^2 + C_2^3C_3 - 4C_2^5\right] e^{(k)^6} + O(e^{(k)^7}),$$

where $C_k = (1/k!)[F'(\alpha)]^{-1}F^{(k)}(\alpha)$, $k = 2, 3, 4, \ldots$, and $e^{(k)} = x^{(k)} - \alpha$.

In the numerical section we use some elements of family (1), obtained by choosing different weight functions which satisfy the conditions of Theorem 1. Specifically, we propose the weight functions:

Procedure 1. The method denoted by NAJC1 is obtained from the weight functions:

$$\begin{aligned} H(t) &= \frac{1}{2}(t - I), \\ G(t) &= [I + t]^{-1}\left(2I - t + t^2\right). \end{aligned}$$

Procedure 2. The weight functions

$$\begin{aligned} H(t) &= \frac{1}{2}(t - I), \\ G(t) &= I + \frac{1}{2}(t - I)^2, \end{aligned}$$

provide the scheme denoted byNAJC2.

3. Numerical results

In this section we analyze the efficiency of our methods and compare them with classical ones, applied to some nonlinear systems. The classical methods used are Newton', Traub' and Jarratt's ones of convergence order 2, 3 and 4 respectively, whose iterative expressions are:

Newton (N)	$x^{(k+1)} = x^{(k)} - [F'(x^{(k)})]^{-1}F(x^{(k)})$,
Traub (T)	$y^{(k)} = x^{(k)} - [F'(x^{(k)})]^{-1}F(x^{(k)})$, $x^{(k+1)} = y^{(k)} - [F'(x^{(k)})]^{-1}F(y^{(k)})$,
Jarratt (J)	$z^{(k)} = x^{(k)} - \frac{2}{3}\,[F'(x^{(k)})]^{-1}F[x^{(k)}]$, $x^{(k+1)} = x^{(k)} - \frac{1}{2}\,[3F'(z^{(k)}) - F'(x^{(k)})]^{-1}(3F'(z^{(k)}) - F'(x^{(k)}))[F'(x^{(k)})]^{-1}F(x^{(k)})$.

In our tests, we have used the following numerical settings: variable precision arithmetics of two hundred and fifty digits in Wolfram Mathematica 8.0; moreover, in each iterative method we have used the stopping criteria $||F(x^{(k+1)})|| + ||x^{(k+1)} - x^{(k)}|| < 10^{-100}$ and the approximated computational order of convergence ρ (see [5]) obtained by

$$p \approx \rho = \frac{\ln(||x^{(k+1)} - x^{(k)}||/||x^{(k)} - x^{(k-1)}||)}{\ln(||x^{(k)} - x^{(k-1)}||/||x^{(k-1)} - x^{(k-2)}||)}.$$

From this value, we have provided two practical indices to measure the computational efficiency: the approximated efficiency index

$$\tilde{I} = \rho^{1/d} \tag{2}$$

and the approximated computational index

$$\tilde{I}_c = \rho^{1/op}, \tag{3}$$

being d and op the number of functional evaluations and the number of operations (products and quotients) per iteration, respectively.

We check the computational efficiency of the proposed schemes NAJC1 and NAJC2 by using the nonlinear systems:

(a) $F_1(x) = (f_1(x), f_2(x))^T : x = (x_1, x_2)^T$, $f_i : \mathbb{R}^2 \to \mathbb{R}$, $i = 1, 2$, $\alpha \approx (3{,}47063096, -2{,}47063096)$, where

$$f_1(x) = e^{x_1}e^{x_2} + x_1 \cos x_2,$$
$$f_2(x) = x_1 + x_2 - 1.$$

(b) $F_2(x) = (f_1(x), f_2(x), f_3(x))^T : x = (x_1, x_2, x_3)^T$, $f_i : \mathbb{R}^3 \to \mathbb{R}$, $i = 1, 2, 3$, $\alpha \approx (2{,}14025, -2{,}09029, -0{,}223525)$, where

$$f_1(x) = x_1^2 + x_2^2 + x_3^2 - 9,$$
$$f_2(x) = x_1x_2x_3 - 1,$$
$$f_3(x) = x_1 + x_2 - x_3^2.$$

(c) $F_3(x) = (f_1(x), f_2(x), f_3(x), f_4(x))^T : x = (x_1, x_2, x_3, x_4)^T$, $f_i : \mathbb{R}^4 \to \mathbb{R}$, $i = 1, \ldots, 4$, $\alpha = (\pm\frac{1}{\sqrt{3}}, \pm\frac{1}{\sqrt{3}}, \pm\frac{1}{\sqrt{3}}, \pm\frac{2}{\sqrt{3}})$, where

$$\begin{aligned} f_1(x) &= x_2x_3 + x_4\,(x_2 + x_3)\,, \\ f_2(x) &= x_1x_3 + x_4\,(x_1 + x_3)\,, \\ f_3(x) &= x_1x_2 + x_4\,(x_1 + x_2)\,, \\ f_4(x) &= x_1x_2 + x_1x_3 + x_2x_3 - 1. \end{aligned}$$

We denote by ε_i the value of $|f_i(x^{(k+1)})|$, being $x^{(k+1)}$ the last iteration calculated and f_i each one coordinate functions of F.

Method	Iter	ρ	$\tilde{I}$	$\tilde{I}_c$	ε_1	ε_2	Time (s)
N	8	1.9999	1.1734	1.1078	7.5993e-174	0	0.004658
T	6	3.0000	1.3841	1.1251	5.8838e-206	0	0.006098
J	4	3.9887	1.1174	1.0715	2.0217e-113	0	0.004620
NAJC1	4	6.0051	1.1259	1.0451	0	0	0.009178
NAJC2	4	6.0028	1.1289	1.0462	0	0	0.008030

Table 1: Results of system (a) by using $x^{(0)} = (4, -3)^T$.

Method	Iter	ρ	$\tilde{I}$	$\tilde{I}_c$	ε_1	ε_2	ε_3	Time (s)
N	13	1.9948	1.0281	1.0201	3.4121e-125	2.7759e-125	1.0794e-125	0.007766
T	-	-	-	-	-	-	-	-
J	8	3.9940	1.0301	1.0158	0	0	0	0.009805
NAJC1	5	4.9496	1.0646	1.0171	0	0	0	0.013722
NAJC2	6	4.9329	1.0716	1.0190	0	0	0	0.013029

Table 2: Results of system (b) by using $x^{(0)} = (12, -2, -1)^T$.

Method	Iter	ρ	$\tilde{I}$	$\tilde{I}_c$	ε_1	ε_2	ε_3	ε_4	Time (s)
N	10	2.0244	1.0249	1.0249	6.5830e-102	6.5830e-102	6.5830e-102	2.7466e-103	0.007272
T	7	3.0909	1.0356	1.0162	2.9862e-145	2.9862e-145	2.9862e-145	7.8319e-147	0.009802
J	5	4.1871	1.0349	1.0141	6.5830e-102	6.5830e-102	6.5830e-102	2.7466e-103	0.007952
NAJC1	5	6.4193	1.0493	1.0104	0	0	0	0	0.017668
NAJC2	5	6.1729	1.0520	1.0110	0	0	0	0	0.014849

Table 3: Results of system (c), $x^{(0)} = (5, 5, 5, -1)^T$.

Unlike the methods NAJC1 and NAJC2 which provide good results in the three examples, Traub's method diverges in the system (b), possibly because the initial approximation

is far from the solution. In addition, if we observe the data of each of the Tables 1 to 3, we note that Newton and Traub's methods shoot up the number of iterations when the initial estimate is far apart of the solution.

4. Conclusions

The new sixth-order methods NAJC1 and NAJC2 belonging to the class of procedures designed by using weight matricial functions have satisfactory overall properties of convergence and stability, even for initial estimations far apart from the solution as we have seen in the numerical section.

Referencias

[1] M. Abad, A. Cordero, J.R. Torregrosa. Fourth- and Fifth-order methods for solving nonlinear systems of equations: an application to the Global positioning System, *Abstract and Applied Analysis*, Article ID:586708 10 pages doi: 10.1155/2013/586708, 2013.

[2] F. Awawdeh. On new iterative method for solving systems of nonlinear equations, *Numerical Algorithms*, 5(3):595–609, 2010.

[3] D.K.R. Babajee, A. Cordero, F. Soleymani, J.R. Torregrosa. On a novel fourth-order algorithm for solving systems of nonlinear equations, *Journal of Applied Mathematics*, Article ID:165452 12 pages doi: 10.1155/2012/165452, 2012.

[4] A. Cordero, J.L. Hueso, E. Martínez, J.R. Torregrosa. A modified Newton-Jarratt composition, *Numerical Algorithms*, 55:87–99, 2010.

[5] A. Cordero, J.R. Torregrosa. Variants of Newton's method using fifth-order quadrature formulas *Applied Mathematics and Computation*, 190:686–698, 2007.

[6] A. Cordero, J.R. Torregrosa, M.P. Vassileva. Pseudocomposition: a technique to design predictor-corrector methods for systems of nonlinear equations *Applied Mathematics and Computation*, 218(23):1496–1504, 2012.

[7] A. Cordero, J.R. Torregrosa, M.P. Vassileva. Increasing the order of convergence of iterative schemes for solving nonlinear systems, *Journal of Computational and Applied Mathematics*, 252:86–94, 2013.

[8] M. T. Darvishi, Norollah Darvishi, SOR- Steffensen-Newton Method to Solve Systems of Nonlinear Equations, *Applied Mathematics*, 2(2):21–27, doi: 10.5923/j.am.20120202.05, 2012.

[9] P. Jarratt. Some fourth order multipoint iterative methods for solving equations, *Mathematics Computation*, 20:434–437, 1966.

[10] M. Petković, B. Neta, L. Petković, J. Džunić. Multipoint methods for solving nonlinear equations, Elsevier, 2013.

[11] J.R. Sharma, R.K. Guha, R. Sharma. An efficient fourth order weighted-Newton method for systems of nonlinear equations, *Numerical Algorithms* 62(2): 307–323, 2012.

[12] J.R. Sharma, H. Arora. On efficient weighted-Newton methods for solving systems of nonlinear equations, *Applied Mathematics and Computation* 222: 497–506, 2013.

[13] F. Soleymani, T. Lotfi, P. Bakhtiari, A multi-step class of iterative methods for nonlinear systems, *Optimization Letters*, doi: 10.1007/s11590-013-0617-6, 2013.

[14] J.F. Traub, Iterative methods for the solution of equations. New York, Chelsea Publishing Company, 1982.

Solution of the Lambda modes problem of a nuclear power reactor using an h-p finite element method

A. Vidal[†] [*], R. Fayez[†] D. Ginestar[‡], and G. Verdú[†]

([†]) Instituto de Seguridad Industrial: Radiofísica y Medioambiental,

Universitat Politècnica de València, Camino de Vera s/n, 46022, València, Spain

([‡]) Instituto Universitario de Matemática Multidisciplinar,

Universitat Politècnica de València, Camino de Vera s/n, 46022, València, Spain,

November 30, 2013

1 Introduction

The neutron diffusion equation is an approximation of the neutron transport equation that states that the neutron current is proportional to the gradient of the neutron flux by means of a diffusion coefficient. This approximation is analogous to the Fick's law in species diffusion and to the Fourier law in heat transfer. For a given configuration of a nuclear reactor core it is always possible to force its criticality dividing the neutron production rate by a positive number, λ, obtaining a neutron balance equation. This equation is known as the Lambda modes problem,

$$\mathcal{L}\Phi = \frac{1}{\lambda}\mathcal{M}\Phi \ , \tag{1}$$

where $\mathcal{L}$ is the neutron loss differential operator and $\mathcal{M}$ is the neutron production operator.

[*]e-mail: anvifer2@etsid.upv.es

Therefore this turns the formulation into a differential generalized eigenvalue problem. The fundamental eigenvalue (the one with the largest magnitude) shows the criticality of the reactor core and its corresponding eigenfunction describes the steady state neutron distribution in the core. Next sub-critical eigenvalues and their corresponding eigenfunctions are interesting because they have been successfully used to develop modal methods to integrate the time dependent neutron diffusion equation [1]. Also the subcritical modes have been used to classify BWR instabilities.

In this work, an *h*-*p* finite element method is used to obtain the dominant lambda modes associated with a configuration of a reactor core. This method allows using heterogeneous meshes, and leads to different refinements such as *h*-refinement and *p*-refinement. An *h*-*p* finite element method has been implemented using the open source finite elements library Deal.II [2]. With the help of the library, the code proposed is dimension independent and can manage different cell sizes and different types of finite elements. In order to solve the resulting algebraic eigenvalue problem from the spatial discretization of the Lambda modes problem the SLEPc library [3] is used.

2 Discretization of the problem

The Lambda modes equation in the approximation of two groups of energy is considered. This equation can be expressed as [1],

$$\begin{pmatrix} -\vec{\nabla}(D_1\vec{\nabla}) + \Sigma_{a1} + \Sigma_{12} & 0 \\ -\Sigma_{12} & -\vec{\nabla}(D_2\vec{\nabla}) + \Sigma_{a2} \end{pmatrix} \begin{pmatrix} \phi_1 \\ \phi_2 \end{pmatrix} = \frac{1}{\lambda} \begin{pmatrix} \nu\Sigma_{f1} & \nu\Sigma_{f2} \\ 0 & 0 \end{pmatrix} \begin{pmatrix} \phi_1 \\ \phi_2 \end{pmatrix}, \tag{2}$$

where D_g, $g = 1, 2$ are the diffusion coefficients, Σ_{ag}, Σ_{fg} and Σ_{12} are the macroscopic cross sections of absorption, fission and scattering, respectively. In the same way, ϕ_1 and ϕ_2 are the fast and thermal neutron fluxes.

A Galerkin finite element method [4] is used leading to an algebraic eigenvalue problem with the following block structure,

$$\begin{pmatrix} \mathbf{L_{11}} & 0 \\ -\mathbf{L_{21}} & \mathbf{L_{22}} \end{pmatrix} \begin{pmatrix} \tilde{\boldsymbol{\phi}}_\mathbf{1} \\ \tilde{\boldsymbol{\phi}}_\mathbf{2} \end{pmatrix} = \frac{1}{\lambda} \begin{pmatrix} \mathbf{M_{11}} & \mathbf{M_{12}} \\ 0 & 0 \end{pmatrix} \begin{pmatrix} \tilde{\boldsymbol{\phi}}_\mathbf{1} \\ \tilde{\boldsymbol{\phi}}_\mathbf{2} \end{pmatrix}, \tag{3}$$

where $\tilde{\boldsymbol{\phi}}_\mathbf{1}$ and $\tilde{\boldsymbol{\phi}}_\mathbf{2}$ are the corresponding algebraic vector of weights that represent the fast neutron flux and the thermal neutron flux respectively.

The matrices elements are given by

$$L_{ij} = \sum_{e=1}^{N_t} \Bigg(D_1 \int_{\Omega_e} \vec{\nabla} N_{1i} \vec{\nabla} N_{1j} \mathrm{d}V - D_1 \int_{\Gamma_e} N_{1i} \vec{\nabla} N_{1j} \mathrm{d}\vec{S} \; + \\ + (\Sigma_{a1} + \Sigma_{12}) \int_{\Omega_e} N_{1i} N_{1j} \mathrm{d}\vec{S} + D_2 \int_{\Omega_e} \vec{\nabla} N_{2i} \vec{\nabla} N_{2j} \mathrm{d}V \; + \\ - D_2 \int_{\Gamma_e} N_{2i} \vec{\nabla} N_{2j} \mathrm{d}\vec{S} + \Sigma_{a2} \int_{\Omega_e} N_{2i} N_{2j} \mathrm{d}V - \Sigma_{12} \int_{\Omega_e} N_{2i} N_{1j} \mathrm{d}V \Bigg) \; , \quad (4)$$

$$M_{ij} = \sum_{e=1}^{N_t} \left(\nu \Sigma_{f1} \int_{\Omega_e} N_{1i} N_{1j} \mathrm{d}V + \nu \Sigma_{f2} \int_{\Omega_e} N_{1i} N_{2j} \mathrm{d}V \right) \; , \quad (5)$$

where N_{gi} is the prescribed shape function for the $i-$th node. For simplicity, the shape functions used are part of Lagrange finite elements [4]. Ω_e ($e = 1, ..., N_t$) are the reactor subdomains in which the reactor domain is dived. In the same way, Γ_e are the corresponding subdomain surfaces which are part of the reactor frontier.

To solve the algebraic eigenvalue problem a Krylov-Schur method is used from the SLEPc library [3]. First, the generalized problem is reduced to an ordinary eigenvalue problem,

$$\mathbf{L_{11}^{-1}} \left(\mathbf{M_{11}} + \mathbf{M_{12}} \mathbf{L_{22}^{-1}} \mathbf{L_{21}} \right) \tilde{\boldsymbol{\phi}}_{\mathbf{1}} = \lambda \tilde{\boldsymbol{\phi}}_{\mathbf{1}} \; , \quad (6)$$

which is solved for the n dominant eigenvalues and their corresponding eigenvectors. In this way, for each matrix-vector product it is necessary to solve two linear systems associated with the L_{11} and L_{22}, to avoid the calculation of their inverse matrices. These systems are solved by means of an iterative scheme as the preconditioned GMRES method. Particularly, a Cuthill-McKee reordering is performed to reduce the bandwidth of the matrices, together with an incomplete LU factorization of the matrices is used for the preconditioning.

3 Numerical Results

To study the performance of the *h-p* finite element method to determine the Lambda modes of a nuclear reactor, three different benchmark problems have been considered. To validate the results of the implemented code first

a 2D homogeneous reactor has been studied, since an analytical solution can be found for this problem. Also more realistic reactors, as the BIBLIS 2D reactor and the IAEA 3D reactor have been studied.

The numerical results show that h-refinement is not a better strategy than increasing the polynomial degree uniformly because of the smoothness in the solutions for the fluxes and the computational cost of evaluating the error estimator. For example, in the IAEA 3D Reactor, a coarse mesh with 4579 cells with $p = 3$ gives better results ($\bar{\varepsilon} = 0.79\%$ and $\epsilon_{eig} = 8.1$ pcm) than a h-refined mesh with 20609 cells and $p = 2$ ($\bar{\varepsilon} = 1.54\%$ and $\epsilon_{eig1} = 87$ pcm), even though the first one is faster (97.5 s against 108.2 s). Also, it is observed that the errors behaviour for the first eigenvalue and its corresponding eigenvector are similar to the errors for the second eigenvector. It can be concluded that the best strategy for a real reactor, with a moderate computational cost, is to use finite elements with cubic polynomials in a coarse mesh.

4 Conclusions

In this contribution, we have presented an adaptive finite element algorithm for the Lambda modes problem. This method allows using high order finite elements with heterogeneous meshes. In this way, to increase the accuracy of the solution it is possible both to refine the spatial mesh and to increase the degree of the polynomials in the finite element method. To study the performance of the method to compute the dominant eigenvalues and their corresponding eigenvectors of a nuclear power reactor, different benchmark problems have been analysed, using different meshes and configurations of the computations. From all the analyses performed is concluded that the method converges if the mesh is refined or the degree of the polynomial expansions is increased, being the last strategy the most convenient one to obtain accurate results with a moderate computational cost.

Acknowledgements

This work has been partially supported by the Spanish Ministerio de Ciencia e Innovación under project ENE2011-22823, the Generalitat Valenciana under projects PROMETEO/2010/039 and ACOMP/2013/237, and the Universitat Politècnica de València under project UPPTE/2012/118.

References

[1] G. Verdú, D. Ginestar, V. Vidal, and J.L. Muñoz-Cobo. 3D Lambda-modes of the neutron-diffusion equation. *Annals of Nuclear Energy*, 21(7):405 – 421, 1994.

[2] W. Bangerth, R. Hartmann, and G. Kanschat. deal.II – a general purpose object oriented finite element library. *ACM Trans. Math. Softw.*, 33(4):24/1–24/27, 2007.

[3] Vicente Hernandez, Jose E. Roman, and Vicente Vidal. SLEPc: A scalable and flexible toolkit for the solution of eigenvalue problems. *ACM Trans. Math. Software*, 31(3):351–362, 2005.

[4] O. C. Zienkiewicz, R. L. Taylor, and J. Z. Zhu. *The finite element method: its basis and fundamentals.* Butterworth-Heinemann, 2005.